LAPPEENRANNAN TEKNILLINEN KORKEAKOULU
LAPPEENRANTA UNIVERSITY OF TECHNOLOGY

UDK 536.7:
621.57:
62-135:
62-947

TIETEELLISIÄ JULKAISUJA
RESEARCH PAPERS
56

JARI BACKMAN

ON THE REVERSED BRAYTON CYCLE WITH HIGH SPEED MACHINERY

Thesis for the degree of Doctor of Technology to be presented with due permission for public examination and criticism in Auditorium of the Student House of Student Union at Lappeenranta University of Technology, Lappeenranta, Finland on the 19th of December 1996, at noon

Lappeenranta
1996

ISBN 951-764-089-7
ISSN 0356-8210

Turbine design is easy.
Elementarily it is a hole in the wall
Per-Holger Sahlberg 1913-1995

Jari Backman
UDK 536.7: 621.57: 62-135: 62-947
Key words Reversed Brayton cycle, heat pump, refrigeration, dehumidifier, high speed technology

On the Reversed Brayton Cycle with High Speed Machinery

ABSTRACT

This work was carried out in the laboratory of Fluid Dynamics, at Lappeenranta University of Technology during the years 1991-1996. The research was a part of larger high speed technology development research.

First, there was the idea of making high speed machinery applications with the Brayton cycle. There was a clear need to deepen the knowledge of the cycle itself and to make a new approach in the field of the research. Also, the removal of water from the humid air seemed very interesting.

The goal of this work was to study methods of designing high speed machinery for the reversed Brayton cycle, from theoretical principles to practical applications.

The reversed Brayton cycle can be employed as an air dryer, a heat pump or a refrigerating machine. In this research the use of humid air as a working fluid has an environmental advantage, as well.

A new calculation method for the Brayton cycle is developed. In this method especially the expansion process in the turbine is important because of the condensation of the water vapour in the humid air. This physical phenomena can have significant effects on the level of performance of the application. Also, the influence of calculating the process with actual, achievable process equipment efficiencies is essential for the development of future machinery. The above theoretical calculations are confirmed with two different laboratory prototypes.

The high speed machinery concept allows one to build an application with only one rotating shaft including all the major parts: the high speed motor, the compressor and the turbine wheel. The use of oil free bearings and high rotational speed outlines give several advantages compared to conventional machineries: light weight, compact structure, safe operation and a higher efficiency at a large operational region.

There are always problems when theory is applied to practice. The calibrations of pressure, temperature and humidity probes were made with care but still measurable errors were not negligible. Several different separators were examined and in all cases the content of the separated water was not exact. Due to the compact sizes and structures of the prototypes, the process measurement was slightly difficult.

The experimental results agree well with the theoretical calculations. These experiments prove the operation of the process and lay a ground for further development.

The results of this work give very promising possibilities for the design of new, commercially competitive applications that use high speed machinery and the reversed Brayton cycle.

ACKNOWLEDGEMENTS

This work started from the visions to find applications that use high speed technology. I and Pekka Sahlberg were encouraged to investigate the Brayton process and search for suitable process connections. In a very short time this led to the design of the process programme, and later to many interesting research activities around our test facilities.

I wish to express my sincere thanks to my friend and colleague Lic. Tech. Pekka Sahlberg. He worked by me through almost all the research. The inspiration and devotion to combine theory to practice have greatly influenced our work.

I am indebted to my mentor, Associate Professor Jaakko Larjola. He is a huge dynamo in high speed technology. I have not yet been in a position, where he could not give answers to my problems. Also, I would like to thank M. Sc. Hannu Esa from his valuable contribution in the area of turbo machines.

I thank all the team members of high speed technology in Lappeenranta, Tampere and Helsinki. It is an honour to work in this multi scientific team that consists of experts in all areas of modern engineering. The high speed technology is indeed on the edge of commercial success.

Especially Lab. Tech. Petri Pesonen has given a precious touch to all our test facilities with the help of his colleagues Ilpo Taipale, Juha Haikola, Erkki Nikku and Jouni Ryhänen.

The Department of Energy Technology has to my mind a unique atmosphere that makes it easy to feel at home, despite the long working hours. Here we have specialists in thermodynamics, power engineering, electrical engineering, economics and environmental engineering meeting daily at the coffee corner. I thank all my friends at the Department for having a good time.

I would like to express my thanks to the official pre-examiners, Professor Manfred Rautenberg, University of Hannover, and Professor Carl-Johan Fogelholm, Helsinki University of Technology, for their valuable corrections and comments. Also, I wish to thank Professor Pertti Sarkomaa for his comments and advices during the manuscript reviewing.

I am obliged to Mrs Sinikka Talonpoika for language revision.

I am grateful for the financial support from the Finnish Cultural Foundation and Lappeenranta University of Technology. I also would like to appreciate the interest that the Technology Development Centre Finland (TEKES) has shown to the high speed technology research.

I am indebted to my parents, Inkeri and Leo, for their love and support. I also want to thank my grand parents and brothers for all the care during these years. I wish to thank my uncle Tom for his interest in my academic activities.

Most of all, I want to thank my wife Sinikka for her encouragement and understanding during all the years of my research. There are no words, just feelings.

Lappeenranta, November 1996 *Jari Backman*

CONTENTS

NOMENCLATURE

Symbol	*Units*	*Definition*
A	m^2	area
b	m	air gap width in the electric motor
c	m/s	absolut velocity of fluid
c_p	kJ/(kg,K)	specific heat capacity in constant pressure
c_n	m/s	absolut velocity component in the axial direction
c_u	m/s	absolut velocity component in the radial direction
c_v	kJ/(kg,K)	specific heat capacity in constant volume
c_f	dimensionless	friction coefficient of the segment of radial bearing
c_f	dimensionless	friction coefficient of the air gap in electric motor
c_m	dimensionless	friction coefficient of the free end of rotor
c_m	dimensionless	friction coefficient of a closed rotating disc
d	m	diameter
d	-	uncertainty
E_s	kWh/kg, Wh/g	specific electric energy
F	N	force
g	m/s^2	gravity
h	kJ/kg	specific enthalpy
k	dimensionless	roughness coefficient of surface
l	m	length of electric motor
L	m	length of radial bearing
m	kg	mass
M	kg/kmol	mol mass
M	Nm	torque
n	dimensionless	number of radial bearing segments
N	1/s	rotational speed
N_s	dimensionless	specific speed
p	Pa	pressure
P	W	power
P_{ab}	W	power due to friction losses in the axial magnetic bearing
P_{ag}	W	power due to friction losses in the air gap of motor
P_{fe}	W	power due to friction losses at the free end of motor
P_{mf}	W	power due to cooling mass flow in the air gap of motor
P_{mt}	W	power due to mechanical losses in the motor
P_{rb}	W	power due to friction losses in the radial bearing
q	W/kg	heat per mass flow
q_m	kg/s	mass flow
q_v	m^3/s	volume flow
r	m	radius
R	m	radius of radial bearing
R	kJ/(kg,K)	gas constant
Re	dimensionless	Reynolds number
s	kJ/(kg,K)	specific entropy
s	m	cascade blade distance
T	K	temperature
u	m/s	circumferential velocity of fluid
v	m^3/kg	specific volume, $1/\rho$
V	m^3	volume
w	m/s	relative velocity of fluid
w	dimensionless	mass fraction of fluid component
x	dimensionless	mole fraction of fluid component
z	m	elevation
α	°	angle of the absolut velocity vector

α_t	dimensionless	turbine flow factor
β	°	angle of the relative velocity vector
γ	dimensionless	specific heat capacity ratio, c_p/c_v
ε_r	dimensionless	coefficient of performance of refrigeration machine
ε_h	dimensionless	coefficient of performance of heat pump
η	dimensionless	efficiency
Λ	dimensionless	radial bearing compressibility coefficient
μ	dimensionless	ratio of molecular masses between water vapour and air
μ	Ns/m^2	dynamic viscosity
υ	dimensionless	blade speed ratio
π	dimensionless	pressure ratio
ρ	kg/m^3	density, 1/v
σ	MPa	tension
τ	m^2/N	compressibility
τ_0	m	clearing between radial bearing and shaft
φ	%	relative humidity, RH
ω	dimensionless	humidity(ratio)
ω	rad/s	angular velocity

subscripts

0	ambient
1..4	reversed Brayton cycle operation points, static state
01..04	reversed Brayton cycle operation points, total state
air	air component
des	design
el	electric, electrical
ice	ice component
inv	inverter
mech	mechanical
p	polytropic
vap	water vapour component
s	isentropic
spec	specific
TS	total to static
TT	total to total
w	water based component
wat	water liquid component

superscripts

'	saturation

1 INTRODUCTION

The Department of Energy Technology at Lappeenranta University of Technology (LUT) has studied the use of high speed technology since 1981. In the 1990s the research concentrated on co-operation between the Department of Energy Technology at Lappeenranta University of Technology (LUT), the Department of Electrical Engineering at Helsinki University of Technology (HUT) and the High Speed Tech Oy Ltd in Tampere.

The Brayton cycle is familiar to many from gas turbines, where turbomachinery and combustors convert fuel to electricity. This means that the cycle produces work with the generator in the cycle. In normal cases the working fluid in the compressor is air and in the turbine exhaust gas. The reversed Brayton cycle has the same turbomachinery elements as a gas turbine — a compressor and a turbine — but not a combustor. Because there is no energy input and the pressure levels in both turbomachinery components are equal, the cycle needs work to compensate for the losses. This means that the electric machine must be a motor.

The reversed Brayton cycle has one particularly interesting feature. Because the heat exchange is not pressure dependant, the order of compression and expansion can be easily reversed. This fact gives more flexibility in the design of the applications because it is possible to design a sub-[1] or over-pressure cycle.

The purpose of this thesis was to examine the reversed Brayton process in detail and to design high speed prototypes. With these prototypes the theoretical calculations were to be verified with measurements. In the calculations and the experiments the significance of humid air was to be very important.

In this work the following methods of research have been adapted:

First, making the theoretical calculations of the reversed Brayton cycle for humid air. Chapter 2 presents the theoretical calculation principles and Chapter 3 introduces the calculation programme. These calculations take into account the real humid air compression and expansion, pressure losses and efficiencies.

---

[1] *This study uses the terms sub-pressure or sub-atmospheric instead of the term vacuum, which is slightly errative in this context.*

Secondly, verifying the theoretical calculations with experimental measurements. The two test facilities and the measurement results are presented in Chapter 4.

Thirdly, investigating application feasibilities in the view of the results, and this is done in Chapter 5.

The reversed Brayton cycle is an old invention referred fairly widely. There are several documents of process applications that refer to patents, prototypes and commercial devices. In the reviewed literature the process itself have been called with several different names: reversed Brayton cycle, reverse Brayton cycle, Joule cycle, air heat pump. Because the design of this disseratation is focused on cycles, where power is needed, the term reversed is used.

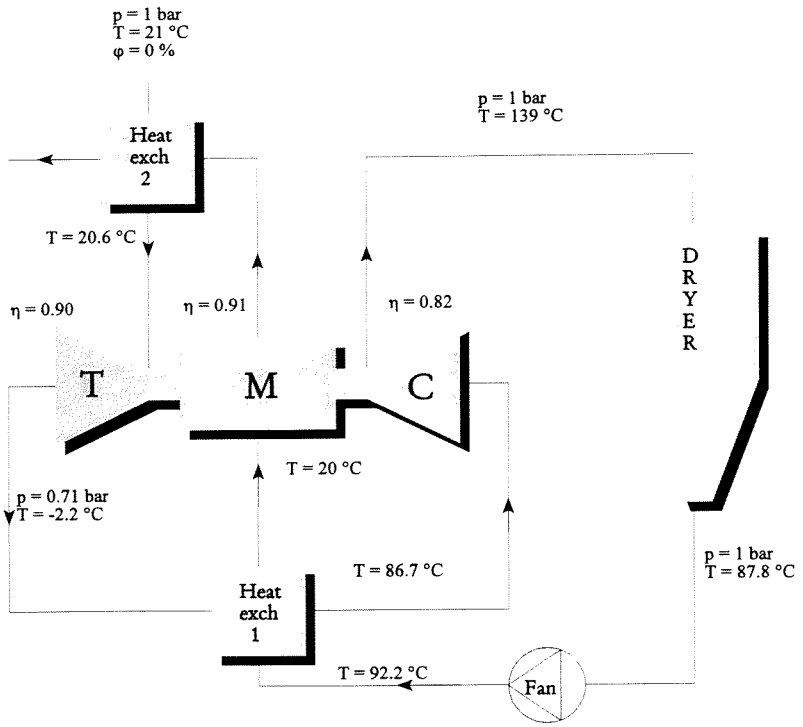

Figure 1. The AirResearch reversed Brayton cycle. T=turbine, M=motor, C=compressor

/AirResearch 1979/ describes the performance of a sub-atmospheric reversed Brayton cycle applied for milk dryers. The working fluid was air and the theoretical calculations were made between dryer exhaust and supply temperatures. The reversed Brayton cycle performance was compared with a Rankine cycle for a known milk dryer facility. These comparisons included a dryer-only heat pump and a heat pump where the exhaust gas heated the inlet gas. The report includes

specific cycle design but there is no mention of actual devices. In this report the mass flow, 0.453 kg/s, and the electric power, 13.7 kW, are very close to those of the first experimental prototype reported in this thesis. There also is a preliminary heat exchanger design that compares three major heat exchanger types. The maximal temperature is 92 °C, which is about 30 degrees higher than the temperatures in this study.

The main disadvantage of the calculations is that the cycle pressure losses are ignored, compressor and turbine efficiencies are fixed at a reasonably high level and the ambient air is considered totally dry.

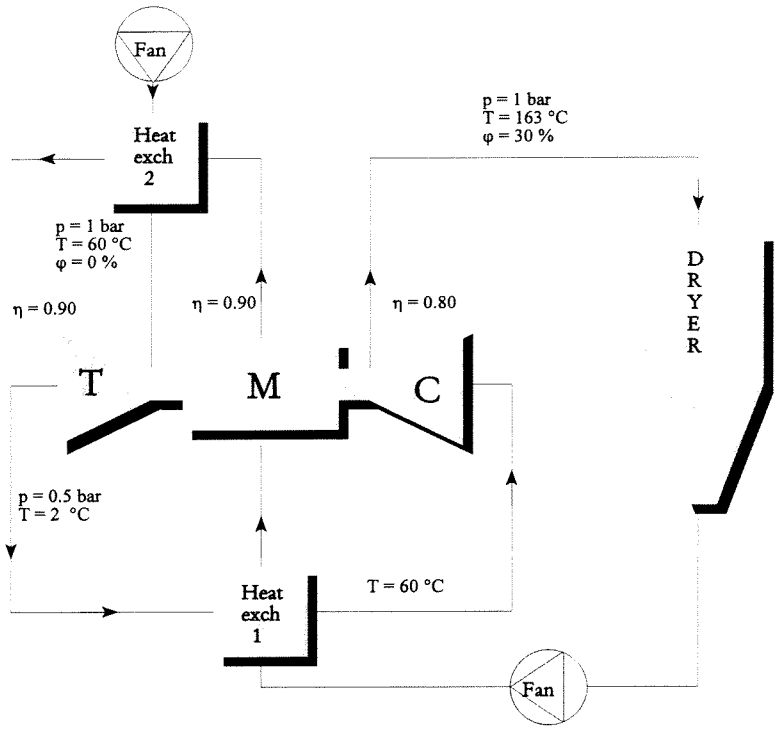

Figure 2. The Cercem reversed Brayton cycle. T=turbine, M=motor, C=compressor

A French enterprise Compagnie Electro-Mecanique (Cercem) has studied industrial drying. /Flaux 1984/ describes the developing of a prototype for a high temperature reversed Brayton cycle designed to operate in the drying industry. A typical installation would be a milk powder atomization drier. The study includes the comparison of three possible cycle modes; open, semi-open and closed cycle. The author adopted the open cycle where the electric power needed is 223 kW and the maximum cycle temperature is 163 °C. The exhaust, moist air from the drying system, is used through a heat exchanger to warm the sub-atmospheric air.

/Kajima 1995/ describes a reversed Brayton cooling device that is used to freeze ice hockey rinks, bobsleighing tracks and air cooling systems. Here an over-pressure cycle is used, where the air is first compressed to higher pressure, then the heated air is cooled close to inlet temperature with for example water. After water cooling the air is cooled with return air from the refrigerating process and finally run through the turbine. The air temperature after the turbine is significantly below the freezing point water of water. This cold air is delivered for refrigerating purposes. The overall power requirement is 400 kW and the air mass flow is 8,5 kg/s. The air is dried in an adsorption device before the compressor, so the working fluid is dry air. As can seen in the Figure 3, the cycle is closed.

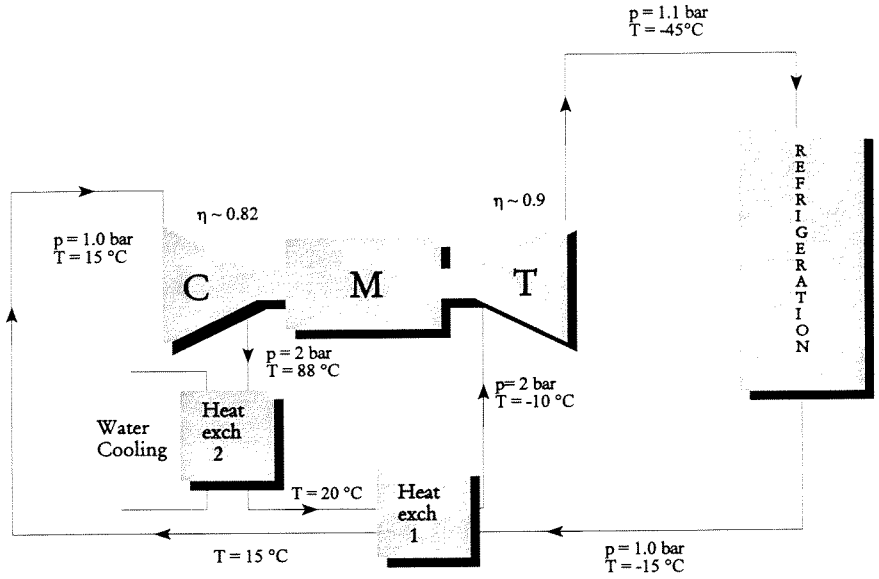

Figure 3. The Kajima cooling device principle. T=turbine, M=motor, C=compressor

/Dunn 1976/ describes the design and the results of a closed Helium-Xenon-cycle Brayton unit. This unit is an application, which was intended to demonstrate energy conversion technology in space. The system is designed to produce up to 10 kW net continuous electric power for at least five years. One test unit accumulated over 21 thousand hours of operation with no apparent failure. The cycle included very high temperatures - turbine inlet temperature 871 °C - and a reasonably high rotational speed of 36 000 rpm. This study introduces an apparatus based to technology similar to that of the present study.

High speed technology is a solution that does away with the gearbox: a high speed electric machine drives the rotor of the turbine, compressor or pump, or the spindle of the milling machine directly. By using suitable bearings it is possible to make the high-speed solution completely oil-free and hermetic, which provides additional benefits.

High speed technology was probably first used in the production of liquid helium /Swift and Sixsmith 1982/: the very low temperature and requirement of purity made it impossible to use gear-boxes or conventional bearings. By using a high speed rotor with gas or magnetic bearings it was possible to achieve the compression and expansion required for the liquefaction of helium without any oil.

Oil-free high speed technology is also widely used in the helium circulators of nuclear reactors /Decker 1976/, in small ORC-power plants for special applications /Bronicki 1982/, in air-circulation systems in aeroplanes, in ultra high speed motors required to scan the laser beam, in some milling and grinding machines /SMM 1984/ and in some space applications /Habermann and Brunet 1984/, /Dunn 1976/. All these are applications, where small size and oil free operation are very important, or where a very high speed is required.

The high speed technology research in Finland has been all-inclusive research that aims at designing a whole process facility. The technology consists of fluid engineering, mechanical engineering, electrical engineering and control engineering.

The research of high speed technology at Lappeenranta University of Technology, at Helsinki University of Technology and in High Speed Tech Oy Ltd includes activities in the following areas:

- static and dynamic fluid bearings /Sallinen 1993/
- active magnetic bearings /Lantto and Antila 1995/
- high speed electric machine construction
- electric control engineering
- turbomachinery design /Larjola et al 1995/
- cooling construction.

The high speed technology theories are applied in several test facilities in waste heat utilization /Larjola et al 1991b/, low pressure compressors /Backman 1989/, high pressure pumps /Larjola et al 1995/, refrigeration compressors and reversed Brayton cycles /Sahlberg 1993/.

The bearing technology is based on oil free gas dynamic, hydro dynamic or electromagnetic bearings that have very long operational cycles and are also practically maintenance free.

The technical high speed solutions are still today on the level of high technology and there are not many commercial applications. The main obstacles are the electric components (the inverter and the motor) and the bearings, which have been the top priorities of the high speed technology research in Finland.

The research helps high speed technology to spread to more conventional applications, such as compressors and small power plants. One major reason for this is the decreased price of suitable inverters and bearings. In this view the reversed Brayton cycle is a very attractive choice in applying high speed technology.

2 THE REVERSED BRAYTON CYCLE

In the Brayton cycle the working, gaseous medium consists of two isobars and two isentropes. The process in the Brayton cycle generates work to be used, but the term reversed explains that the obtainable cycle needs external work. This can be electric, pneumatic or hydraulic etc. power. The most common way is to use an electric motor to provide this work.

The performance of the reversed Brayton cycle is characterised so that the compressor takes care of the pressure difference and the turbine takes care of the mass flow, and this counteraction at given speed defines the operational points of the cycle.

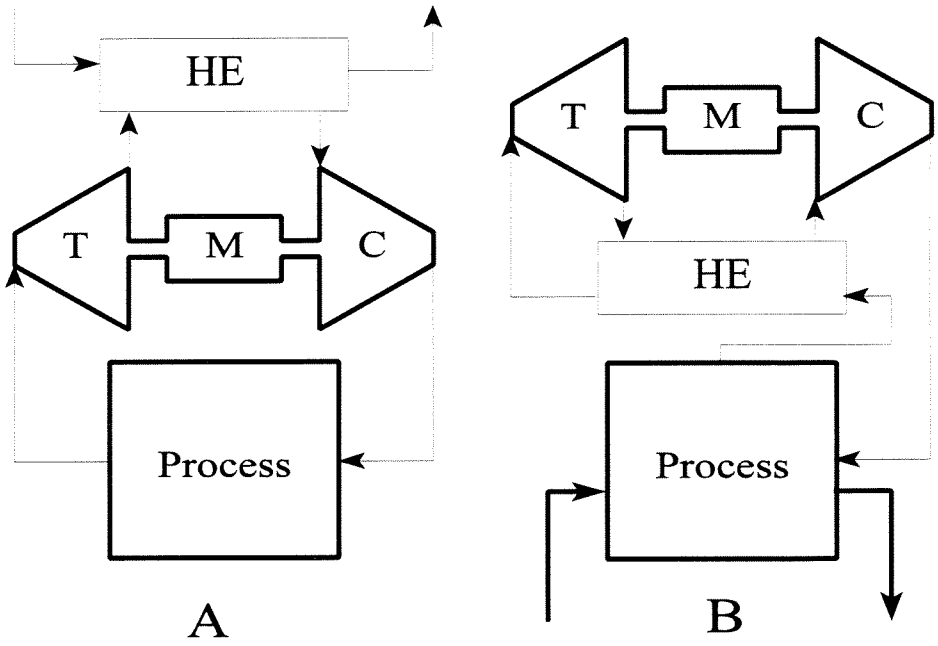

Figure 4. Example of closed (**A**) and open (**B**) reversed Brayton cycle

A typical application of the Brayton cycle is the gas turbine while the humidifier, ventilation system, cryogenic machine or heat pump are typical applications of the reversed Brayton cycle. In principle the reversed Brayton cycle can be either open - the fluid medium is constantly changed - or closed. The loop is also defined open if the Brayton cycle is closed but the interface process is open. This is the case when only part of the actual process air flow is forwarded to the Brayton cycle. In the closed loop there is no material transfer between the process and the environment, Fig. 4.

The limits for the process values in the reversed Brayton process are quite wide. There are no such limits that are familiar to common organic cycles as critical temperature and pressure, evaporation pressure, etc. In the cryogenic applications -80 °C could be considered as the lower limit and in heat pumps the upper limit would be around 300 °C. The pressures vary from about 0.1 bar to 10 bar. The limits are mostly set by material restrictions and, finally, according to economical estimations.

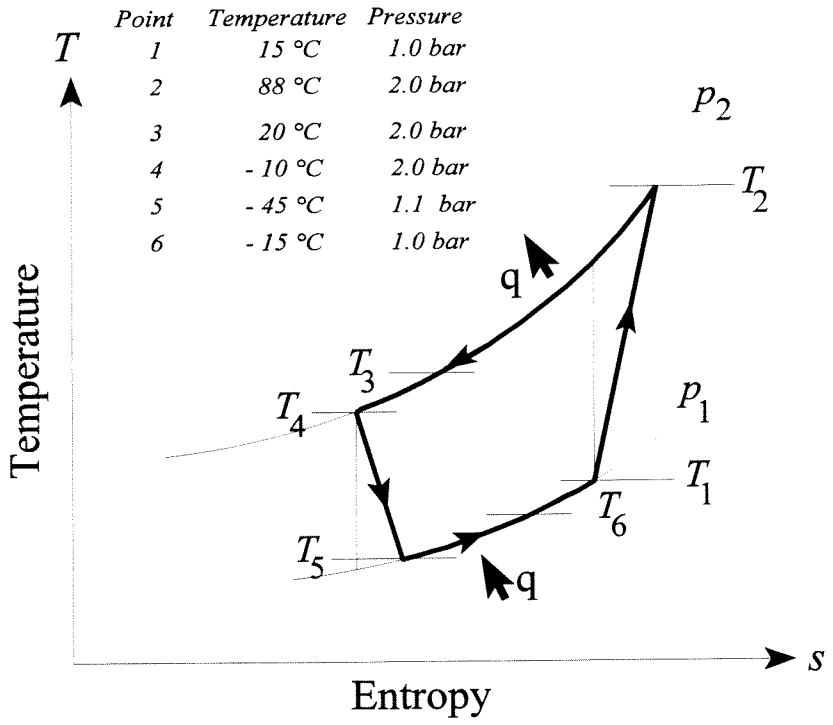

Figure 5. The *T,s*-chart of the reversed Brayton cycle in Fig. 3.

Several examples of different open, reversed Brayton cycles were described in Chapter 1. The cycle chart is usually described as a *T,s*- or *h,s*-chart as shown in Fig. 5.

The necessity of good efficiencies in the pressure cycles is the main reason for the fact that there still are so few commercial applications that use the reversed Brayton cycle.

The many published calculation models are quite coarse and simple. The main compression/expansion losses are taken into account but usually the pressure losses are ignored. With even moderate losses and efficiencies the calculations usually result with low overall cycle efficiencies.

When the surrounding air is used as a medium, it is usually treated as dry, e.g. the water vapour in the air is ignored. But for example during the expansion the water vapour pressure can drop beneath the wet point and part of the water vapour condenses to water. The quantity of water is not large but the phenomenon influences the enthalpy of the fluid because the vaporization heat is considerable.

In this thesis a calculation model is introduced which includes the actual turbomachinery efficiencies, the pressure losses and the use of humid air.

2.1 Humid air and perfect gas

The ambient air is a mixture of several gases. Normally dry air consists of nitrogen, oxygen and argon to over 99.6%. The rest are small amounts of large number of different gases. Air is catalogued with specific molecular weights (M_i) and gas constants (R_i), and it is assumed to be a perfect gas.

Humid air is a mixture of dry ambient air and water vapour. The amount of water vapour that there can be in humid air (thermodynamical equilibrium assumed) is a function of temperature and thus varies. Vapour in this context means gas that is near to liquefying.

The enthalpy in the real gas phase is defined as a function of the pressure and the temperature that thermodynamically describe the gas particle motions. This relevance complicates calculations because in most processes that include air, the average distance between particles is usually so large that there are only weak attractive forces among the particles. The approximation of perfect gas usually simplifies these calculations by neglecting the intermolecular forces /Anderson 1990/. A gas is defined as perfect gas when it governs the equation of state /Liepmann and Roshko 1957/

$$pv = R_i T \tag{1}$$

where $v = V / m$. The specific gas constant R_i varies for each gas and is related to the universal gas constant R, so for air $R_i = R / M_i$. The result is very close to the absolute value if the density is close to zero. In the cases where the air pressure is between 0.5 and 10 bars and the temperature is between 250 and 600 K, the error is less than 0.5 % calculated from table values. In water vapour the error is lower than 1% when $p < 0.5$ bar and $T > 250$ K /Vargaftig 1975/.

If we ignore intermolecular forces, we can also express enthalpy and internal energy only as functions of the temperature along the isobar and isochor[1] /Anderson 1990/

$$dh = c_p dT \tag{2}$$

$$du = c_v dT \tag{3}$$

Here the enthalpy and the inner energy vary only with temperature.

If the specific heats were chosen as constants, calorimetrically perfect gas would be used. Because the specific heat capacity of dry air varies from $c_p = 1.002$ to $c_p = 1.016$ when the temperature rises from $T = 0$ °C to $T = 100$ °C, the use of a conveniently chosen value for calorimetrically perfect gas gives a very small error. In this research humid air is examined and therefore the use of calorimetrically perfect gas is not preferable here.

The entropy change of the system is always positive, which tells us in what direction the process evolves. The entropy of ideal gas is a function of both temperature and enthalpy. The entropy definition $\Delta q = Tds$ can be differentiated with the help of the first law of thermodynamics and we obtain for perfect gas

$$ds = c_p \frac{dT}{T} - R\frac{dp}{p} \tag{4}$$

An isentropic process is defined to be adiabatic and reversible. Thus the isentropic change of state is obtained from Eq. (4) by setting $ds = 0$ and integrating

$$\begin{aligned} & c_p \frac{dT}{T} = R\frac{dp}{p} \\ \Rightarrow\ & \bar{c}_p \ln\frac{T_2}{T_1} = R\ln\frac{p_2}{p_1} \\ \Rightarrow\ & \frac{p_2}{p_1} = \left(\frac{T_2}{T_1}\right)^{\frac{\bar{c}_p}{R}} \end{aligned} \tag{5}$$

---

[1] *a process is called isobar, when the pressure is constant, and isochor when the specific volume is constant*

Equation (5) relates pressure and temperature for an isentropic process, and is of great importance in the compressor and turbine design procedures. The mean specific heat capacity in constant pressure is defined $\overline{c_p} = c_p[(T_1+T_2)/2)]$. For small pressure ratios ($\pi < 4$) and normal temperatures (250 K $< T <$ 500 K), the temperature difference after the process would be smaller than 0.1 degrees in comparison with the value obtained by accurate integration.

2.1.2 The Dalton gas mixture model

We have assumed that humid air can be treated as a perfect gas mixture. To calculate the mixture the Dalton gas mixture model has been used. The law of Dalton declares /Liepmann and Roshko 1957/: that the total pressure of the ideal gas mixture is equal to the sum of the partial pressures, i.e. individual gas component pressures. Thus, we get the equation

$$p = p_{air} + p_{vap} \tag{6}$$

and the individual gas component's pressure is the outcome of the multiplication of the total pressure of the mixture and the mole fraction

$$p_{vap} = x_{vap} p \tag{7}$$

$$p_{air} = x_{air} p \tag{8}$$

The water vapour pressure in air is regulated by the temperature so that it can be only as high as the pressure of saturated water vapour. If the mole fraction of the vapour is greater than the temperature allows, the rest of the water is in liquid (water) or solid (ice or snow) state. The quantity of water vapour is defined by relative humidity φ [1]

$$\varphi \equiv \frac{p_{vap}}{p'_{vap}} \tag{9}$$

The amount of dry air is kept constant through the expansion process, and thus it is convenient to define the mass fraction of the flow mixture as function of the mass flow and to call it humidity

---

[1] *Relative humidity is often abbreviated as RH*

$$\begin{aligned} \omega_{vap} &\equiv \frac{m_{vap}}{m_{air}} \\ \omega_{ice} &\equiv \frac{m_{ice}}{m_{air}} \\ \omega_{wat} &\equiv \frac{m_{wat}}{m_{air}} \end{aligned} \tag{10}$$

and these together form the water-based humidity in air

$$\omega_w = \omega_{vap} + \omega_{wat} + \omega_{ice} \tag{11}$$

The mole fractions in the gas phase can be written

$$\begin{aligned} x_{air} &= \frac{n_{air}}{n_{air} + n_{vap}} = \frac{\mu}{\omega_{vap} + \mu} \\ x_{vap} &= \frac{n_{vap}}{n_{air} + n_{vap}} = \frac{\omega_{vap}}{\omega_{vap} + \mu} \end{aligned} \tag{12}$$

where $\mu = M_{vap} / M_{air}$

The mass fractions in humid air are

$$\begin{aligned} w_{air} &= \frac{m_{air}}{m_{air} + m_{vap} + m_{wat} + m_{ice}} = \frac{1}{\omega_w + 1} \\ w_{vap} &= \frac{\omega_{vap}}{\omega_w + 1} \\ w_{wat} &= \frac{\omega_{wat}}{\omega_w + 1} \\ w_{ice} &= \frac{\omega_{ice}}{\omega_w + 1} \end{aligned} \tag{13}$$

From equations (12),(7), (8) and (9) we get the water vapour humidity in Eq. (10)

$$\omega_{vap} = \mu \frac{p_{vap}}{p_{air}} = \mu \frac{p'_{vap}}{\frac{p}{\varphi} - p'_{vap}} \tag{14}$$

The condensation of water vapour is possible if the inlet relative humidity and the pressure ratio of the turbine are suitable. According to the Dalton gas mixture model the condensation or sublimation temperature depends solely from the partial pressure of the water vapour.

The thermodynamical properties of humid air are calculated by weighing the mixture mass components using Eq. (13)

$$\begin{aligned} h &= \frac{1}{\omega_w + 1}(h_{air} + \omega_{vap} h_{vap} + \omega_{wat} h_{wat} + \omega_{ice} h_{ice}) \\ s &= \frac{1}{\omega_w + 1}(s_{air} + \omega_{vap} s_{vap} + \omega_{wat} s_{wat} + \omega_{ice} s_{ice}) \end{aligned} \tag{15}$$

The humid air gas constant R is calculated by weighing the gaseous components by their mole fractions in Eq. (12)

$$M = \frac{1}{\omega_{vap} + \mu}(\mu M_{air} + \omega_{vap} M_{vap}) \tag{16}$$

$$R = \frac{R_u}{M} \tag{17}$$

The water vapour has surprisingly large effects on the thermodynamical properties of humid air when compared to those on dry air. For example at 40°C the gas constant R (which is often considered constant) grows from 287 J/(kg,K) to 311 J/(kg,K) when the relative humidity is increased from 0% to 100%. This effect is smaller in the specific heat ratio γ, because the effect in both specific heats is in the same direction.

2.1.3 Thermodynamical state property correlations

The thermodynamical changes in a process are usually examined in the h,s-chart and therefore specific enthalpy and specific entropy have to be made relative with a physical reference point. If the reversed Brayton process is calculated by hand, many iterative and labourious calculations have to be made.

According to the definition of perfect air above, enthalpy will be expressed as a function of temperature and entropy as a function of both temperature and pressure.

To simplify the property correlations of the humid air process, the reference point is chosen to equal the point of water saturation at the triple point, T_{ref} = 273,16 K and p_{ref}=611.3 Pa, where all three phases can be represented simultaneously.

The values of specific heat capacity in constant pressure /Vargaftig 1975/ can be expressed with a regressional third degree polynomial fit

$$c_p(T) = a_1 + a_2 T + a_3 T^2 + a_4 T^3 \tag{18}$$

where the constants for the region 200 K ≤ T ≤ 1800 K are for dry air

a_1 = 9.82076E-1 kJ/ (kg,K)
a_2 = 1.64395E-5 kJ/ (kg,K^2)
a_3 = 2.25868E-7 kJ/ (kg,K^3)
a_4 = -8.81495E-11 kJ/ (kg,K^4)

and for water vapour

a_1 = 1.80768E-1 kJ/ (kg,K)
a_2 = 1.79273E-5 kJ/ (kg,K^2)
a_3 = 6.80617E-7 kJ/ (kg,K^3)
a_4 = -2.22443E-10 kJ/ (kg,K^4)

The specific enthalpy of water vapour and air can be expressed with similar regression coefficients when Eq.(18) is placed into Eq.(2) and integrated

$$\begin{aligned}\Delta h &= h(T) - h(T_{ref}) = \int_{T_{ref}}^{T} (a_1 + a_2 T + a_3 T^2 + a_4 T^3)\, dT \\ &= a_1(T - T_{ref}) + \frac{a_2}{2}(T^2 - T_{ref}^2) + \frac{a_3}{3}(T^3 - T_{ref}^3) + \frac{a_4}{4}(T^4 - T_{ref}^4)\end{aligned} \tag{19}$$

Here the reference temperature is chosen to be T_{ref} = 273.16 K in which temperature the enthalpies for dry air and water vapour are $h_{air}(T_{ref})$ = 0 kJ/kg and $h_{vap}(T_{ref})$ = 2501.3 kJ/kg. The latter equals to latent heat between water and water vapour in the chosen reference point.

The specific entropy of water vapour and air can be expressed by integrating Eg.(4)

$$\begin{aligned}\Delta s &= s(T,p) - s(T_{ref}, p_{ref}) = \int_{T_{ref}}^{T} \left(\frac{a_1}{T} + a_2 + a_3 T + a_4 T^2\right) dT - \frac{R_u}{M} \int_{p_{ref}}^{p} \frac{1}{p} dp \\ &= a_1 \ln\left(\frac{T}{T_{ref}}\right) + a_2(T - T_{ref}) + \frac{a_3}{2}(T^2 - T_{ref}^2) + \frac{a_4}{3}(T^3 - T_{ref}^3) - \frac{R_u}{M} \ln\left(\frac{p}{p_{ref}}\right)\end{aligned} \tag{20}$$

The reference point values are for dry air and vapour are

$$s_{air} = 0 \text{ kJ/(kg,K)}$$
$$s_{vap} = h_{vap}(T_{ref}) / T_{ref}$$

The specific enthalpy of water is based on the values /Keenan et al 1978/ fitted by a third degree polynomial fit

$$h_{wat}(T) = a_1 + a_2 T + a_3 T^2 + a_4 T^3 \tag{21}$$

where the constants for the region 273.16 K $\leq T \leq$ 500 K are

a_1 = -1287 kJ/kg
a_2 = 5.54968 kJ/ (kg,K)
a_3 = -4.29195E-3 kJ/ (kg,K^2)
a_4 = 4.47921E-6 kJ/ (kg,K^3)

Because water is practically incompressible, the specific entropy of water is obtained by evaluating Eq. (4) in the following way

$$ds = \frac{dh}{T} - \frac{v}{T} dp = \frac{dh}{T} = s(T) \tag{22}$$

and differentiating Eq.(21)

$$\begin{aligned} dh_{wat} &= (a_2 + 2a_3 T + 3a_4 T^2) dT \\ \Rightarrow s_{wat}(T) &= \int_{T_{ref}}^{T} (\frac{a_2}{T} + 2a_3 + 3a_4 T) dT \\ &= a_2 \ln(\frac{T}{T_{ref}}) + 2a_3 (T - T_{ref}) + \frac{3a_4}{2} (T^2 - T_{ref}^2) \end{aligned} \tag{23}$$

When suitable conditions exist, it is possible that the process is moved to an area where the condensated water is ice. Therefore, we have to make regressional fittings also in this area. The specific enthalpy of ice is based on the values /Keenan et al 1978/ fitted by second degree polynomial fit

$$h_{ice}(T) = h_{ice}(T_{ref}) + a_1 + a_2 (T - T_c) + a_3 (T - T_c)^2 \tag{24}$$

where the constants for the region 233.15 K $\leq T \leq$ 273.16 K are

$a_1 = 0$
a_2 = 2.10340 kJ/ (kg,K)
a_3 = 3.66290E-3 kJ/ (kg,K^2)

The reference point for ice enthalpy is h_{ice} = -333.43 kJ/kg, which is the melting heat of water. Parameter T_c = 273.15 K is the 0 °C used in the original correlation.

The specific entropy of ice is expressed as with water from Eq. (23)

$$\begin{aligned} dh_{ice} &= (a_2 + 2a_3(T - T_c))\,dT \\ \Rightarrow s_{ice}(T) &= s_{ice}(T_{ref}) + \int_{T_{ref}}^{T} \left(\frac{a_2 - 2a_3T_c}{T} + 2a_3\right) dT \\ &= s_{ice}(T_{ref}) + (a_2 - 2a_3T_c)\ln\left(\frac{T}{T_{ref}}\right) + 2a_3(T - T_{ref}) \end{aligned} \tag{25}$$

The reference point value for entropy is

$$s_{ice} = h_{ice}(T_{ref}) / T_{ref}$$

The water vapour pressure is expressed with a regressional exponential correlation /Schmidt 1989/

$$p'_{vap}(T) = p_{cr} e^{\left[T_{cr}/T(a_1\tau + a_2\tau^{1.5} + a_3\tau^3 + a_4\tau^{3.5} + a_5\tau^4 + a_6\tau^{7.5})\right]} \tag{26}$$

where τ = 1 - T/T_{cr}, p_{cr} = 220.64 bar and T_{cr} = 647.14 K and the constants for the region 273.16 K ≤ T ≤ 647.14 K are

a_1 = - 7.85823
a_2 = 1.83991
a_3 = - 11.7811
a_4 = 22.6705
a_5 = - 15.9393
a_{61} = 1.77516

The ice vapour pressure is expressed with a regressional exponential fit for the values /Keenan 1978/

$$p'_{ice}(T) = a_1 e^{\left(a_2 - \frac{a_3}{T}\right)} \tag{27}$$

where the constants for the region 233.16 K ≤ T ≤ 273.16 K are

a_1 = 34860760 bar
a_2 = 0
a_3 = 6136.427 K

2.2 One-dimensional compressible flow

The flow in the reversed Brayton cycle with turbomachinery is continuous and direct forwarded. The related flow passages are quite large and the velocities are significant only in the turbomachinery components. The direction of the flow is abruptly changed only in the turbomachinery (sometimes also in the droplet separator). Therefore, there are good possibilities to consider the total cycle for an accurate design assignment. All the major components can be calculated on a level that would realize the commercial manufacturing of reversed Brayton cycle machines.

First we have to recognize the fact that we cannot calculate the flow at a 100% accuracy. It is customary to simplify the process parameters as seen in Chapter 1. The use of turbomachinery means compressible flow, where the use of the Bernoulli equation would be erroneous.

The approach starts by defining the basic flow principles and equations. Compressible flow has variable density, and whenever the fluid meets a change in pressure, there will also be a change in the density. This compressibility is defined as /Anderson 1990/

$$\tau = \frac{1}{\rho}\frac{d\rho}{dp} \tag{28}$$

The compressibility of the fluid also varies in the flow, because the flows are started and maintained by forces on the fluid, caused by changes in the pressure. It can be said that where there are pressure differences there is flow.

Usually the boundary between compressible and incompressible flow is set to be at fluid speeds of 30% of the speed of sound. At a temperature of 300 K and pressure of 1 bar this would mean a density change of around 5%, when air is used as a fluid.

2.2.1 The principles of motion

The first laws of motion were defined by Sir Isaac Newton /Newton 1686/ as axioms of deceleration, action and reaction of mechanics, which are the first profound fluid dynamics analyses. Later, they were developed by Leonhard Euler in 1757 and de Saint Venant in 1839 to equations of continuity, momentum and energy /Anderson 1990/.

The fluid dynamics analysis at this time was based on one-dimensional and inviscous flow. With proper interpretation these equations can still be used to explain the reversed Brayton cycle.

For calculating the properties of the fluid when it flows through the reversed Brayton cycle, a basic model of flow needs to be created, into which physical principles can be applied. From this model the necessary mathematical equations can be formulated that describe the model sufficiently. These equations are derived from several gas dynamics textbooks /Liepmann and Roshko 1957/, /Zucrow and Hoffman 1976/, /Anderson 1990/.

The basic model here is chosen to be a turbomachine with flow paths, illustrated in Fig. 6. The flow of the model is assumed to be one-dimensional, steady-state, compressible and inviscid. The temperatures, pressures and velocities of the flow are represented by their average values.

The specific work P_{spec} done to the system is positive for a turbine (the system delivers work), and negative for the compressor. The heat term q is positive, when the heat is added to the system (heating from the surroundings) and negative, when the heat is subtracted from the system.

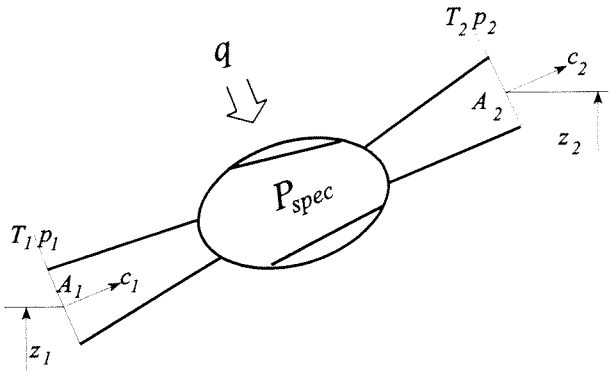

Figure 6. Turbomachine model for flow calculations

The definition of the model does not exclude the complicated, viscous flow inside the turbomachine, but assumes that the flow is unsteady and uniform at the observation points in Fig. 6. To ensure this kind of flow, the areas at the observation points are usually chosen to be quite large. Therefore, the velocities of the fluid are clearly belove the compressible flow limit stated above, but the density

between points 1 and 2 is changed due to the actions of the turbomachine. The compression and expansion processes are defined below with the polytropic and isentropic efficiencies.

Continuity equation

The one-dimensional equivalent of the continuity equation is /Liepmann and Roshko 1957/

$$\rho_1 c_1 A_1 = \rho_2 c_2 A_2 \tag{29}$$

When we look at the reversed Brayton cycle and its components, there are clear inlet and outlet orifices in which the state of the fluid can be measured. Also, the flow is generally constant through the cycle.

There are three exceptions to this constant mass flow:

- if the process is to be used in air drying, part of the water vapour condensates to water and is removed from the cycle. The removal usually takes place after the droplet separator, with a system (pipe, pump etc.) in which the mass flow of the water can be measured. Typically the mass flow of the water is less than 10% of the mass flow of the inlet humid air.
- if there occurs condensation, part of the water will condensate on the surface of the channels, and will affect the above mentioned water mass flow measurement. The error caused by this phenomenon is proportional to the surface area, and is at largest at the beginning of the operation of the cycle. When the surfaces are wet, the water runs more rapidly to the collecting area. These two exceptions can be observed by measuring the relative humidity before and when the cycle has reached the steady state operation.
- in the turbomachinery the gaps between the rotating wheels and the stationary chassis are usually sealed up with contactless seals, such as labyrinth seals, to reduce mechanical losses and ensure a long lifetime. Therefore, there always exist small paths where the air can leak out. The smaller the turbomachinery, the relatively larger gaps have to be used.

Momentum equation

As mentioned above, the flow is compressible and the density is not constant. The momentum equation for one-dimensional flow is /Anderson 1990/

$$p_1 + \rho_1 c_1^2 = p_2 + \rho_2 c_2^2 \tag{30}$$

Energy equation

Energy cannot be created nor destroyed but the form of energy can be changed, and so the energy equation for one-dimensional flow becomes /Zucrow and Hoffman 1976/

$$q + h_1 + \frac{c_1^2}{2} + gz_1 = h_2 + \frac{c_2^2}{2} + P_{spec} + gz_2 \tag{31}$$

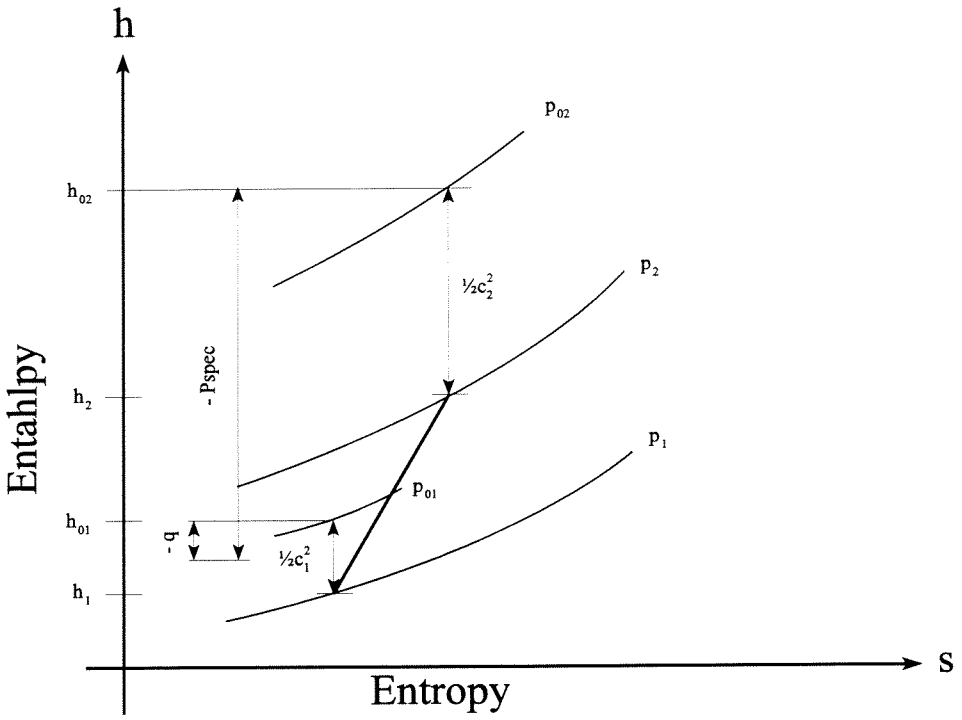

Figure 7. The *h,s*- or Mollier-chart of the turbomachine model

The energy equation of the turbomachine model in Fig. 6 is illustrated for a compressor in Fig. 7. Here the compressor uses work, $-P_{spec}$, and has a heat loss of $-q$ to the surroundings. The potential energy change is ignored[1].

---

[1]*The potential energy of gas is extremely small due the low density of the gas and the compact size of the turbomachinery. For example in the atmospheric conditions, a 10 kW compressor working with the pressure ratio of two, the potential energy is a 0.00002 part of the work needed in the compressor*

2.3 Compressor

The compressor compresses the working fluid to a higher pressure. One can use various kind of compressors to accomplish this. To get high efficiencies in a reversed Brayton cycle and to accomplish the compression, the expansion and the external work on the same shaft, one attractive option is to use turbomachinery. In such a case either axial or radial compressor can be used.

The axial compressor has a higher design efficiency but the radial compressor can be simpler — and thus more economical — to manufacture and be more compact. In an axial compressor there are more stages than tere are in the radial compressor. A trend to prefer radial turbomachinery can be seen in the manufacture of turbochargers, where most compressors have a single radial wheel when the pressure ratio is up to four.

In the turbo compressor, the rotation work is changed to pressure with rotationary and stationary blades. First, the rotor wheel accelerates the flow and the absolute velocity over the blade. During this work also the static pressure usually rises when the relative velocity over the rotor blade decreases. The stator slows the velocity and changes a greater part of the dynamic pressure to static pressure. In a typical compressor the absolute velocities are several hundred metres per second.

In an axial compressor the flow enters an annular channel axially. First there is the rotor cascade and then the stator cascade. After the stator the flow enters the diffuser, where the remaining kinetic energy is partially transformed to static pressure. The diffuser is normally an evenly expanded channel. The high efficiencies are obtained by the highly developed computerized fluid dynamics (CFD), which are very largely used by the compressor manufacturers around the world. The major governing equations were developed by Euler, Navier and Stokes. The first computer programmes for axial compressors were written in the early 60s. Today there are quite good possibilities to achieve isentropic efficiencies higher than 0.90 in commercial series production. In the axial compressor, the area of the channel decreases with the rise of pressure and density, to keep the axial velocity of the flow near constant. Because the flow out of the compressor is axial, the whole machine is quite simple to fit to the surrounding system.

In a radial compressor the flow enters axially, but is then turned radially out from the impeller. The static pressure rises due to the decrease of the relative velocity, but also due to the centrifugal forces. After the impeller the flow enters a radially annular diffuser, in which there can be blades. Because the radius increases, the diffuser can also be made without any blades (parallel diffuser), where the flow is slowed by the free vortex flow. The high complexity of the flow, especially in the rotating

impeller, makes CFD modelling very difficult. There has been much research in analysing the flow and the different viscous phenomena, but there are still no programmes that can calculate the time dependant flow explicitly. The radial compressor needs a gathering body, volute, to assemble the flow to the next phase or to the outlet piping. Usually the volute is a logarithmically increasing passage that ends to a circular outlet, which is easy to connect to piping. The velocities in the volute should be kept low to keep the pressure losses small.

2.3.1 The velocity triangles and the *h,s*-chart of the compressor

The state values of the fluid — pressure rise vs. temperature rise (points 1 to 2 in Fig. 5) — in the compressor are relatively simple to calculate. The velocities of the flow in the rotor can be divided to three velocity vectors:

$\vec{c}$: the absolute velocity of the flow
$\vec{w}$: the relative velocity of the flow
$\vec{u}$: the circumferential (tangential) velocity of the flow

The velocity vectors form a triangle in which the absolute velocity is the sum of the relative and tangential velocities:

$$\vec{c} = \vec{w} + \vec{u} \tag{32}$$

The absolute velocity is formed of two velocity components that are perpendicular to each other:

c_n: the velocity in the axial direction
c_u: the velocity in the radial direction

The value of the absolute velocity is

$$c = \sqrt{c_n^2 + c_u^2} \tag{33}$$

In the diffuser there is no relative velocity. The flow is slowed and the flow angle is changed due to the increase of the diffuser area and the radius. The volute gathers the flow from the diffuser circumferentially, and the volute area is increased in the proportion of gathered gas, in order to keep the flow velocity constant. Finally, the flow is led out in a conical tube, which ends at a desired diameter and is connected to the piping with for example a flange.

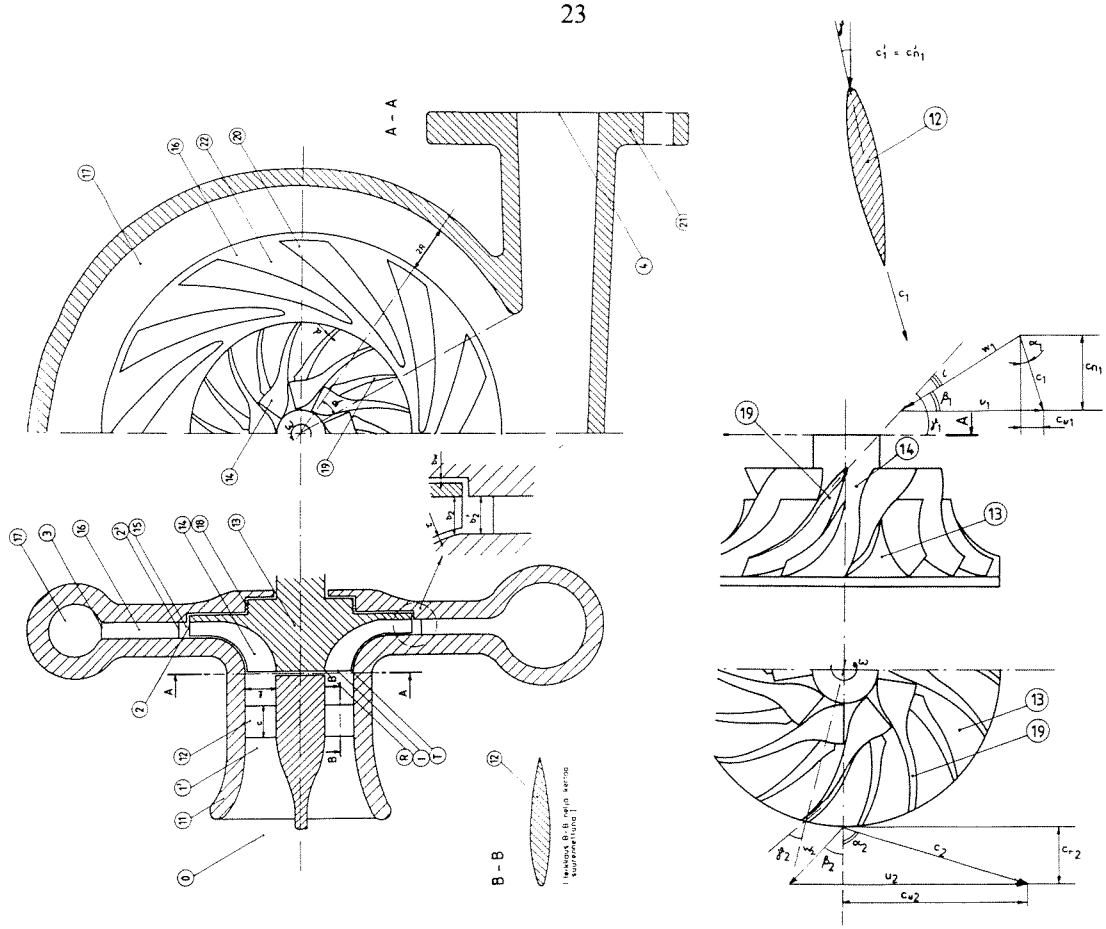

Figure 8. Geometry, velocity vectors and velocity triangles of a radial compressor /Larjola 1988/

The geometry, the velocity vectors and the velocity triangles of a radial compressor are presented in Fig. 8. The rotor blades rotate clockwise and the momentum of the flow is expressed at the inlet and outlet of the rotor with the momentum equation /Dixon 1984/

$$M = F \cdot r_1 + F \cdot r_2 \tag{34}$$

where the force is $F = q_m \cdot c_u$

When we add power $P = \omega \cdot M$ and tangential velocity $u = \omega \cdot r$, we get the Euler turbomachine equation /Dixon 1984/

$$-P = q_m(c_{u1}u_1 - c_{u2}u_2) \tag{35}$$

where the minus sign denotes that power must be put in to obtain compression. When we divide the power with the mass flow q_m, we obtain the specific power P_{spec}, which is an equation that contains only the velocities of the flow

$$-P_{spec} = c_{u1}u_1 - c_{u2}u_2 \tag{36}$$

When the system is assumed to be adiabatic (isolated), and the potential energy change is ignored, the energy balance of the flow system will be according to Eq. (31)

$$h_1 + \frac{1}{2}c_1^2 = h_2 + \frac{1}{2}c_2^2 + P_{spec} = h_3 + \frac{1}{2}c_3^2 + P_{spec} = h_4 + \frac{1}{2}c_4^2 + P_{spec} \tag{37}$$

The *h,s*-chart shows that the work is done only in the impeller, and the enthalpies h_{02} and h_{03} are the same. If the outlet of the compressor is not directed to another compressor, the pressure rise that is calculated from the velocity at the volute exit is lost. Consequently, the actual pressure obtained by the compressor is the static pressure p_4.

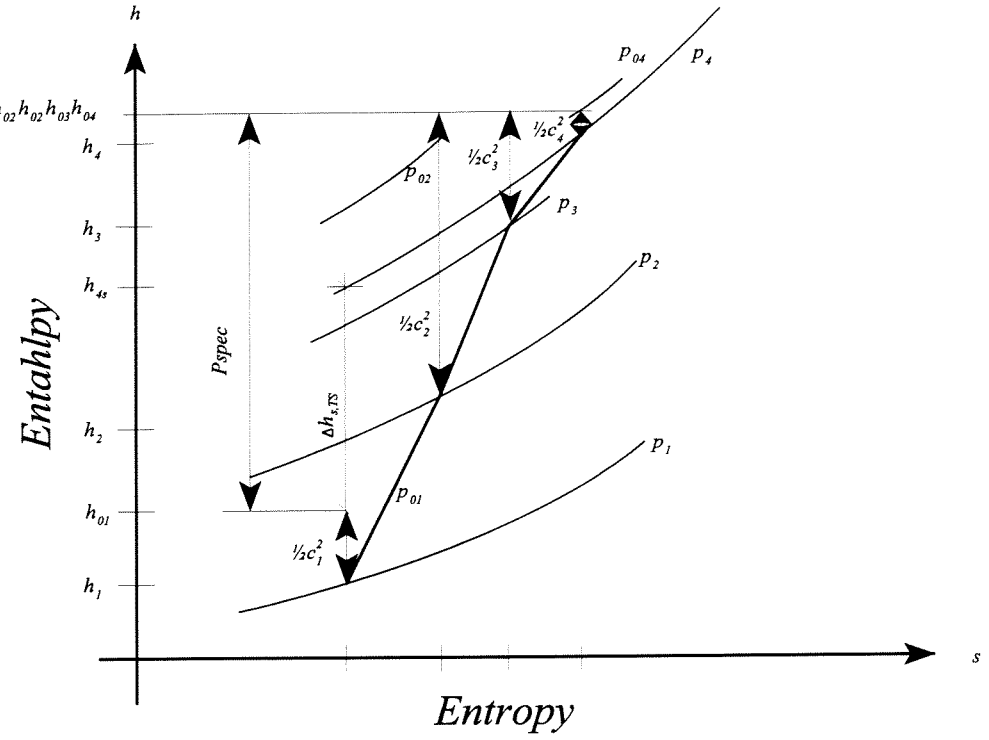

Figure 9. The *h,s*- or Mollier-chart of the compressor

The polytropic process from pressure p_1 to pressure p_4 is defined with the polytropic efficiency, which can be best seen as an angle coefficient in Fig. 5 between compression points 1 and 2. It can be defined as /Larjola 1988c/

$$\eta_p = \frac{vdp}{dh} \tag{38}$$

By integrating and applying the perfect gas definition, Eq. (38) becomes

$$\frac{T_4}{T_1} = \left(\frac{p_4}{p_1}\right)^{\frac{R}{\bar{c}_p \eta_p}} \tag{39}$$

Equation (39) is used to calculate the compression process values.

2.3.2 The efficiency of the compressor

The efficiency of a machine determines its capability to work in comparison with the ideal work. There can be several definitions of the efficiency, and this can cause difficulties, when different machines are compared to each other.

In the *h,s*-chart the phases are defined between the inlet and outlet flanges. The ideal process is defined to be the isentropic process between the total inlet and static outlet conditions. This is chosen, because the kinetic energy at the outlet cannot be used[1]. The real process is between the total conditions at inlet and outlet. This definition will include the aerodynamic losses caused by the turbulence of the internal gas friction and by the friction between the gas and flow passages. Also the pressure drops at the inlet and the outlet are noted.

The ideal enthalpy rise is h_{s4}-h_{01} and the actual enthalpy rise is h_{04}-h_{01}. The efficiency is defined by the isentropic efficiency in the compressor, and the index includes the letters to define the state between the total inlet state and the static outlet state. The isentropic efficiency is thus

$$\eta_s = \frac{\Delta h_{s,TS}}{\Delta h_{TT}} = \frac{h_{4s} - h_{01}}{h_{04} - h_{01}} \tag{40}$$

2.3.3 Off-design capabilities

When a compressor is designed, it is assumed to operate at one point. If the inlet conditions, pressure and temperature, or rotation speed, piping and valve pressure losses etc. vary from this design point, the performance of the compressor changes.

---

1 *It might be argued that in the over pressure cycle most of the compressor outlet speed can be used in the droplet separation channel and could therefore be counted in the ideal process. This would be right if the speed in the channel were not slowed down as much as in test facility I. To keep identical basic definitions to both cycles, this conventional approach was chosen.*

A kinetic compressor operating with constant speed has two limiting points concerning the mass flow. The phenomenon below the minimum mass flow operation point is called stalling, where the flow will be detached from the rotating blade. Typically the unstable flow begins to pulsate in the impeller. The impeller may be destroyed, if the stalling is allowed to continue a longer time. It is absolutely important to operate with mass flows above the stalling point.

When the mass flow is increased enough, the velocity in some point of the compressor reaches the velocity of sound of the fluid. In the compressor this means that the mass flow cannot be increased, and the flow will be choked.

The compressor manufacturers provide compressor maps that are usually tested at essential operation points /Watson and Janota 1982/. It is very common that the abscissa of the map gives the mass flow and the ordinate gives the pressure ratio. There are several constant speed lines from stalling to choking. The efficiency equality curves help detecting of the best operation regions.

The map also includes two very important parameters: the reference pressure and temperature. When the compressor is used with different inlet conditions, the aerodynamic performance differs from that on the map. This will be taken into account with off-design calculation, in which a kinematic similarity is used.

The kinematic similarity requires that the model and the compressor have the same length-scale ratio and the same time-scale ratio. The relations of the velocities are kept equal /Dixon 1984/, and in this way operation of the compressor can be estimated at a large range.

The off-design calculation is very sensitive especially in the sub-pressure cycle, because here the compressor inlet conditions change, and the interpretation of the compressor map becomes more complex. In normal cases the map mass flow is calculated from the actual mass flow with the equation /Glassmann 1972/, /Watson and Janota 1982/

$$q_m = q_{m,des} \frac{p}{p_{des}} \sqrt{\frac{T_{des} R_{des}}{TR}} \tag{41}$$

The map constant speed is calculated from the actual speed

$$N = N_{des} \sqrt{\frac{TR}{T_{des} R_{des}}} \tag{42}$$

2.4 Turbine

The turbine design is very critical in a reversed Brayton cycle, because the power generated in the turbine decreases the amount of electrical power needed in the motor. A turbine operating with a good efficiency can be the factor that helps cross the threshold of the economical utilization of the cycle.

We have chosen two main types of turbines: an axial and a radial inflow turbine. The choice of the turbine type depends on many things, which can be the manufacturing costs, the flow paths of the cycle, the rigidity of the shaft, the leakage questions, the foreign particles in the flow etc. The axial turbine is commonly used in the commercial applications of medium or large size turbomachines, but in small machines there are more often radial inflow turbines.

The flow in the axial turbine is less complex than the flow in the radial turbine, and therefore one can achieve higher efficiencies. Also foreign particles that in humid air expansion coagulate with water droplets run through the axial turbine without greater problems. This can be a very serious erosion problem in the radial inflow turbine, because the flow direction is inwarded. There can be a situation, where the flow forces thrust the foreign particles to swirl into the rotor impeller passage. The problem arises from the fact that the centrifugal force pushes the particles back out from the impeller. If the particles are stuck to circulate back and forth between the impeller and the stator, there will very rapidly be serious erosions, especially in the rotating impeller blades / Wilson 1991/.

When the humid air flow expands through the turbine, part of the water vapour condensates to water droplets or sublimates to ice particles. When this occurs, the expansion process becomes more complex to calculate.

The blades in a high efficiency axial turbine can be very complicated in shape. Depending on the manufacturing methods, the costs of the axial turbine cascades are often higher than with the radial turbine.

The flow enters the turbine first through the stator, in which the pressure is turned to speed. In the axial turbine the stator is an annulus shaped blade cascade, and in a radial turbine the blades are on an annulus ring. The axial stator blades are 3-dimensional and they together form the blade cascade. The radial stator blades are 2-dimensional on a ring and they form separate nozzle passages for the flow.

In the axial turbine the rotor cascade resembles the stator cascade very much, but in the radial turbine the impeller wheel differs considerably from the stator. The impeller blades conform passages that are 3-dimensional and in which the flow is turned 90 degrees.

With the help of a diffuser, the main part of the kinetic energy after the rotor is turned to pressure to prevent it from dissipating to heat.

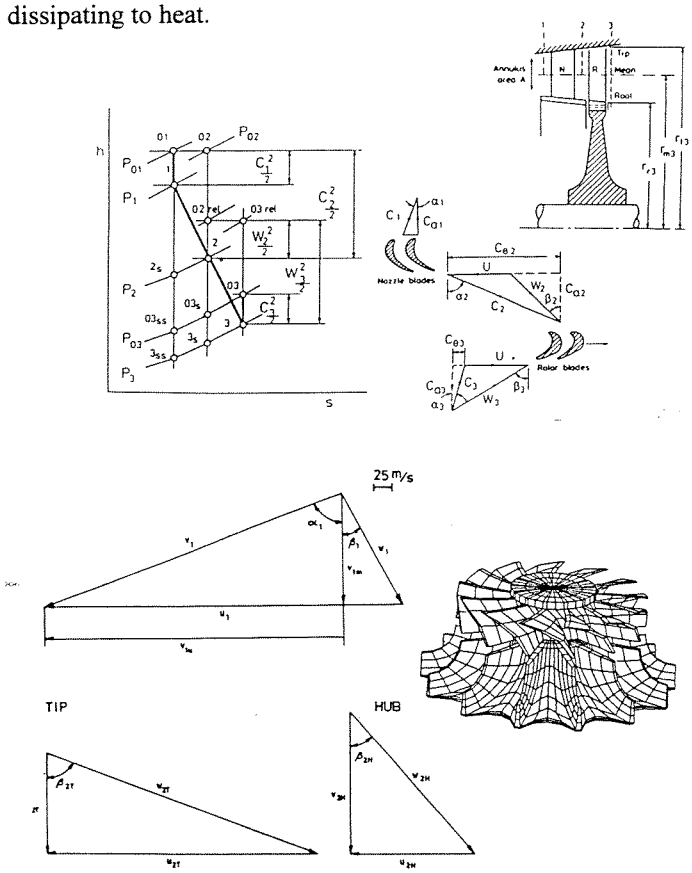

Figure 10. Axial turbine geometry and velocity triangles (top) and radial turbine geometry and velocity triangles (bottom) /Larjola et al 1987/.

2.4.1 Velocity triangles and efficiency of the turbine

The turbine velocity triangles in Fig. 10 resemble those of the compressor very much. From the triangles, the enthalpy drop and the power output can be calculated as described in Chapter 2.3.1. In the momentum equation either the order of the triangle parameters are changed or the sign of the specific power is switched

$$P = q_m(c_{u1}u_1 - c_{u2}u_2) \tag{43}$$

Particularly in the axial turbine, where the hub-tip-ratio λ is large enough (λ > 0.85), the velocities and the fluid parameters can be assumed to be constant. This means that the radial equilibrium can be neglected and the blades can be straight, and the streamline radius is constant. This simplifies the equation to

$$P = q_m \, u \, (c_{u1} - c_{u2}) \tag{44}$$

When the system is assumed to be adiabatic and the potential energy change is ignored, the energy balance of the flow system becomes slightly different as for the compressor

$$h_1 + \frac{1}{2}c_1^2 = h_2 + \frac{1}{2}c_2^2 = h_3 + \frac{1}{2}c_3^2 + P_{spec} \tag{45}$$

There is no work in the nozzle and $h_{01} = h_{02}$.

The isentropic and polytropic efficiencies are defined in the same way as in the compressor, but because the losses increase entropy, the real values are larger than in the ideal process. Therefore, the isentopic efficiency of the turbine is

$$\eta_s = \frac{\Delta h_{TT}}{\Delta h_{s,TS}} = \frac{h_{01} - h_{03}}{h_{01} - h_{s4}} \tag{46}$$

The efficiency of the turbine is defined in contrast to the isentropic, ideal process and as in the compressor, the isentropic process is between the total inlet state and the static outlet state. The kinetic energy is assumed to be lost after the turbine. The real process is defined between the total inlet state and the total outlet state.

2.4.2 Condensing and the *h,s*-chart of the turbine

The expansion process differs physically from compression, when the water vapour in the humid air begins to condensate. In the thermodynamic equilibrium of the flow, the water vapour pressure in humid air cannot exceed the pressure of saturated water vapour in corresponding temperature.

During the expansion in the turbine, the temperature (and the corresponding saturated water vapour pressure) decreases more rapidly than the pressure of the water vapour component in the humid air. This means that part of the water vapour condenses to water or sublimes to ice ($T < 273{,}16$ K). During this phase shift the water vapour delivers heat that corresponds to the difference between the vapour and liquid enthalpies. If the water vapour sublimes, this difference is between the vapour and

solid enthalpies. Due to this internal heat delivery, the temperature of the fluid after the expansion is higher than it would be without this partial vapour phase change.

Condensation is theoretically defined to be either homogeneous or heterogeneous. Homogeneous (also called spontaneous) condensation occurs due to the random agglomeration of vapour molecules in totally clean flow conditions, and is believed to be the major condensation process. Heterogeneous condensation occurs around foreign solid particles and on the walls of the flow channel. This nucleation phenomenon is believed to have only a small influence in the condensation process /Moore and Sieverding 1976/.

Homogeneous nucleation is a very sensitive process and laboratory results have shown that accurate prediction of droplet size distributions is very difficult. Also, the heat transfer speed in the nucleation area is restricted by many factors. Typically the whole process takes only 10-20 μs in a shock-like front, and the temperature of the different fluid components differ, which in return causes an entropy rise in the mixture. Furthermore, the condensing is not immediate /Moore and Sieverding 1976/.

In vapour turbines, depending on the rate of expansion and the pressure, the vapour becomes supercooled by 30-40 °C before condensing. Nucleation formation and growth are prevented by surface tension. The droplets are very small and their surface-to-volume ratio is very high (droplets are in clusters of less than 20 molecules /Young 1989/), and the nucleation is blocked by the free energy barrier. This supercooled fluid is in a non-equilibrium state, and in subsonic flow the condensation causes a small drop in the pressure.

Subcooling is defined in the steam turbine with the Wilson point, which is the maximal supercooling temperature before condensing starts. If there also occurs heterogeneous condensation (dust, ions, salt) supercooling is smaller, and condensing can even start just after crossing the saturation line. This condensation is obvious if there are foreign particles. The smaller the particles, the less supercooling /Moore and Sieverding 1976/.

Expansion calculation during operation around the saturation zone is based on a quasi-static expansion, in which the system after the turbine is in thermodynamical equilibrium. The state parameters are at every moment defined by the equation of state, and there is no supercooling in the vapour.

In the theoretical expansion process with humid air there exists a four-phase zone /Sahlberg 1988/ that is due to the fact that the triple point of humid air is not a discrete point, but a zone restricted by the isotherm 0.01 °C. The zone is wedge shaped, and the tip is on the cutting point of the phase

boundaries of vapour/water and vapour/ice. In this region there are four components and three phases; air, water vapour, water and ice. Furthermore, at the isobars the amounts of dry air and water vapour are constant. When the expansion state is above this zone under the saturation line, the fluid contains two components (air and water) and two phases (gas or vapour and liquid). In manual calculation with the *h,s*-chart this four-phase zone is easily observed, but due to the narrow area, the numerical approach requires closer attention.

There has been very little research done on humid air water vapour condensation in expansion. Some approaches have been noted in /Heikkinen et al 1992/ and /Ling and Li 1988/, but the methods differ from the approach presented below. In the calculations of this thesis it is assumed that all the water exists as water vapour, which means that there are no water droplets in the inlet flow. The default parameters in the turbine expansion are the turbine inlet pressure and temperature (both stagnation and static), the turbine isentropic efficiency, the static pressure after the turbine and the relative humidity. From this data the humidity and stagnation enthalpy can be directly calculated. The calculation procedure requires several iteration loops within each other:

- the temperature after the expansion T_{3ss} is first guessed with the help of the isentropic equation, where the specific heat capacity ratios are calculated at the inlet mixture
- in this temperature the corresponding pressure of saturated steam p'_{h3s} is calculated, and from this we get the humidity ω'_{h3s} that corresponds to 100% relative humidity. If the humidity is greater than the humidity at the inlet ($\omega_{h1} < \omega'_{h3s}$), there occurs no condensation in the turbine. If the humidity is smaller, part of the water vapour condensates to water.
- the total mixture specific entropy change is calculated. The separate component entropy change is calculated, and the possible alteration in the partial pressures depending on the mole fractions in the gas phase is observed. If the total specific entropy change does not equal nil, the temperature guess is corrected. The course is obtained from the specific entropy change. If it is negative, we have to increase the temperature and vice versa.

When the iteration converges with desired accuracy, the isentropic enthalpy h_{3ss} after the turbine is calculated from the temperature T_{3ss} and humidity portions. The actual enthalpy h_{03} is calculated with the help of the efficiency. Also this enthalpy calculation has iteration loops that resemble those above.

The method can be illustrated with the *h,s*-chart of humid air. The calculations with the chart are hampered with the fact that the *h,s*-chart of humid air is dependent on the inlet air consistency. If

humidity in the inlet changes, another *h,s*-chart with different water vapour mass portion in the air should be used.

2.4.3 Off-design performance

The off-design performance of the turbine can be evaluated with the blade speed ratio, ν, and the nozzle flow approximation.

The blade speed ratio is physically defined with the help of dimensional analysis /Glassman, 1972/

$$\upsilon = \frac{u}{\sqrt{2\Delta h_{sTS}}} \tag{47}$$

For the first theoretical calculations the flow can be considered isentropic and the turbine reaction level to zero. Then the isentropic total-to-static efficiency can be derived to be only a parabolic function of the blade speed ratio /Glassman 1975/

$$\eta_{stTS} = 4\upsilon\sin(\alpha_2) - 4\upsilon^2 \tag{48}$$

Though this equation is achieved with considerable generalizations, it gives good results in actual turbines. The maximal value of the efficiency is derived for the chosen outlet angle from Eq. (67). When the reaction level is increased, the maximal blade speed ratio increases. In turbo chargers with wide operational range, the blade speed ratio is also dependent on the pressure ratio /Watson and Janota 1982/.

The blade speed ratio is a very good tool to make preliminary calculations of the turbine dimensions. It is then easy to fit the turbine to the other components of the reversed Brayton cycle. When the turbine inlet conditions and the pressure ratio are known, the isentropic enthalpy and the mean circumferential speed can be calculated. The rotational speed is known from the compressor calculation, and the mean diameter is found. The tip and hub radius can be calculated from the continuity equation.

The throat capacity tells the mass flow dependency of the rotational speed, the pressure ratio and the fluid inlet conditions. This is applied with a semi empiric nozzle flow approximation that considerably simplifies calculations. In the first test facility it also proved to be quite exact. The approxima-

tion was first evaluated by Saint Venant /Anderson 1990/.

$$q_m = \frac{Ap_3}{\sqrt{T_3}} \sqrt{\frac{2\bar{c}_p}{R^2}\left[\left(\frac{p_4}{p_3}\right)^{\frac{2\,(\bar{c}_p - R)}{\bar{c}_p}} - \left(\frac{p_4}{p_3}\right)^{\frac{2\,\bar{c}_p - R}{\bar{c}_p}}\right]} \tag{49}$$

In the iterative off-design calculation, the pressure ratio is preliminarily determined by the compressor calculations. This pressure ratio is then used to calculate the turbine mass flow (pressure losses and water separation included), which in turn is again used to calculate the compressor pressure ratio. The calculation is continued until the pressure ratios and mass flows are equal, both in the turbine and in the compressor.

2.5 High speed motor

The reversed Brayton cycle needs power supplied through rotational work. In a high efficiency turbomachinery the power required by the cycle can be reduced to less than a half of the compressor power. The rotational work can be produced in many ways.

The electric motor has good advantages that have enlarged the use of motors in numerous places in the world. The size of the motor is rather compact and electricity is properly available in many places. The electric machine technology has developed greatly during the last century, and the drive can be easily connected to turbomachinery. There are large amounts of commercial products from 1200 MW power production steam turbines to 1000 W vacuum cleaners.

When conventional electric machines are used, the rotational speed is set to the net frequency, in which 50 Hz corresponds 3 000 rpm. In the Brayton cycle the compressor and turbine rotational speeds are usually much higher. The processes studied in this thesis concern rotational speeds over 10 000 rpm, and therefore use mechanical means (gear or belt drive) have to be used to change the speed of the conventional drive. Although this can be done, the efficiency can be very low due to the high losses.

During the last two decades, the development of the technology to control the speed of electric machines electrically has been quite rapid. Frequency inverters can vary the speed of the conventional machines, but they can also be used to supply a higher frequency to the machine. This way it is possible to have higher rotational speeds in the electric machine.

The development of the power semiconductors has advanced so that in 1985 the power-speed-limit of the commercial inverters was 20 kW / 30 000 rpm, in 1990 it was 100 kW / 30 000 rpm and in 1995 it reached 100 kW / 150 000 rpm.

For special purposes, the reversed Brayton cycle could use an air turbine drive, in which pressurized air drives a separate air turbine. The air turbine would be mounted to the same shaft with the other turbomachinery. This kind of technology is used in dental drills.

2.6 Water droplet separator

The reversed Brayton cycle operation often requires that the condensed water be removed from the cycle. This is usually an optimization problem, because, especially in the drying and heat pump applications, it is essential for good cycle characteristics that the energy and pressure losses are kept small.

The basic operational idea in a flow separator is to use centrifugal forces to separate the heavier water droplets from lighter humid air. Following separators were considered:
- vertical cyclone separator.
- corrugated plate separator.
- mesh pad mist eliminator or knitted wire mesh separator.

2.7 The reversed Brayton process and high speed technology

It is a demanding task to design working, high efficiency machinery that includes turbomachinery, high speed electric machinery and long operational life bearings. The design parameters have to be chosen from a wide range, and they have meet high demands to give the process the possibility to perform at a high efficiency.

The basic requirement for the high cycle efficiency is to have high efficiency turbomachinery. Usually this means rotational speeds that exceed the synchronic speed. For example the speeds of vehicle turbo chargers are often in the range of 100 000 rpm. This is over 30 times the synchronic speed, and it is almost impossible to realize the electric drive with a conventional gearing system.

In this research we have decided to use conventional kinetic turbomachinery to achieve both the compression and expansion processes. The high speed electric motor and the turbomachinery are

directly coupled on the same shaft without any gears and clutches. The frequency change of the supply from the electric net (50 or 60 Hz) is made with the means of an electric inverter. The high speed technology involves a totally new construction of the main process equipment, which in many cases requires a new approach to the system. The advantages from this technology are:

- maintenance and oil-free operation. There is no gearbox, and the oil-free fluid or magnetic bearings have a long lifetime. These bearings operate without mechanical contact between the bearing and the rotor.
- high efficiency. The turbomachinery, high speed inverter and electric machine design includes internal adaptation that ensures that all individual components are working with high efficiency. The research on electric machines at LUT and HUT indicates that high speed electric machines can be designed with significantly high efficiencies.
- small and compact size. When the rotational speed is increased, the size of the machinery is decreased, often dramatically. The outer diameter of the compressor, the turbine or the pump disc is inversely proportional to the rotational speed. The volume of the electric machine is inversely proportional to the speed in the 3rd power.
- low specific price. The economical studies show that the specific price of the machinery decreases, when the rotational speed increases at the same manufacturing levels. One main reason is the reduced size and volume of the machinery.

The use of an inverter makes it possible to control the rotational speed to obtain the optimal operation of the process. This advantage does mean an increase in the price of the machinery but this investment is obligatory to realize the high speed.

The inverter supplies the motor with the high frequency current that generates the high speed rotation. This means the use of powerful transistors, but there have been very few commercial inverters to give 100 A, 800 Hz current that would rotate a 50 kW motor with the rotational speed of 48 000 rpm. Because of the high production costs and the very low demand of today, the industry has not been interested in developing such machines, although there have been theoretical ideas to exploit the reversed Brayton cycle.

In the 90s, the use of inverters in Finland has shown definite increase, which explains why the rapid development of power transistors has made a breakthrough in the control of electrical machines.

3. THE PROCESS CALCULATION PROGRAMME - BCD

In the early stage of the research, the process calculations proved to be very iterative and time consuming to accomplish the required accuracy. The researchers, and later the product development and marketing personnel, could benefit from a reliable process calculation programme that provides explicit data about the performance and the components of the machine.

The Brayton Cycle Design (BCD) programme gives a realistic view of the most significant process parameters and coefficients. Especially the analysis of the phenomenon of water vapour condensing to water or sublimation to ice is very important.

The programme was generated in Turbo-Pascal[1] computer language, and was based on the equations and fluid property correlation functions mentioned in Chapter 2.

Following simplifications are used in the calculations:

- the system is assumed to be adiabatic. This means that there is no heat transfer to the surroundings. This is a common practise, when the temperature differences are moderate as here. This assumption can be confirmed with a thermal insulation of the machinery as was done with the test facilities in this thesis.
- the power of the cooling is omitted. The cooling construction is very dependent on the machine and the distribution of the losses. Therefore the general calculation of the power is complicated. The cooling construction of Test Facility II was ca. 10% of the total power, Fig. 39.
- the flow is assumed to be one-dimensional, steady-state and homogenous. The water vapour condensing in the turbine can cause errors, but the errors are mainly included in the efficiency calculation. The turbine performance in the test facilities did not significantly suffer from the condensation.

3.1 The input data

The programme needs the following input data:

- the process connection that will be used. The connection is defined by a single parameter.
- the state values of the humid air: temperature, pressure and relative humidity
- the pressure ratio of either the compressor (over-pressure connection) or the turbine (sub-pressure connection)

---

[1] *Copyright of Borland International, Inc*

- the mass flow of the humid air
- the pressure drops between the calculation points (in the heat tubes, in the droplet separator, in the inlet/outlet piping)
- the isentropic, mechanical and electrical efficiencies
- the droplet separation efficiency

If the user gives the rotational speed of the machine, the programme calculates the turbomachine specific speeds.

3.2 The calculation routines

From the input data, the programme calculates the process iteratively. The different calculation points are executed in the calculation procedures according to the process connection. The state values are calculated with the help of fluid property correlation functions. Several extra routines have been developed to ease the basic calculation of special cycle procedures: drying, coefficient exploration, etc.

The calculation routines are explained below for a simple over-pressure cycle, connection number 1 in Fig. 15. The calculation of a sub-pressure cycle differs only slightly from this. With a more complicated heat exchanger connection the calculation has to make iterative calculations that may involve the whole process.

Compressor

The inlet conditions, the pressure drops at the inlet, and the isentropic efficiency are used to calculate the temperature at the outlet from. Eq. (39) iteratively. The humidity is constant, because the temperature of the fluid and the vapour pressure of water increase.

Heat exchanger

The heat exchanger calculation uses the continuity and energy equations to balance the enthalpies and mass flows. In some regenerative connections, the heat exchanger calculation actively tests that the temperature difference is not lower than allowed between the primary and the secondary side.

Turbine

The turbine pressure ratio is known from the compressor ratio and pressure losses. Equation (49) is used to calculate the approximate flow area of the turbine. The condensation is calculated with the routines explained on page 31.

Off-design

Normally the process is designed to operate at the design point, but the off-design calculation enhances the prediction of the actual machinery operation. This is important once a Brayton machinery has been designed or made, and this machinery is considered to operate at different process conditions. The operation will be determined by the mutual operation of the turbine and compressor.

The user can use a particular compressor map that can be fed to the programme, or use the relative compressor map of the programme. The turbine and compressor operations are calculated with the principles explained in Chapter 2, and often require some iteration loops to match the mass flow and power balances.

3.3 The rapid interactive environment

The programme is based on the Rapid Interactive Environment (RIE) that makes it possible for the user to run the programme with only a few keystrokes, and the user can be acquainted with the programme structure in a short period. Although the programme is easy to use, the user has to understand the process principles to be able to get all the benefits of the programme.

The programme always starts (for a new user) with an info screen collection. There is a total of five info screens that can be viewed in a sequel, and the main features of the programme are explained in these screens. The programme then starts with a default input data, and the results are printed on the screen.

The user can have up to nine different windows during the same session. This has proved to be very useful, when the influence of different input data is compared to the Brayton Cycle process behaviour.

Whenever the user has any doubts that there is some misunderstanding, the on-line help can be looked up on the screen, or the user can glance through the info pages.

The default process calculation is chosen to give instant understanding about the process calculation for the new user. When the results are on the screen (Fig. 11), it is rather easy to employ one's own process parameters, compared with feeding them separately without any knowledge of the calculation procedures.

```
Data  Input  Efficiencies  PressLoss  HeatExch  Optimization  OffDesign
            Reversed Brayton Cycle in over pressure process mode | ©LUT&HST
 <-■->                          NoName.rbc                        Window: 1

 Cycle points                   T        h        p        wi        wh      Fii
                              [ °C ]  [kJ/kg]  [ kPa ]                        %
 0 - Cycle inlet               14.0     24.1    100.0    0.9961    0.0039   39.0
 1 - To Compressor             14.0     24.1     99.5    0.9961    0.0039   38.8
 2 - From Compressor           64.5     75.4    160.0    0.9961    0.0039    4.1
 3 - From heat exchanger       32.0     42.3    157.5    0.9961    0.0039   20.6
 4 - From turbine              -0.1      9.4    101.5    0.9963    0.0037  100.0


 Compressor power      Pc  =   1.13 kW compressor isentropic efficiency = 0.823
 Turbine power         Pt  = 725.81 W  turbine isentropic efficiency    = 0.906
                                       mechanical efficiency           = 0.948
 Motor electric power  Ps  = 438.03 W  motor electrical efficiency      = 0.970
 Refrigeration power   Pre = 323.58 W  refrigeration COP               = 0.739
 Compressor mass flow  qm  =  0.022 kg/s   Turbine mass flow qm =  0.022 kg/s
 Rotational speed      N   =  145728 rpm
 Condensate mass flow  qv  =  0.014 kg/h   Vaporizate power Pva =    0.0 W
 Droplet separation    Ds  = 100.00 %      Specific energy  Psm = 31.56 kWh/kg
 Impeller diameter     Dko =     35 mm     Impeller diameter   Dtu =     30 mm
 Compressor specific speed=   0.70        Turbine specific speed  =   0.76
F1 Help  F2 Save  F6 Graf  F9 Info  F10 Run  Alt+F10 Exit          | 18. 7.1994
```

Figure 11. The BCD-programme screen output at default calculation

The first and last lines are the menu lines. The second line describes the process mode. There is a small RBC-logo in the beginning of the 3rd row to inform that the results are matched to the input data. The logo will disappear when the data is changed by the user. On this line there is also the name of the input file that has the **.rbc**-extension as a default to separate the file from other files in the computer's directory. The last information on this line is the window number.

The rest of the screen is dedicated to the process parameters. First there are the process parameter data in the main points of the cycle. These parameters include the temperature (T), enthalpy (h), pressure (p), the mass fractions of dry air (wi) and water vapour (wh), and the relative humidity of the flow (Fii).

The most valuable calculation data are the component powers and efficiencies, the coefficient of the process and the mass flows. With this data the realistic process flow is possible.

From this screen the user can begin to build a new cycle calculation. The input parameters can be changed in the *Input* Menu that is revoked just by pressing the key I (The letter is highlighted on the first line called the Menu Line). As seen in Fig. 12, only a few parameters of the process fluid values need to be known to make the calculations. In the Input menu the user presses the appropriate highlighted letter, and the programme opens a data input window, in which the user can give a new value to the parameter.

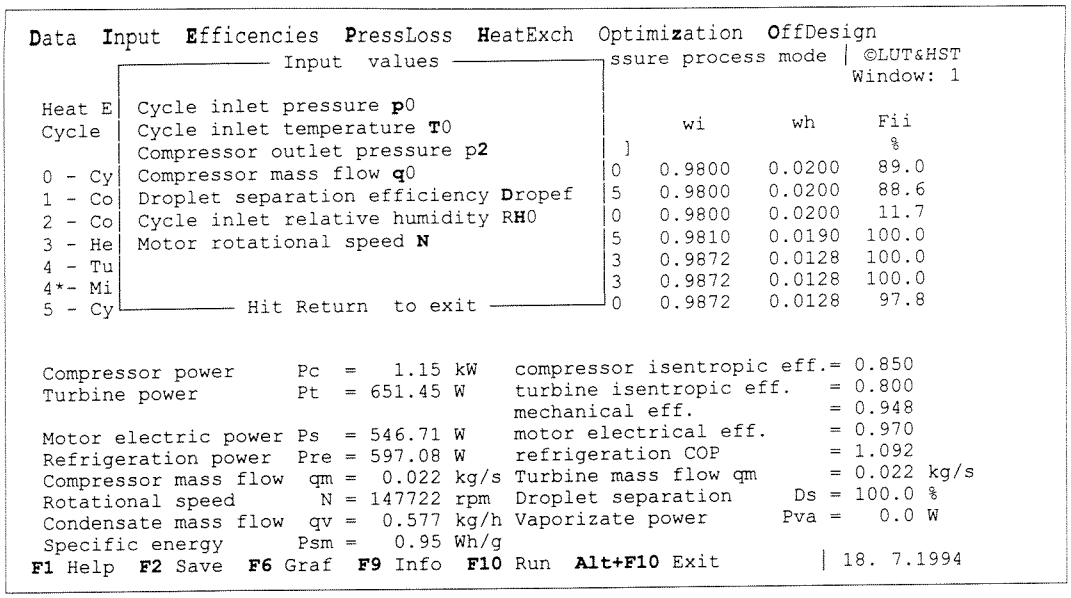

Figure 12. The BCD-programme input menu .

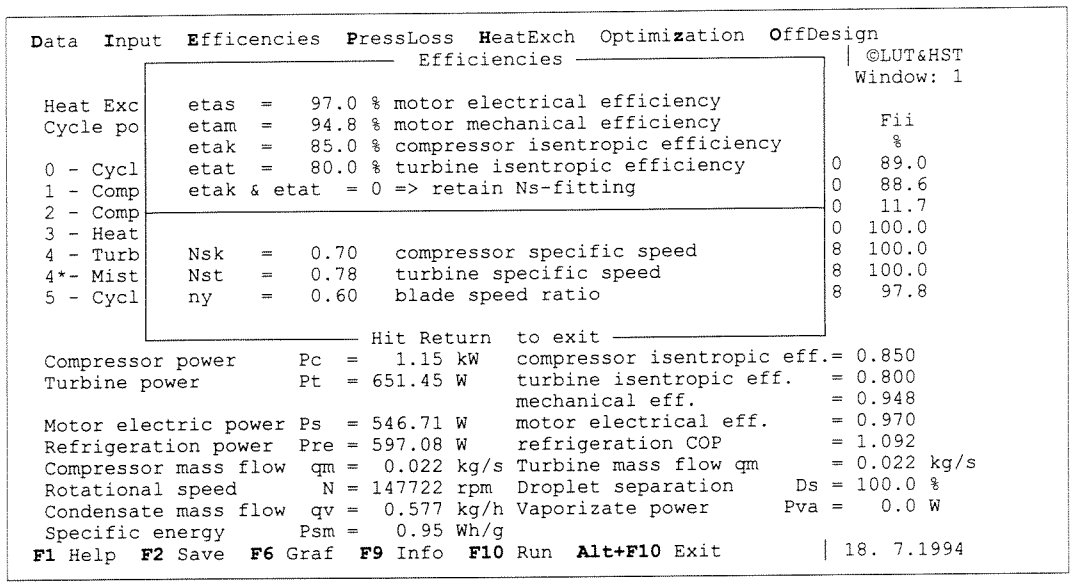

Figure 13. The BCD-programme efficiencies menu.

In the *Efficiencies* Menu (key E, Fig. 13), the efficiencies of the turbomachinery can be changed. The default parameters in the efficiencies are already quite near the actual values. They have been chosen into the programme by using the experience achieved during the prototype testing. This menu also states the main turbo component characteristics. If the turbine or the compressor efficiencies are chosen to be zero, the programme calculates the efficiency according to the speed, the pressure ratio and the mass flow. It should be noted that the programme includes electric and mechanical losses to the calculations.

The pressure losses (key P, Fig 14) are very important in the accurate calculation of the process. The losses are given only to those parts of the process that are currently chosen.

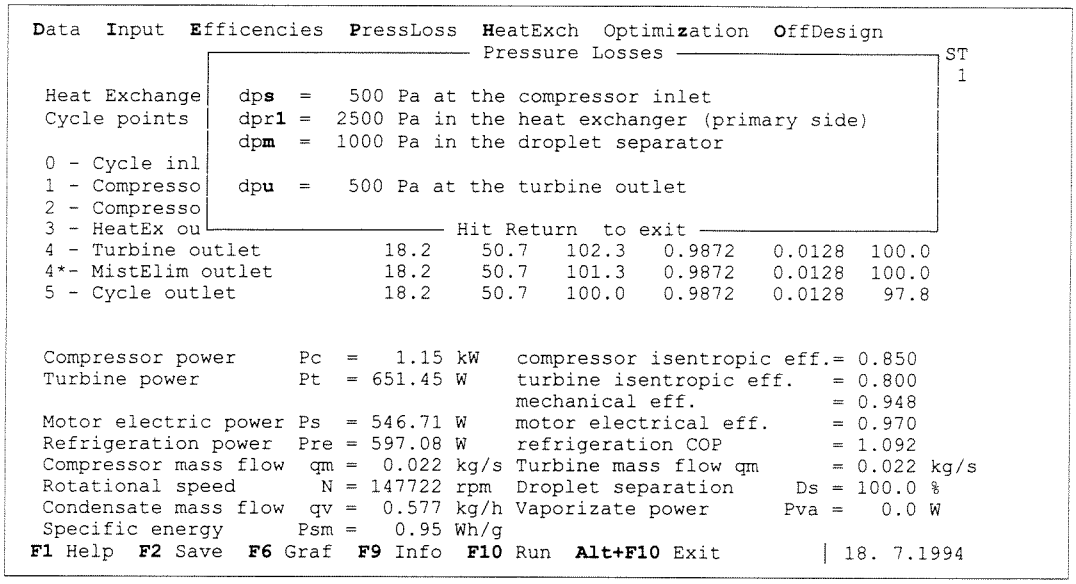

Figure 14. The BCD-programme pressure loss menu.

The use of heat exchangers diversifies the process calculations considerably. The programme can calculate up to nine different heat exchanger connections. There are three main connections for the over-pressure cycle, and six main connections for the sub-pressure cycle (Fig. 15).

The heat exchanger (key H, Fig 16) connections can be chosen from these nine different compositions. In some options the programme asks the outlet temperature of the heat exchanger. In such cases the heating/cooling fluid can be taken from outside the actual process, it can be for example could be running cold water or waste heat from an industrial process. In some cases the process uses internal heat exchange, and then the programme asks for the temperature difference, *dT*, of the heat exchanger. The main connection parameters can be graphically checked with the key F4.

From the *Data* Menu (D-key), the user can open new files to new windows, save the current input data into a new file or in the current file, close the current window, print the output data (as on the screen) to a file or to the printer. If the user has chosen a special compressor, the map with the operation point can also be printed on a laser printer.

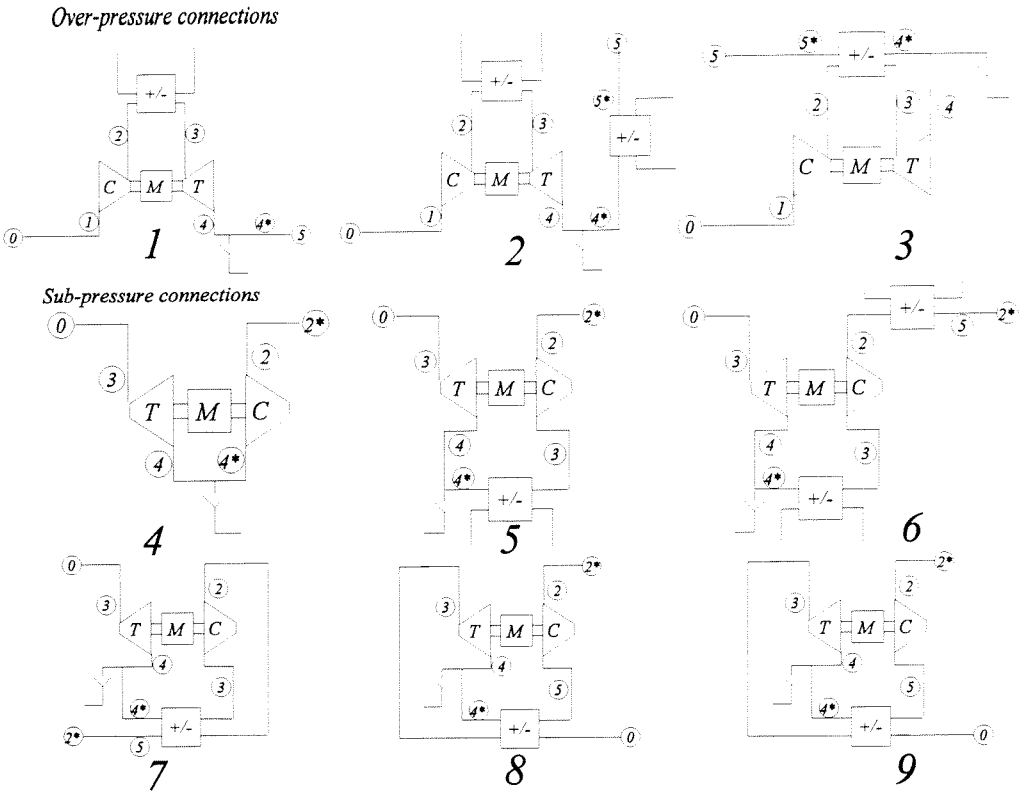

Figure 15. Heat exchanger connections.

```
Data  Input  Efficencies  PressLoss  HeatExch  Optimization  OffDesign
                          Heat Exchangers                          HST
      Current connection number 4                                 : 4
 Heat                   Overpressure connections
 Cycle  1 Primary HE loop between compressor and turbine, give T3
        2 Primary HE loop between compressor and turbine, give T3
 0 - C    Secondary HE loop after turbine, give T5
 3 - T  3 Primary HE loop between compressor and turbine, give T3
 4 - T    Secondary HE loop after turbine, give dT and program gets T5
 4*- M                  Sub pressure connections
 2 - C  *4 No heat exchangers, only turbine, droplet sep. and compressor
 2*- C  5 Primary HE loop between turbine and compressor, give T3
        6 Primary HE loop between turbine and compressor, give T3
          Secondary HE loop after compressor, give T5
        7 Primary HE loop between turbine and compressor, give T3
 Compr    Secondary HE loop after compressor, program gets T5
 Turbi  8 Primary HE loop before turbine, give T3
          Secondary HE loop after compressor, program gets T5
 Motor  9 Primary HE loop before turbine, give dT
 Heati    Secondary HE loop after turbine, program gets T3 and T5
 Turbi                                                        kg/s
 Rotat                  Hit Return to exit                      %
 Condensate mass flow  qv =  1.165 kg/h Vaporizate power      Pva =   0.0 W
```

Figure 16. The BCD-programme heat exchange menu

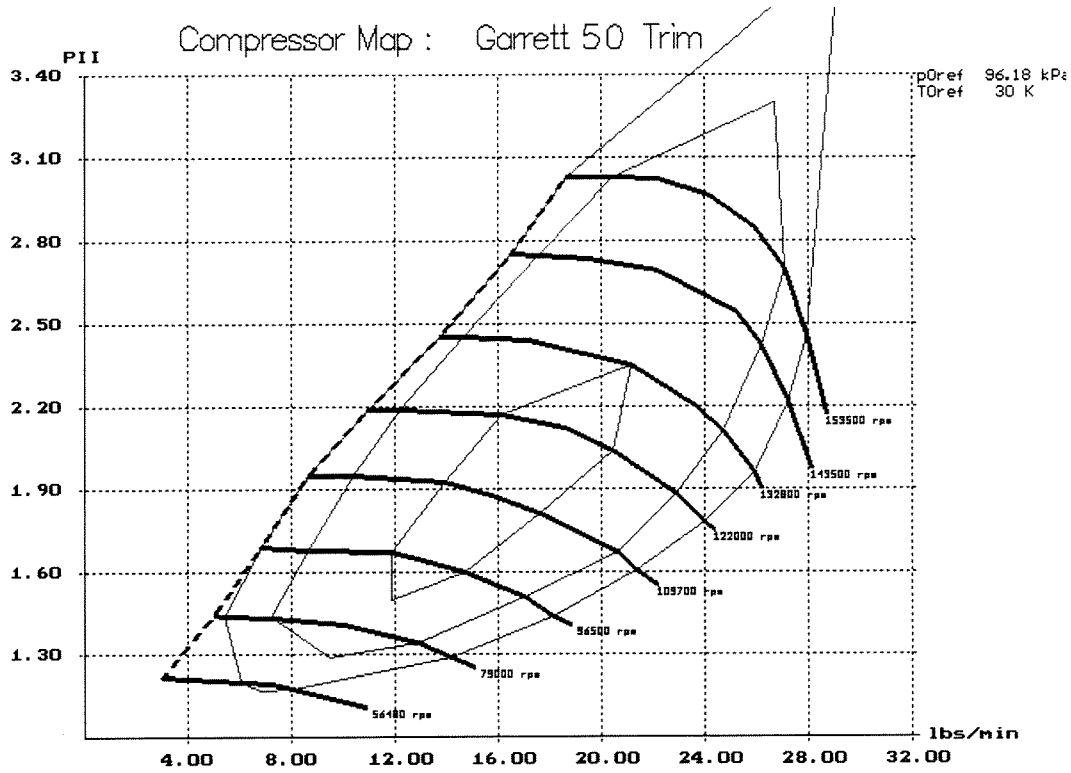

Figure 17. The compressor map as illustrated on the screen.

4. TEST FACILITIES

The theoretical calculations implicated that there could be commercially significant applications using the Brayton cycle with high speed technology. Therefore, the building of test facilities was a vital part of this research. Two test facilities were built and tested to demonstrate the theory.

4.1 Test facility I

In the early stage of the design, it was clear that a prototype was needed to verify the process calculations of the Reversed Brayton Cycle and its components. The first facility was based on the Reversed Brayton Cycle with partial high speed technology. The goals of the first facility (1992-93) were to verify the calculation model and to check the results of the computer programme in favourable operation regions. It was very important was to get results concerning the condensation phenomenon and its effect on the process parameters. The main components were decided to be built from readily available components.

The largest turbomachinery manufacturers were contacted for offers for the turbomachinery parts — the radial compressor and the axia turbine — which would finally determine the drive device. The offers fixed two things very clearly:

1. There were no offers for the axial turbine, although one manufacturer informed of a suitable turbine, but was not interested in giving an offer.
2. The rotational speed of the compressor that would give a good efficiency would be around 15 000 to 30 000 rpm

Because of the latter point, a choice had to made between air turbine drive, belt drive, gear drive and high speed drive. The closer examination of mechanical construction sketches showed that the last alternative was most promising. With cooperation between ABB Motors and ABB Strömberg Drives a slightly modified conventional electric motor and frequency inverter was designed to accomplish the desired power and rotational speed.

The first test facility was tested in the following reversed Brayton cycle process connections:

1. Sub-pressure connection that functions as an air dryer in a heat pump mode. The humid air is first expanded to sub-pressure, then part of the condensated water is removed in the droplet separator, and finally the compressor compresses the remaining air to the atmosphere pressure.

In the first connection, the operational conditions of the test facility were designed to be close to those of commercial air driers. The turbine outlet temperature was chosen to be above the freezing point.

The process design values calculated with the BCD-programme are shown in Fig. 18.

```
            Reversed Brayton Cycle in sub pressure process mode  □ ©LUT&HST
<-■->                        RBC1DES1.RBC                          Window: 1
Heat Exchanger connection number 4
Cycle points                    T       h       p       wi       wh      Fii
                              [ °C ]  [kJ/kg] [ kPa ]                    %
0 - Cycle inlet                20.0    49.6   101.0   0.9884   0.0116   80.0
3 - Turbine inlet              20.0    49.6   100.7   0.9884   0.0116   79.8
4 - Turbine outlet              6.6    27.9    73.0   0.9916   0.0084  100.0
4*- MistElim outlet             6.6    27.9    72.0   0.9916   0.0084  100.0
2 - Compressor outlet          44.5    66.4   101.4   0.9916   0.0084   14.5
2*- Cycle outlet               44.5    66.4   101.0   0.9916   0.0084   14.5


Compressor power      Pc  =  14.96 kW   compressor isentropic eff.= 0.758
Turbine power         Pt  =   8.46 kW   turbine isentropic eff.   = 0.820
                                        mechanical eff.          = 0.948
Motor electric power  Ps  =   7.53 kW   motor electrical eff.     = 0.910
Heating power         Phe =   6.5  kW   heating COP               = 0.858
Turbine mass flow     qm  =  0.390 kg/s Compressor mass flow   qm = 0.389 kg/s
Rotational speed      N   =  20200 rpm  Droplet separation     Ds = 100.0 %
Condensate mass flow  qv  =  4.575 kg/h Vaporizate power      Pva =   3.1 kW
Specific energy       Psm =   1.65 Wh/g
```

Figure 18. The sub-pressure connection design values.

2. Over-pressure connection that functions as a heat pump. The humid air is first compressed to over-pressure, then cooled in a heat exchanger and after that the cooled fluid is expanded in the turbine close to the atmospheric pressure, and the condensated water is removed in the droplet separator. The second connection was chosen so that it would be possible to accomplish it with the same machinery.

The process design values calculated with the BCD-programme are shown in Fig. 19. Depending on the droplet separator efficiency and pressure drop, the cold coefficient of performance (ε_r) would be close to unity, and the heat coefficient (ε_h) would be close to two.

In both connections, the theoretical specific electric power would be less than 2 kWh electricity for each separated kilogram of water.

4.1.1 Compressor

The radial compressor was purchased from French the company Hispano-Suiza, and it was delivered with the impeller wheel, the diffuser plate and the volute scroll. Originally this compressor, model

HS-300, was developed for turbo chargers operating in larger diesel engines. The design was from the year 1963 and the efficiency was rather modest, only 0.77 at the design point.

```
          Reversed Brayton Cycle in over pressure process mode □ ©LUT&HST
<-■->                        RBC1DES2.rbc                          Window: 4
Heat Exchanger connection number 1
Cycle points                  T       h       p       wi       wh      Fii
                           [ °C ]  [kJ/kg]  [ kPa ]                      %
0 - Cycle inlet             20.0     49.6   101.0   0.9884   0.0116   80.0
1 - Compressor inlet        20.0     49.6   100.6   0.9884   0.0116   79.7
2 - Compressor outlet       58.0     88.4   140.0   0.9884   0.0116   14.3
3 - HeatEx outlet           25.0     54.7   139.0   0.9884   0.0116   81.3
4 - Turbine outlet          11.9     33.6   102.3   0.9915   0.0085  100.0
4*- MistElim outlet         11.9     33.6   101.3   0.9915   0.0085  100.0
5 - Cycle outlet            11.9     33.6   101.0   0.9915   0.0085   98.7


Compressor power      Pc  =  20.58 kW   compressor isentropic eff.= 0.760
Turbine power         Pt  =  11.16 kW   turbine isentropic eff.   = 0.820
                                        mechanical eff.          = 0.948
Motor electric power  Ps  =  10.92 kW   motor electrical eff.     = 0.910
Refrigeration power   Pre =   8.49 kW   refrigeration COP         = 0.777
Compressor mass flow  qm  =  0.530 kg/s Turbine mass flow qm      = 0.528 kg/s
Rotational speed      N   =  20700 rpm  Droplet separation    Ds  = 100.0 %
Condensate mass flow  qv  =  5.947 kg/h Vaporizate power     Pva =   4.1 kW
Specific energy       Psm =   1.84 Wh/g
```

Figure 19. The over-pressure connection design values.

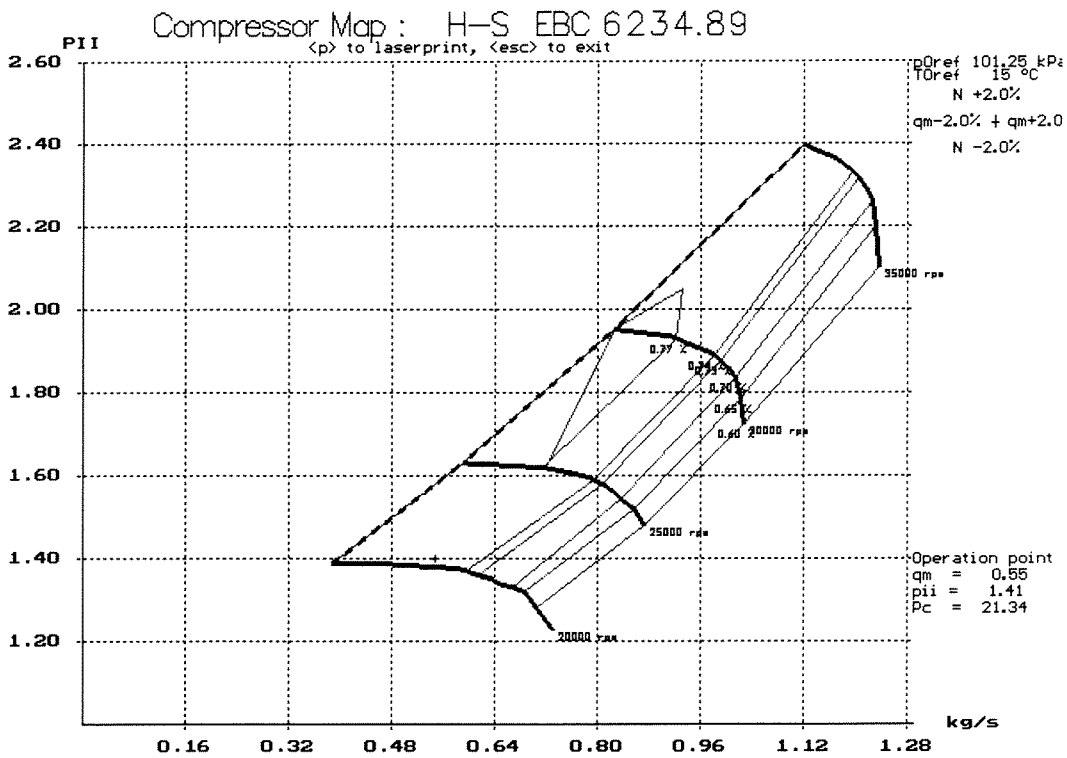

Figure 20. Compressor performance at the sub-pressure cycle design point. Design point marked with '+'

The impeller was made of cast iron, which increased the weight of the compressor in comparison with modern aluminium alloy castings.The compressor operation points are illustrated in Figures 20 and 21, where it can be seen that both process connections are slightly on the lower part of the compressor map, but reasonably good efficiencies can still be achieved with this wheel.

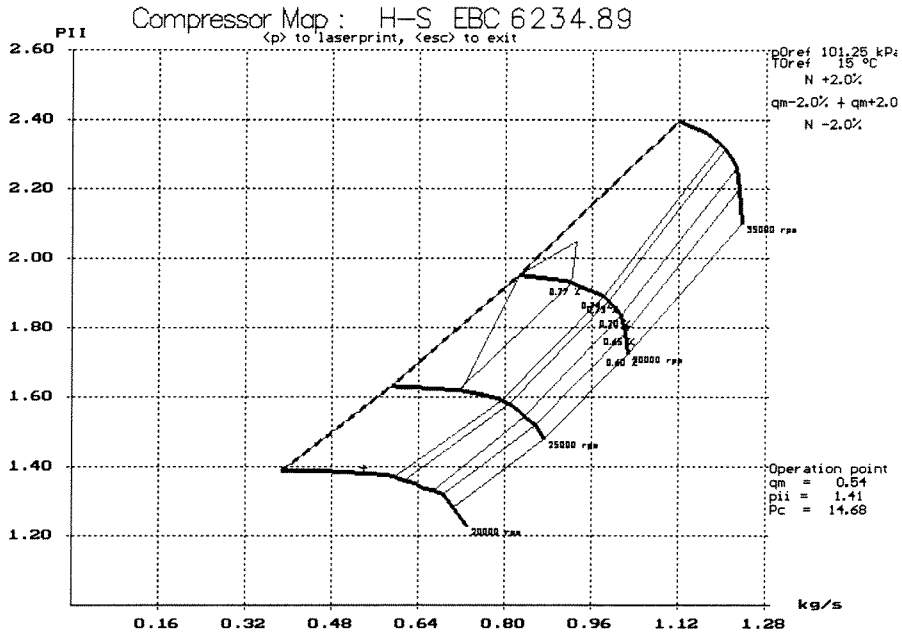

Figure 21. Compressor performance at the over-pressure cycle design point. Design point marked with '+'

4.1.2 Turbine

The turbine wheels were designed at LUT /Sahlberg 1993/ according to the turbine conditions in Fig. 15. The turbine was an axial turbine with straight blades, and the design isentropic efficiencies were $\eta_{stTT} = 0.883$ and $\eta_{stTS} = 0.820$. The turbine diffuser was angular with pressure recovery factor $C_{pr} = 0{,}4$ that leads to an isentropic efficiency of $\eta_{stTT} = 0.845$.

The nozzle and the rotor were manufactured in the Laboratory of Production Technology at Finnish Technical Research Institute. They were made by milling from aluminium alloy mould (AlSiMgPb). Due to the straight blades in the wheels, the work could be done on a three-axis milling machine.

The turbine was separately tested at LUT to get information of the turbine design and off-design performance. When the compressor was not installed, the other end of the motor was free for a

dynamometer connection and the turbine load could be measured. If tested with the whole test facility the turbine load could only be calculated numerically from the mass flow and temperatures. This in practice tends to increase the error marginal, especially when the temperature range is narrow as here, around 10 °C. Also, the turbine test results were needed to be certain that the blade speed ratio and the nozzle flow approximations gave accurate results for this turbine.

The measured parameters were the mass flow, the rotational speed, the turbine inlet pressure and temperature, the turbine outlet pressure and the motor torque.

The test results indicated that the turbine throat capacity was 6% larger than designed. This was apparently caused by an overestimation of the boundary layers. The measured efficiency was 4 percentage points higher than designed, which in turn indicates inaccuracy in the efficiency correlations. However, the achieved design point efficiency $\eta_{tsTS} = 0.86$ is a very encouraging result for one-dimensional design.

From the turbine test results the total-to-static isentropic efficiency and the throat capacity correlation factor α_t as a function of blade speed ratio could be presented /Sahlberg 1993/.

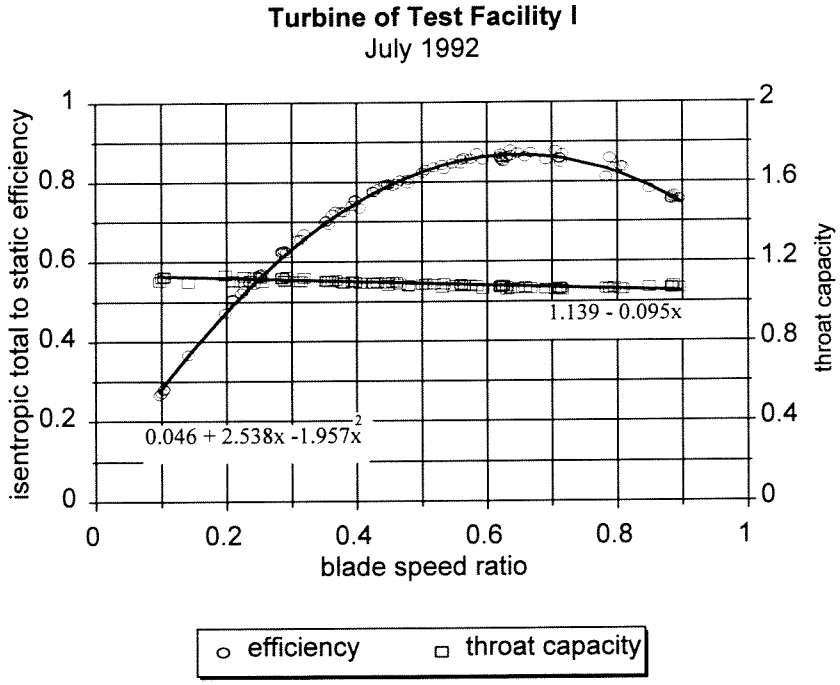

Figure 22. Turbine efficiency in Test Facility I

The curves can be accommodated to fit the measurement points with regression analysis and the corresponding equations are /Sahlberg 1993/

$$\eta_{stTS} = 0.046 + 2.538 - 1.957v^2 \tag{50}$$

$$\alpha_t = 1.139 - 0.095v \tag{51}$$

With this information the operation and performance of the turbine were known relatively well. Also the test instrumentation and data acquisition operated very well.

4.1.3 Motor and frequency inverter

The direct drive was accomplished with two alternative commercial electric motors manufactured by ABB Motors. The motor stators were rewound with thicker and fewer windings and the rotor cooling fans were turned. In this way it was possible to get a load of 11 kW with 20 000 rpm from both motors, when the powers were 3.2 kW and 5.5 kW at 3 000 rpm. The cooling fan was removed because it would not have endured the higher speed. The cooling of the electric motor was made by leading externally pressurized air through the motor chassis into the air gap of the motor at the turbine end, and the air flowed freely out from the motor at the compressor side. The air flow was controlled by monitoring the outlet temperature.

The original ball bearings were replaced by precision ball bearings to last the higher rotational speed.

The unbalance of the rotor increases the effecting forces proportional to the rotational speed, and the balancing has to be more accurate. The balancing was made at LUT.

The mechanical losses of the prototype were measured with the no-load test. The test composition (test rotor with the turbine) was chosen so that the load was equal to those generating mechanical losses at rotation. Compressor wheel losses generally increase the outlet temperature.

In the no-load test the supply voltage was decreased at constant speed. At zero voltage the measured load is theoretically equal to the mechanical losses. The accuracy of the measurement did not entirely depend on the accuracy of the measurement instruments (the dynamometer accuracy was ±2%), because it was not possible to operate the machine with zero voltage (the motor speed decreases at small voltages). The losses had to be interpolated from the measurement values. Secondly, bearing friction tended to change from one measurement to the other. Therefore, the mechan-

ical losses were chosen from the highest value measured from the turbine testing.

The measurements were processed with regression analysis /Sahlberg 1993/, and the mechanical losses for Test Facility I were defined to be

$$P_{mt} = 837\left(\frac{N}{N_0}\right)^{2.27544} \tag{52}$$

The accuracy was determined to be ±50 W, which is equivalent to ± 6%. The overall view of the test facility I is presented in Fig. 21.

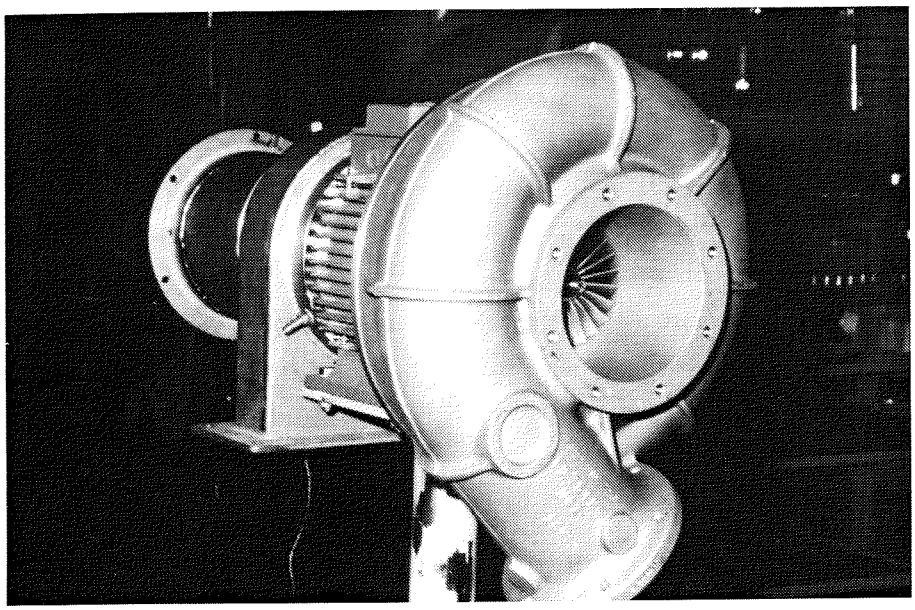

Figure 23. The rotating parts of Test Facility I. The radial compressor in the front, the motor rotor in the middle and the axial turbine at the back.

4.1.5 Heat exchangers and lay-out

To minimize pressure losses in the heat exchangers, the speed of the fluid has to be slowed. This according to the continuity equation, raises the area of the passage and the size of the heat exchanger. The heat exchangers were of the air/water model, and the air size was optimized to give a bearable pressure loss around 100 Pa.

All the pipings between inlet and outlet piping, turbine, compressor, heat exchanger and droplet separators were designed to suitable modules, so that the necessary change between sub- and overpressure connections would be easy. The droplet separator was also built to the same frame. All the

pipings were isolated. The layout design is given in appendix A.

4.1.6 Test arrangements

Test Facility I was tested for the sub-pressure connection in two phases between September 1992 - March 1993 and January - March 1994. The over-pressure tests were done between March and September 1993. The main work during this time was dedicated to improving the test conditions and making necessary changes to the test facility.

Test goals and grounds
The goals of the tests were to operate the test facility at the design point, and to make identical measurements in both connections to get process characteristic that could be compared to those of the design programme. The experimental knowledge about process performance would be valuable in all cases.

The test facility consists of several units that operate at slightly different time responses. To get accurate measurements, the measurements have to confirm each other, and must be obtained with well-calibrated instruments.

The main concern was the air drying capacity of the exit flow, which can be expressed with the heat coefficient of the process (ε_h). The condensation capacity was of great importance and this showed to be an interesting measurement problem, because it involved inaccuracy factors. In these tests the condensation phenomenon was measured in four different ways:

- measurement of the relative humidity, the mass flow, the temperature and the pressure of the fluid both before and after the process. From these values the extracted water could be calculated.

- measurement of the extracted water. This measurement had several inaccuracy factors: the surface of the droplet separator, the separator channels and the piping between the turbine and the compressor (relatively large). The condensation of water drops on the surface always caused a start lag before any water was extracted from the process. Also the droplet separator installation in sub-pressure was problematic, because the place had to be sealed before the tests, and could only be inspected afterwards. Therefore, several adjustments were made to ensure that water flowed to the right place. However, this measurement gave us the lowest value of water condensation, because all the errors decreased this value.

- measurement of the relative humidity, the mass flow, the temperature and the pressure before the turbine, the turbine pressure ratio and the efficiency (as a function of blade speed ratio from the turbine test, Fig. 19).

- by measuring the turbine outlet temperature and assuming negligible sub cooling in the turbine, the saturation temperature could be obtained.

The two first mentioned methods are applied over the whole process, and the two latter methods are concentrated on the turbine. In the simple sub-pressure connection this also includes the whole process, because the turbine is the only place where condensation occurs.

Test arrangements and instrumentation

The test arrangements are illustrated in Fig. 22 (sub-pressure connection) and Fig. 25 (over-pressure connection). When comparing the pictures it can be noted that the instrumentation is identical, and the test arrangements do not differ much from each other. The heat exchangers that were not in use with the sub-pressure connection were left in location to straighten the flow. At the actual test location these differences of the arrangements were even smaller.

The test facility was connected to the normal ventilation system at LUT. The inlet flow was obtained from the fresh air channel, and the outlet flow was directed to the exit channel. The relative humidity of air at the inlet was regulated up to 100% with a Condair TS 660 air moistener.

The measured parameters were the relative humidity (RH) before and after the test facility, and the essential pressures (p) and temperatures (T) in the compressor and the turbine, the mass flow after the compressor (with the pressure difference, dp) over the orifice device, the motor power (P) and the speed (n), and the water extracted from the process (qv).

The instrumentation arrangement and calibration were conducted in the following way:

- Relative pressure transducers TRAFAG 8890.21 were used at the process pressure points. The pressure was measured with three vertical static probe holes (diameters 0.5 mm) each 120° apart circumferentially. The holes were united with a 6 mm tube, in which the pressure was measured. The pressure after the turbine was measured as mentioned above, but there were two 2 mm diameter probe holes in a 70° angle against the flow. This design was somewhat contrary to measurement directions /ISO 5389/, but due to the very complicated structure of the scroll, the correction would have caused a great uncertainty about the surface smoothness.

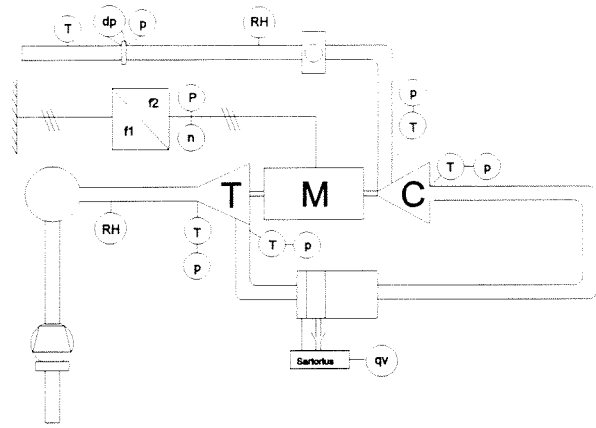

Figure 24. Sub-pressure connection. The inlet air flows first into turbine. Therefore the air first expands to sub-pressure and the compressor compresses it back to atmospheric pressure. The water condensed in the turbine is extracted with the water separator situated between the turbine and the compressor. Due to the extraction, the air leaving the compressor is drier and warmer.

- The pressure difference of the mass flow orifice device was measured with a Valmet DP3 pressure transducer. The manufacturer accuracies were ± 1.2 kPa for the Trafag and ±0.3 kPa for the Valmet transducers. Because the pressures measured in the test facility were relatively small (pressure difference over the compressor is about 30 kPa), there was a need to perform calibration. All probes were frequently calibrated with the Beamex DM2 pressure calibrator, which operates within 0.01 kPa error at operational scale. The calibration procedure was made with the whole measuring equipment so that the reference pressure was compared to the output of the appropriate data acquisition channel. Also, the less accurate Trafag pressure sensors were subjected to a one month long drift and repetition measurement with the Beamex DM2 calibrator. This measurement showed a standard deviation of 0.23 kPa. For a single test measurement this would mean an accuracy of ± 0.45 kPa, with 95% confidence /Sirén 1995/.

- Mass flow was measured with a SFS-ISO 5167 standard orifice device. The standard gives an error of ±0.5 %, when the piping distances are adequate /SFS-ISO 5167-1/. Here the straight length before the orifice device was more than 30 times the pipe diameter.

- The relative humidity was measured with Vaisala HMP 132Y-sensors, which were equipped with PT100 thermometers. The manufacturer accuracy is ±3%-units when the relative humidity is above 75%. This requires a calibration once a year. We made frequent calibrations with a salt bath, and found that calibrations done once a week resulted in a difference less than 1 percentage unit. The PT100 accuracy was ± 0.25 °C, but these thermo sensors were extremely sensitive to the inverter electromagnetic disturbance. At a startup the temperature jumped more than 1 °C. Therefore the gas temperatures were measured with thermocouples.

- The temperature probes were mainly K-type thermocouples with 0.35 mm conductor diameter. The thermocouples in the compressor were situated at the flanges. Because the turbine outlet temperature depends directly from the relative humidity of the expanded air, the rapid response of the thermocouple is important. Therefore, K-type thermocouples with 0.15 mm were used for this temperature measurement. The thermocouples in the turbine were situated just before the stator ring and after the rotor wheel. The thermocouple manufacturer accuracy is ± 1 °C. The thermocouple values were monitored on site in several long term measurements (24-hour closed loop), in which the maximal deviation of the thermocouple values was 1.1 °C. Because the absolute accuracy in temperature is significant when we calculate the water vapour content, the absolute level was defined with a precision mercury thermometer (accuracy ± 0.1 °C) and an external PT100 sensor (accuracy ± 0.05 °C). The accuracy in temperature after this procedure was estimated to be ± 0.5 °C.

- The momentarily extracted water was measured with a Sartorius 1413 MP8 scale. The scale accuracy (± 2 g) was not significant, because the extracted water amount could be measured later, as well.

- The motor power and speed were obtained from the inverter. The values were checked by measuring the electric values before and after inverter with two Norma AC-Power Analyzers. The slip — the percentage difference of the supply and rotational frequencies — was determined to be 3% from these values.

Data aquisition

The data acquisition of the process parameters requires a quick and accurate system. In an early stage it was evident that programme which gives real time information of the process operation would be beneficial. The available commercial data acquisition programmes were rejected because the calculation of the parameters involves rather complicated functions from the raw data.

All the parameters were measured with electrical sensors and the quantities were directed to data acquisition unit Fluke Hydra 2620 A that gathered the information from these 19 signals in less than 1 second. Fluke Hydra operates with mechanical relays that ensure a low disturbance in data acquisition. It was directed with an IBM PC-based computer via RS-232 serial bus, through which also the signals were sent to the computer.

The computer ran the Tripleap-programme based on the QuickBasic[1] computer language. This programme initiated and directed Fluke Hydra, calculated all process values needed in the analyses, saved these values along with the raw measurement data and printed the results on the screen. The programme's real time capability is described with the fact that all this was done within six seconds.

The programme output could be chosen from four different screens: one text screen (Fig. 25) where all process parameters were printed basically in the same way as in the BCD-programme, and three graphic screens showing the time rate of water condensing, the main temperatures or relative humidities and turbo efficiencies (Fig. 26). From these graphics it was possible to watch different unsteady phenomena and choose the possible steady state measurement points. The graphic views were evaluated during the tests from practical needs and they were of real use during the test.

Because all the raw sensor data were saved, the tests can be simulated with the same programme, if there are corrections in process calculation equations or in the calibration data. It also serves as an excellent demonstration programme.

4.1.7 Test results—sub-pressure cycle

There were 35 different sub-pressure connection tests, which lasted 51 hours in total. The longest test took 4.5 hours. After the start, when the desired rotational speed was achieved, it took about 10 minutes for the temperatures to stabilize. However, the water extraction did not begin until all the surfaces in the separator channel had become wet and this took approximately fifteen minutes. In Fig. 24 are the graphic output results of the longest test, starting before the end of the first hour. Changes in the process are mainly caused by variations in the inlet relative humidity. The intervals between measurements were 30 seconds and the whole test lasted 4.5 hours. The test scale value is modified with a constant, because a considerable amount of water, 4 litres, did not flow out from the droplet separator during the test.

---

[1] *Copyright of Microsoft Corporation*

Data aquisition programme TRIPLAP

```
Time  11:25:53          04.03.93  LUT/Energy Technology
 Reversed Brayton        T        h        p        yi       yh        RH
 Sub pressure          [ C ]   [kJ/kg]  [ kPa ]                        %
         0.    704.     474.     116.
 0 - Inlet state        17.3     38.8    101.6   0.9916   0.0084     69.2
 4 - Turbine outlet      3.5     18.8     76.7   0.9937   0.0063    100.0
 5 - Diffuusor out       2.9
 1 - Compressor in       3.9     19.7     75.9   0.9938   0.0062     94.1
 2 - Compressor out     40.4     56.7    104.4   0.9938   0.0062     13.7


 Compressor power     Pk  = 14.749 kW  compressor efficiency    = 0.722
 Turbine power Pt         =  7.684 kW  turbime efficiency       = 0.867
 Heat power           Phe =  7.083 kW  heat Coefficient Of Pr.  = 0.859
 Electric power       Ps  =  8.245 kW  eletromech. efficiency   = 0.857
 Mass flow turbine    qmt =  0.399 kg/s     qmeq =  0.400 kg/s
 Mass flow compresso qmk  =  0.398 kg/s     qmeq =  0.521 kg/s
 Rotational speed      N  =  19646 rpm      Neqt =  19566 rpm
 Water condensing     qmv =  3.021 kg/h     Neqk =  20035 rpm
 Evaporation power     P  =  2.098 kW       Nyy  =  0.617
 Water mass flow   qvw_s  =  2.099 kg/h
1EXIT     2Cont      3Ltilat     4Vesigr     5Tunnus     6FILETRIPLi6   7Step
```

Process design programme BCD

```
 Data  Input  Efficencies  PressLoss  HeatExch  Optimization  OffDesign
            Reversed Brayton Cycle in sub pressure process mode  | ©LUT&HST
 <-■->                      TRDESAP.RBC                          Window: 3
 Cycle points                  T        h        p        wi       wh      Fii
                             [ °C ]   [kJ/kg]  [ kPa ]                      %
 0 - Cycle inlet              17.3     38.8    101.6   0.9916   0.0084    69.2
 3 - Turbine inlet            17.3     38.8    101.6   0.9916   0.0084    69.2
 4 - Turbine outlet            3.1     19.0     76.7   0.9938   0.0062   100.0
 4*- MistElim outlet           3.1     19.0     75.8   0.9938   0.0062   100.0
 2 - Compressor outlet        39.7     56.1    104.4   0.9938   0.0062    14.3
 2*- Cycle outlet             39.7     56.1    101.6   0.9938   0.0062    13.9


 Compressor power      Pc  =  14.78 kW  compressor isentropic eff.= 0.722
 Turbine power         Pt  =   7.91 kW  turbine isentropic eff.   = 0.867
                                        mechanical eff.          = 0.921
 Motor electric power  Ps  =   8.02 kW  motor electrical eff.     = 0.930
 Heating power         Phe =    6.9 kW  heating COP               = 0.855
 Turbine mass flow     qm  =  0.399 kg/s Compressor mass flow   qm = 0.398 kg/s
 Rotational speed      N   =  19646 rpm  Droplet separation     Ds = 100.0 %
 Condensate mass flow  qv  =  3.146 kg/h Vaporizate power      Pva =   2.2 kW
 Specific energy       Psm =   2.55 Wh/g
F1 Help  F2 Save  F6 Graf  F9 Info  F10 Run  Alt+F10 Exit        | 29. 5.1995
```

Figure 25. The measured and the design sub-pressure process compared with each other at a stabilized test point.

The measured process values (from a quasi stationary moment of the process) evaluated with the design programme values give quite a good similarity.

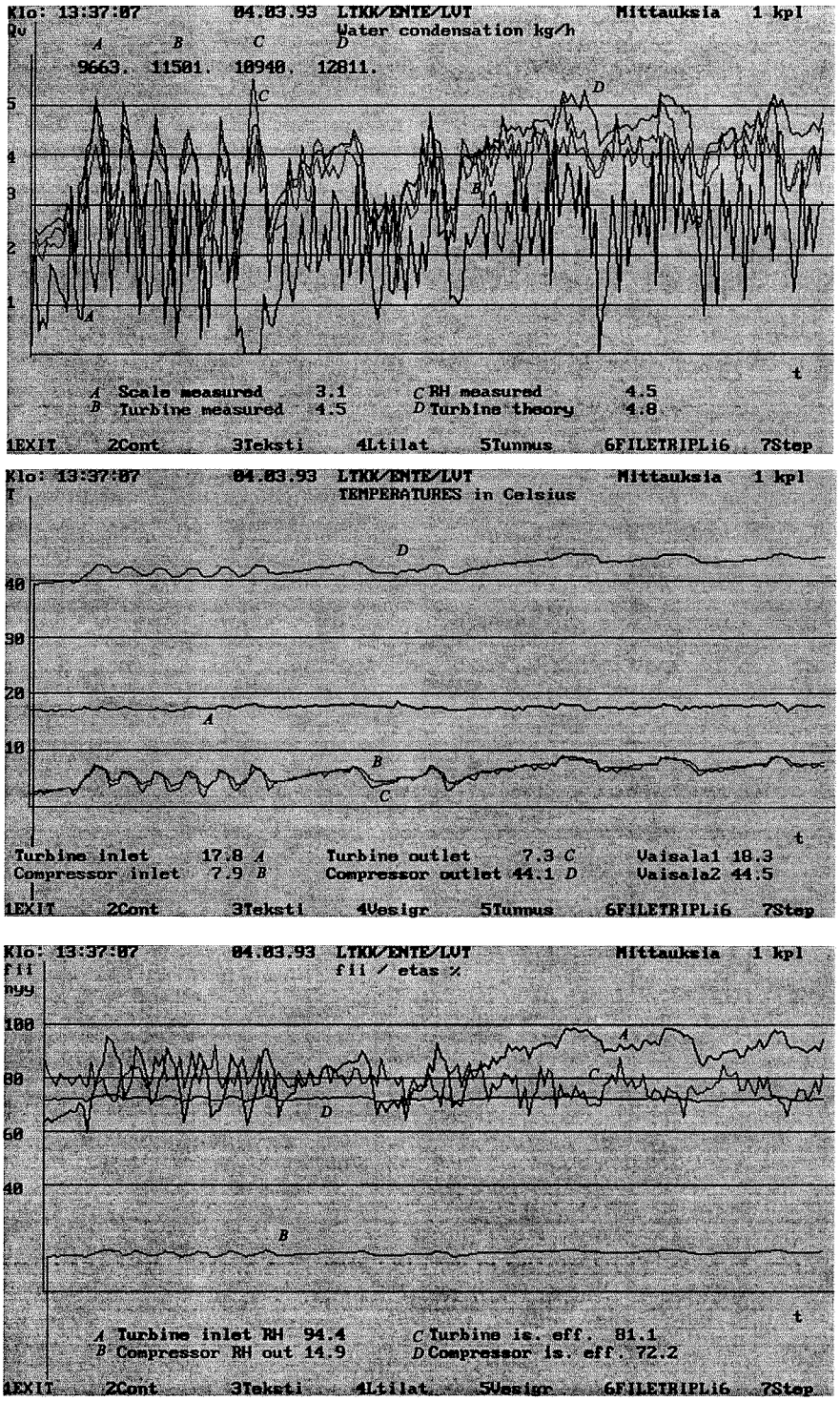

Figure 26. The output screens of the TRIPLAP-programme

4.1.8 Test results — over-pressure cycle

The over-pressure connection was installed by changing the sub-pressure connection parts to a slightly different order

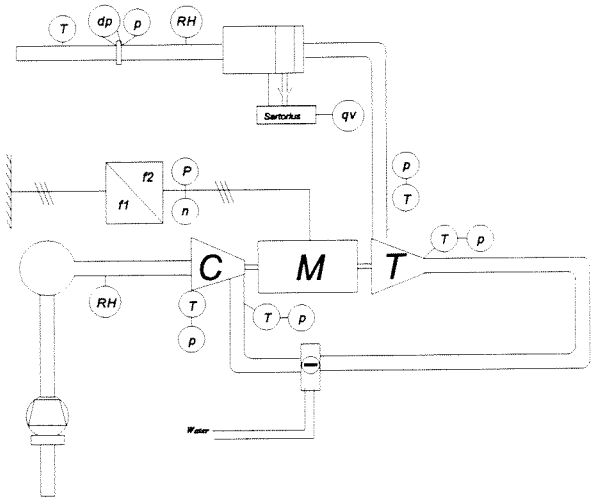

Figure 27. Over-pressure connection. The inlet air flows first to the compressor, in which the fluid is compressed to over-pressure, and the turbine expands it back to atmospheric pressure. The water condensed in the turbine is extracted with the water separator situated after the turbine.

The data acquisition and the programme were modified to the changes and the programme was named TRIPLYP. The tests were made from March to September in 1993. There were 23 separate tests that lasted 37 hours in total. The longest test took about 4 hours. The testing was made to three different types of droplet separators. The test facility operated better step by step. Fig. 28 shows one quasi steady operational point and Fig. 29 shows the different water condensation measurements, the main temperatures and efficiencies from the same test.

Data aquisition programme TRIPLYP

```
Time 10:40:30          02.06.93  LUT/Energy Technology      Measurements 30 pts
 Reversed Brayton        T        h        p        yi       yh       Fii
 Over-pressure         [ C ]   [kJ/kg]  [ kPa ]                        %
       2561.   5255.   3937.    4230.
 1 - Compressor in      16.0     36.9    100.7   0.9918   0.0082    72.6
 2 - Compressor out     53.0     74.6    137.5   0.9918   0.0082    12.7
 3 - Turbine in         23.7     44.7    137.2   0.9918   0.0082    65.0
 4 - Turbine out         9.8     25.4    107.0   0.9934   0.0066   100.0
 5 - Mist elim exit      9.5     25.4    102.9   0.9930   0.0070   100.0


 Compressor power     Pk  = 19.310 kW  compressor efficiency    = 0.726
 Turbine power        Pt  =  9.895 kW  turbine efficiency       = 0.869
 Heat power           Plä = 15.326 kW  heat coefficient of pr. = 0.999
 Electric power       Ps  = 11.687 kW  electromech. efficiency = 0.806

 Turbine mass flow   qmt =  0.512 kg/s    qmeq =  0.384 kg/s
 Compressor mass flow    =  0.512 kg/s    qmeq =  0.516 kg/s
 Rotational speed      N =  19986 rpm     Neqt =  19690 rpm
 Water condensing    qmv =  2.893 kg/h    Neqk =  19951 rpm
 Evaporation power     P =  2.009 kW      Nyy  =  0.640
 Water mass flow   qvw_s =  1.597 kg/h

1EXIT     2Cont      3TempGra    4WaterGra   5EffGra     6FILETRIPLYi6  7Step
```

Process design programme BCD

```
 Data  Input  Efficencies  PressLoss  HeatExch  Optimization  OffDesign
            Reversed Brayton Cycle in sub pressure process mode  | ©LUT&HST
  <-■->                    CH5CASE2.RBC                          Window: 1  Heat
Exchanger connection number 1
  Cycle points              T       h       p       wi       wh      Fii
                         [ °C ]  [kJ/kg]  [ kPa ]                      %
  0 - Cycle inlet          16.0    36.9    100.7   0.9918   0.0082   72.6
  1 - Compressor inlet     16.0    36.9    100.6   0.9918   0.0082   72.5
  2 - Compressor outlet    53.2    74.9    137.7   0.9918   0.0082   12.5
  3 - HeatEx outlet        23.7    44.8    137.2   0.9918   0.0082   61.4
  4 - Turbine outlet        9.3    26.8    107.0   0.9932   0.0068  100.0
  4*- MistElim outlet       9.3    26.8    103.0   0.9932   0.0068  100.0
  5 - Cycle outlet          9.3    26.8    100.7   0.9932   0.0068   94.1


  Compressor power     Pc  =  19.45 kW   compressor isentropic eff.= 0.726
  Turbine power        Pt  =   9.23 kW   turbine isentropic eff.   = 0.869
                                         mechanical eff.          = 0.862
  Motor electric power Ps  =  12.23 kW   motor electrical eff.     = 0.970
  Refrigeration power  Pre =   5.22 kW   refrigeration COP        = 0.427
  Compressor mass flow  qm =  0.513 kg/s Turbine mass flow qm      = 0.512 kg/s
  Rotational speed       N =  19646 rpm  Droplet separation     Ds = 100.0 %
  Condensate mass flow  qv =  2.515 kg/h Vaporizate power      Pva =   1.7 kW
  Specific energy      Psm =   4.86 Wh/g
F1 Help  F2 Save  F6 Graf  F9 Info  F10 Run  Alt+F10 Exit        | 29. 5.1995
```

Figure 28. The measured and design sub-pressure process compared with each other at a stabilized test point.

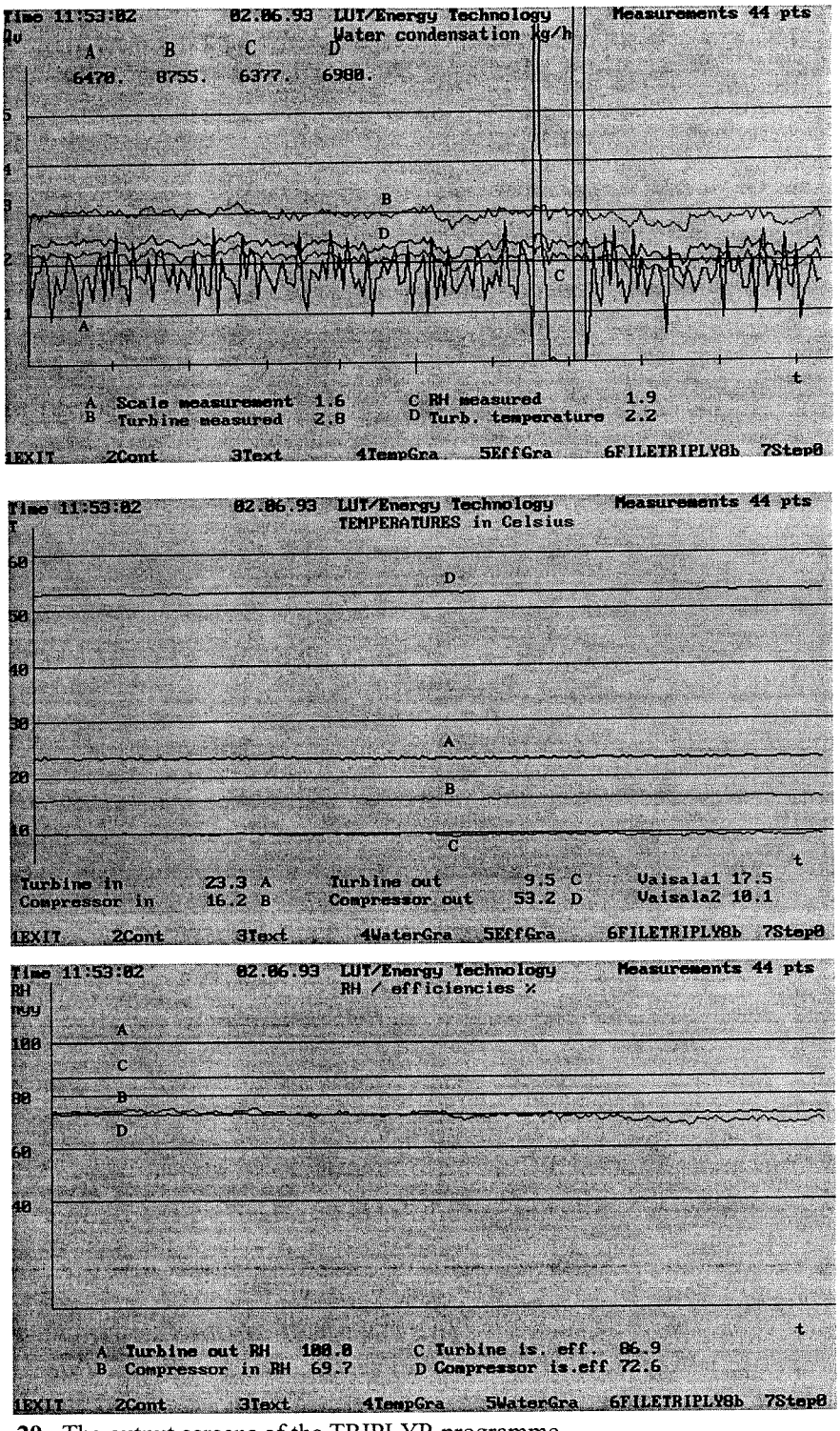

Figure 29. The output screens of the TRIPLYP-programme

The tests in September 1993 with the over-pressure cycle concentrated on testing different droplet separators in a similar test arrangement.

Following separators were used:

ACS mesh pad eliminator from ASC Inc,USA. Stainless steel. Medium priced. Guaranteed to separate 95% of droplets that are bigger than 5 μm. Estimated pressure loss around 300 Pa, Fig. 30.

Lechler corrugated plate separator from Lechler GmbH, Germany. PPTV-plastic. Expensive, tailor-made. Guaranteed to separate 99.9% of droplets that are bigger than 17..20 μm. Estimated pressure loss less than 100 Pa.

Munters corrugated plate separator from Germany. GLASdek (resembles cardboard). Inexpensive, large series. No separation data. Estimated pressure loss less than 100 Pa.

The ACS separator was also equipped with a customized net separator to increase separation. During the test programme it was decided to do one test without any separator.
The results were the following:

Table 1. Droplet separator results

Test name	Droplet separator	Scale g	Surfaces g	Total g	Condensation g	Efficiency %
TRIPLYi6	ACS+net error ±	3817	1528	5345	7 265 1 360	73,6 14,6
TRIPLYi7	ACS error ±	3333	1235	4568	6 635 1 100	68,8 09,8
TRIPLYi8	Lechler +Munters error ±	3408	1442	4850	8 861 2 160	54,7 10,7
TRIPLYi9	Lechler error ±	2134	365	2499	6 210 2 300	40,2 10,9
TRIPLYiA	No separator error ±	-	2142	2142	5 904 1 470	36,3 07,3

The results and visual experiences from the outlet flow showed that the separation degree was always less than 100%. The droplets also gathered to the surfaces of the separator channel and the tests did not last long enough to eliminate this influence on the test results. However, with the different droplet separators, the flow was apparently smoother and there was not so much water on the

surfaces after the tests. The error was calculated with ±2% maximal deviation of the relative humidity and ±0.3 °C of temperatures around the turbine.

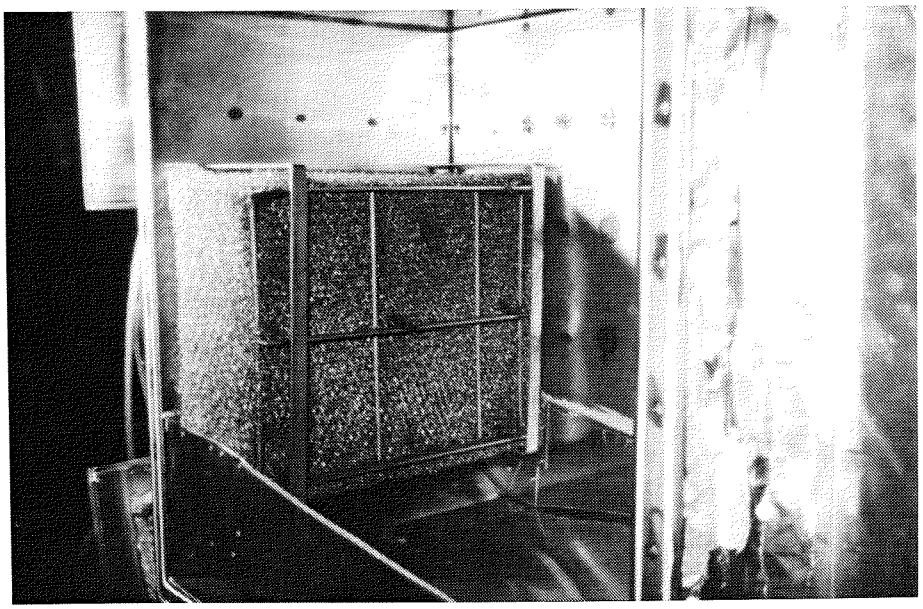

Figure 30. The ACS droplet separator in Test Facility I.

4.1.9 Errors and uncertainty

The comparisons with theoretical values should take into account the possible errors and uncertainties of the test arrangements /ISO 5389/:

- accuracy of measurements
- errors due to the inaccuracy or uncertainty in the thermodynamic properties of the process medium
- errors due to unsteady conditions during the test

The main errors occured with the relative humidity and the temperatures. They affected the water vapour content of the cycle. The measuring programme was used in numerical error analysis, in which the measured values were changed according to the error margins. From this calculation the sensitivity to these changes could be evaluated. When these margins were implemented to the test results, the utmost values in the desired cycle variables were obtained.

The above procedure gives the extreme margins of error, which can be reduced by statistical error analysis, where the uncertainty is defined

$$d_y = \pm \sqrt{\sum_{i=1}^{n} \left(\frac{\partial Y}{\partial X_i} \right)^2 dx_i^2} \tag{53}$$

The three main parameters to be analysed were the water condensation mass flow $q_{m,wat}$, the inlet motor power P_{el} and their ratio; the specific energy consumption E_s that is the used electric energy per the condensated water mass. The condensation mass flow is

$$q_{m,wat} = q_{m,c}(w_{vap0} - w_{vap1}) \tag{54}$$

where the water vapour mass fraction for both points is

$$w_i = \mu \frac{p'_{vap,i}}{\frac{p_i}{\varphi_i} - p'_{vap,i}} \tag{55}$$

The motor input power can be evaluated to be

$$P_{el} = \frac{P_c - P_t}{\eta_{inv}\eta_{mech}\eta_{el}} = \frac{q_{m,c}(h_{03} - h_{02}) - q_{m,t}(h_{00} - h_{04})}{\eta_{inv}\eta_{mech}\eta_{el}} \tag{56}$$

Because of the complicated equations, the uncertainty derivation of Eq. (53) is done in blocks according to Appendix B. When we use the values for sub-pressure cycle (Fig. 25) and the uncertainties mentioned previously, we get the measured values at one point

condensation mass flow $q_{m,wat}$ = 3.02 kg/h ±0.69 kg/h
electric input power P_{el} = 8.25 kW ± 0.57 kW
from these two E_s = 2.73 kWh/kg$_{wat}$ ± 0.67 kWh/kg$_{wat}$

The values for over-pressure cycle calculations we get from Fig. 28 and the values are respectively

condensation mass flow $q_{m,wat}$ = 2.89 kg/h ±0.66 kg/h.
electric input power P_{el} = 11.69 kW ± 0.89 kW
from these two E_s = 4.04 kWh/kg$_{wat}$ ± 1.05 kWh/kg$_{wat}$

The droplet separation results were not conclusive. In the sub-pressure cycle the droplet separation level was 80% and in the over-pressure cycle 70% of the theoretical separation value. But the errors in the relative humidity sensors can at utmost limits be so extensive that the accuracy can vary up to

30%. Therefore, the measurements could not be directly used to evaluate the droplet separation efficiency or to substantiate the water extraction as planned originally. The error margins of the sensors were analysed before actual tests by empirical tests, where the inlet relative humidity was adjusted a level where there would not occur any condensation. In these cases the calculated humidities were within a few per cent, which indicated much smaller errors in the sensors.

4.1.10 Discussion on Test Facility I

The operation of the test facility proved to be reliable. There were only some problems with the bearings during the separate turbine testing. The mechanical system was reliable and the inverter functioned without any faults. The design was found to fill the requirements stated earlier and the test facility was operative.

The start sequence was 40 seconds, during which time the nominal rotational speed was achieved. The test needed one person to supervise the humidifier and the water container, which had to be emptied about twice an hour. The noise at the test facility was over 85 dB, because there was no noise filter design.

The most problematic element was the Condair humidifier that was not capable to attain stationary humidification circumstances at the nominal design conditions — RH 80%, 20 °C — but resulted in ca. five minute oscillation with some 20 per cent amplitude. Despite several service jobs and control manoeuvres, the oscillation remained in a long term test (over one hour). In some tests the inlet relative humidity was originally high and the humidifier operated in a more stable manner. The problem from the oscillation was the time responses of different components of the cycle. Especially, observing of the turbine operation that included visual condensing showers was somewhat distracted, but fortunately the oscillation cycles were much longer than previously.

Because the test facility was installed in to the University ventilation system, the pressure levels at the beginning and end of the cycle were different. This was the reason why the isentropic work in the compressor was higher than that in the turbine. If the pressure levels had been the same, the specific electric power would have been approximately 20% lower.

The installation and calibration of the test facility were time consuming. Also, the development of the data acquisition programmes took time. That is why the test programme lasted nine months.

The automated data acquisition system eased substantially the making of the tests and their analysing. The programmes have proved to be very useful in demonstrating the test facility and the cycle.

The droplet formation was very difficult to verify. The theory indicated that the droplet sizes could vary from micro metres to hundred micrometers. Visually, in the channel after the turbine, a few sudden sprays of apparent water that occurred in an interval of some seconds could be seen. During the experiments there were clear water bubble formations and small water streams along the surfaces. To examine the droplet size in the flow itself, laser droplet size measurement was made by the Laboratory of Energy Engineering and Environmental Protection at Helsinki University of Technology.

In these measurements a laser beam is sent through the channel perpendicular to the flow. The droplets in flow distract in the light and scatter light observed in the receptor lens. The receptor data is statistically analysed and the droplet size distribution can be calculated. Unfortunately, the test channel proved to be too wide for qualitative test results, and the scatter radius was larger than the receptor could measure. However, the Laboratory could conclude from the data that the droplet size is smaller than five micro metres, although the exact size distribution could not be obtained. This result conforms roughly with our expectations.

It was extremely difficult to extract water from of the test facility, especially in the sub-pressure cycle tests, despite all the efforts made to correct this problem.

4.2 Test Facility II

The second test facility was built with high speed technology in the years 1994-95. It was designed to function as an air drier in the operational range of commercial air driers, and it was planned to be a serious reference for further development of commercial Reversed Brayton Cycles.

The main goals for the prototype were set as follows

- high speed technology applied in all possible parts
- overall efficiency of the turbomachinery above 80%
- electrical efficiency above 85%
- no external cooling

The first test facility operated at the rotational speed of 20 000 rpm and consumed 11 kW of power. Although the operation was satisfactory, there was a need to make the second test facility clearly

smaller. This would mean an increase in the operational speed and a decrease of power. A clearly significant limit would be around 2 kW, which could be supplied in common households.

The theoretical optimum in the cycle pressure ratio would be 1.2-1.3 that would mean also smaller condensing flow, as will be seen in Chapter 5. When the drying capacity becomes more important, the optimum pressure ratio increases. The cycle for sub-pressure was determined with the BCD-programme in the following way.

The main components are discussed below, but it can be directly seen from Fig. 31 that the temperatures are quite moderate at the design circumstances. The maximal temperature is around 60 °C and the minimal temperature is around 10 °C. Because of the decreased mass flow compared to Test Facility I, the amount of condensed water would be around one litre per hour.

```
 Data  Input  Efficencies  PressLoss  HeatExch  Optimization  OffDesign
            Reversed Brayton Cycle in sub pressure process mode  | ©LUT&HST
 <-■->                        TRDESAP.RBC                        Window: 3
 Heat Exchanger connection number 4
 Cycle points                    T        h        p        wi        wh      Fii
                               [ °C ]   [kJ/kg]  [ kPa ]                      %
 0 - Cycle inlet                25.0     65.6    100.0    0.9841    0.0159   80.0
 3 - Turbine inlet              25.0     65.6     99.7    0.9841    0.0159   79.8
 4 - Turbine outlet              8.1     34.8     64.2    0.9895    0.0105  100.0
 4*- MistElim outlet             8.1     34.8     63.2    0.9895    0.0105  100.0
 2 - Compressor outlet          63.1     90.9    100.4    0.9895    0.0105    7.4
 2*- Cycle outlet               63.1     90.9    100.0    0.9895    0.0105    7.3


 Compressor power      Pc  =   3.57 kW   compressor isentropic eff.= 0.720
 Turbine power         Pt  =   1.97 kW   turbine isentropic eff.   = 0.840
                                         mechanical eff.          = 0.826
 Motor electric power  Ps  =   2.28 kW   motor electrical eff.     = 0.850
 Heating power         Phe =    1.6 kW   heating COP               = 0.697
 Turbine mass flow     qm  =  0.064 kg/s Compressor mass flow   qm = 0.064 kg/s
 Rotational speed      N   =  87300 rpm  Droplet separation     Ds = 100.0 %
 Condensate mass flow  qv  =  1.252 kg/h Vaporizate power      Pva = 849.7 W
 Specific energy       Psm =   1.82 Wh/g
F1 Help  F2 Save  F6 Graf  F9 Info  F10 Run  Alt+F10 Exit        |  5. 6.1995
```

Figure 31. Test facility II design parameters in the sub-pressure cycle

4.2.1 Compressor

The design of the compressor wheel in a small scale is quite demanding, because small errors can easily lower the efficiency of the wheel. Therefore, the design advanced in three different paths: manufacturing with own design, manufacturing with outside design and buying a commercial compressor.

Own design

Centrifugal compressor design is even today based on empirical knowledge. The test facility wheel was preliminary designed with the design data of LUT high speed research /Larjola et al 1987/, /Larjola 1988c/, /Backman 1989/.

As can be seen in Fig. 32, the isentropic efficiency $\eta_{scTS} = 0.82$ (printed in bold), which can be considered very good. Because the design is based on empirical data, the efficiency has to be verified by testing the possibly manufactured wheel with a proper arrangement /ISO 5389/. However, the final design and manufacturing was not made during this research.

```
Data  Input  Impeller  Diffuser  Speed  Boundaries  Iteration  OffDesign
              Centrifugal compressor 1-D flow design program       | ©LUT
   ☺                          RBC2COMP.CCF                        Window: 2

Fluid :Air (humid)     Compressor case:Testilaitteisto                RH 100.0

 STATE  p      T      h      v     cn     d1t    d1h      N      qm      Ns      P
--------kPa-----K-----kJ/kg---m3/kg---m/s-----m--------m--------rps----kg/s----------kW----
  1    58.85 277.4   4.28   1.35  95.6 0.036  0.013    1455   0.064   0.939    3.21
 01    62.50 282.0   8.94
 STATE  p      T      h      v      c      d       b      etas    cpr      N2
--------kPa-----K-----kJ/kg---m3/kg--m/s-----m--------m-------------------------------
  2    85.77 313.2  40.48   1.05 193.3 0.061 0.0046 0.874             18
 02   104.97 331.6  59.16


  3    99.48 330.1  57.69   0.95  54.3 0.109 0.0046 0.791   0.714
 03   101.04 331.6  59.16
  4   100.42 331.0  58.55   0.95  34.9 0.047         0.822   0.600
-------------------------------VELOCITY TRIANGELS-------------------------------
TRIANGLE    c      cu      cr      w      u      alfa    beta   gamma    iota    Mach
   1       95.6    0.0    95.6   191.3  165.7    0.0    30.0    30.1     0.1    0.57
   2      193.3  173.5    85.2   136.6  276.6   63.9    51.4    40.0   -11.4    0.55
13:39:33
F1 Help  F2 Save  F6 Graf  F9 Info  F10 Run  Alt+F10 Exit          |  6. 6.1995
```

Figure 32. Main centrifugal compressor data for Test Facility II. Design by Jari Backman.

The wheel stresses due to the rather low circumferential speed $u_2 = 276.6$ m/s will not be critical. For a conventional impeller wheel, an approximate equation /Backman 1989, Larjola 1987/ can be used

$$\sigma_m \equiv 0.3 \rho u^2 \tag{57}$$

where σ_m : the nominal tension
ρ : the density of the wheel

The tension from Eq. 57 is for aluminium ($\rho = 2700$ kg/m^3) $\sigma_m = 62$ MPa, but the commonly used aluminium alloys can easily endure 200 MPa /Backman 1989/.

Outside design

During the design it was decided to get offers for the design of the compressor wheel. After some consideration the offer from the Institute of Fluid Mechanics at Hannover University in Germany was accepted. Their offer included the design of the impeller wheel, the unbladed stator and the scroll. Also, the stresses of the wheel were to be calculated.

The Institute of Fluid Mechanics has several decades of experience in the design of radial turbomachines. Their design is based on the experience and tests from numerous orders in the area of radial machines. The results (Fig. 33) were quite near to those of our own design.

```
 Data  Input  Impeller  Diffuser  Speed  Boundaries  Iteration  OffDesign
                Centrifugal compressor 1-D flow design program      | ©LUT
   ☺                        RBC2HAN.CCF                            Window: 2
Fluid :Air (humid)      Compressor case:Testilaitteisto             RH  0.0 %

 STATE  p      T      h      v     cn     d1t    d1h      N      qm     Ns      P
--------kPa-----K-----kJ/kg---m3/kg--m/s------m--------m---------rps----kg/s----------kW----
  1    58.38  276.7   3.59   1.36  102.7  0.036  0.013    1455   0.064  0.918   3.27
 01    62.50  282.0   8.87
 STATE  p      T      h      v      c      d      b      etas    cpr    p/p01   N2
--------kPa-----K-----kJ/kg----m3/kg-m/s------m--------m-------------------------------
  2    85.93  311.7  38.32   1.07  206.2  0.060  0.0043 0.523           1.37    16
 02   108.16  332.9  60.00                               0.939          1.73


  3    97.04  322.9  51.84   0.98  127.8  0.096  0.0043 0.742   0.513   1.55
 03   105.68  332.9  60.00                               0.896          1.69
  4   100.00  332.9  60.00   0.96   98.2  0.028          0.800   0.600   1.60
-------------------------------VELOCITY TRIANGELS-------------------------------
TRIANGLE     c      cu      cr      w       u      alfa    beta   gamma    iota    Mach
   1       102.7    0.0   102.7   190.9   160.9    0.0    57.5    55.4     2.0    0.57
   2       206.2  186.9    87.2   136.4   273.8   65.0    45.1    30.0   -15.1    0.56
13:50:20
 F1 Help  F2 Save  F6 Graf  F9 Info  F10 Run  Alt+F10 Exit          |  6. 6.1995
```

Figure 33. Main centrifugal compressor data for Test Facility II. Design by Hannover University. Some of the data calculated by Jari Backman

Two wheels were manufactured but they were not tested for the Test Facility II.

Commercial compressor

After contacts with major centrifugal compressor manufacturers, a compressor wheel with surrounding equipment was ordered from Garrett. The performance map of the compressor wheel TRIM 50 is illustrated in Figure 17. This compressor is from a vehicle engine turbo charger, in which the peak efficiency is not very important. Therefore, the performance map shows that the maximal isentropic efficiency $\eta_{scTS} = 0.72$ is considerably lower than the efficiencies of the other wheels.

In all the above cases the compressor was equipped with an unbladed stator and a logarithmical scroll.

4.2.2 Turbine

As with the first test facility, it was difficult to find turbine manufacturers and the design was decided to be made by the research group at LUT. A numerical method was developed to use the empirical data found in the literature. The turbine was chosen to be an axial turbine with diffuser in the outward direction from the machine (in Test Facility I the diffuser was inwards directed). The hub-tip-ratio λ was larger than 0.85 so that the blades could be made straight.

The turbine efficiency calculations were based on three different efficiency determinations described in /Ainley and Mathieson 1957/, /Traupel 1968/, /Dunham and Came 1970/, /Dixon 1978/ and /Kacker and Okapuu 1981/. In these determinations the losses of the turbine are divided to:

- internal aerodynamic losses that are born from
  - fluid viscous friction
  - boundary layers in the blades and flow channels
  - turbulence and mixing
- internal frictional losses between the rotationary and stationary parts of the turbine
- external energy losses

The stator and rotor cascades were made by the Sahlberg-method, in which the blade geometry is added to the mean stream line with geometrical means.

The isentropic efficiency was designed to be $\eta_{stTS} = 0.84$, which in the view of the results of the first test facility was considered realistic.

4.2.3 Motor and frequency inverter

The rotational speed was set to 87 300 rpm, which means that the motor has to rotate 1 455 revolutions per second. The increase in speed results in a much smaller motor size /Jokinen 1988/, which in turn is a clear benefit in cost. The motor was designed by the HST motor design group. The research on high speed motors at Lappeenranta University of Technology and at Helsinki University of Technology has concentrated on three major areas:

- motor efficiency. To get a high efficiency from a smaller motor with a high speed current, much scientific work has been done. The current is supplied with the inverter, and it is complicated compared to the normal sinusoidal current. Usually this means increased electrical losses.

- inverter technology. Because the demand of high frequency inverters is still rather small, the manufacturers have not contributed very much in developing high speed inverters. This research has been done in cooperation with Finnish inverter manufacturers.
- cooling solutions. The high circumferential velocity of the motor rotor causes friction in the air surrounding the rotor /Larjola et al 1991c/. Firstly, the friction takes up mechanical power and secondly, it dissipates to heat in the air gap and this heat has to be removed from the motor. Finally, more problems are caused by the mass flow of the cooling fluid, which in turn generates more losses /Larjola et al 1991c/, too.

Motor

The electric motor can be either synchronous or asynchronous. In the synchronous motor the rotor rotates at the speed of the stator frequency and in principal the electrical efficiency is higher than in the asynchronous motor. The problem with this type of motor tends to be the rigidness of the rotor that especially with fluid bearings cannot be tolerated. The rotor has to be made either of dynamo discs or permanent magnets. Although the LUT and HUT research has decided to concentrate on asynchronous electric machines, there are also promising results of permanent magnet synchronous machines /Malmqvist and Chudi 1995/.

The efficiency of an asynchronous motor with inverter current depends on many circumstances. There are various choices of how to coil the stator, and how to manufacture the rotor. The HUT research group has made theoretical calculations concerning the electromagnetical effect of the inverter current.The manufacturing test programme of the rotor electromagnetic surface, made by HST also, has given various solutions for different circumferential speed regions.

The electricity research group at LUT has studied the possibilities of enhancing the efficiency of the solid asynchronous motor and these test results have also been very promising /Pyrhönen 1991/.

A solid rotor with copper coating was chosen for Test Facility II. The surface was ground smooth to ensure small friction losses from the rotating shaft. The motor is a 3-phase induction motor with the nominal power of 5 kW, which exceeded the design cycle power of 2.3 kW (Fig. 31). The motor efficiency was not tested, because the gas bearings are very sensitive to the external load, which makes a dynamometer connection difficult. The rotor losses were estimated to be 180 W, the stator losses 130 W and the electrical efficiency η_{el} = 85%.

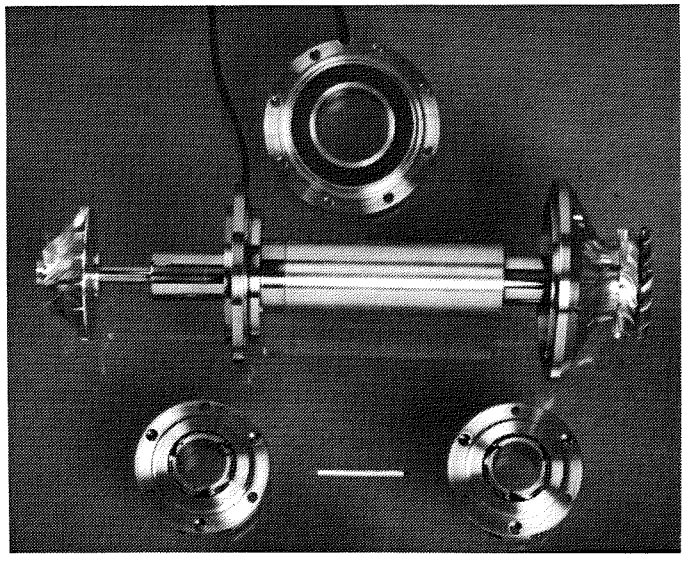

Figure 34. The rotating parts of Test Facility II. Radial compressor on the left, axial turbine on the right, radial gas dynamic bearings at the bottom, motor rotor in the middle and axial magnetig bearing on top. The scale can be seen from the 5 cm match between the radial bearings. Photo Vesa Mikkonen

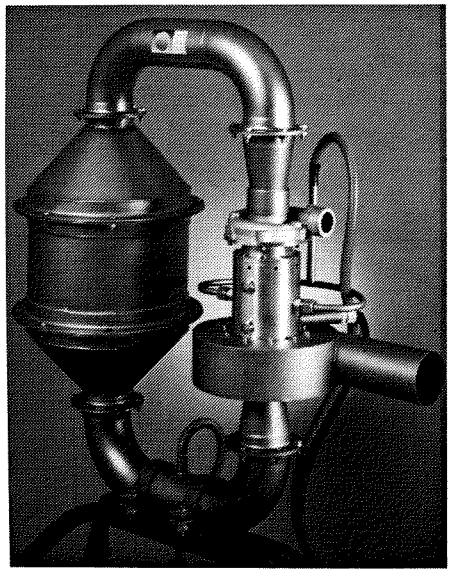

Figure 35. Test Facility II, sub-pressure connection. The rotating part vertically in front in the order: compressor, motor and turbine. The droplet separator can be seen at the back. Photo vesa Mikkonen

Inverter

The inverter was delivered by the Finnish company Oy Vacon Ab. The Vacon 2.2 CX inverter was custom designed for a high speed technology drive.

The test facility layout drawing is presented in Appendix C and the test facility in the sub-pressure connection is in Fig. 35.

Cooling

The exact cooling losses are complex to calculate, because they depend very strongly on the surfaces of the stator and the rotor. Also, the heat transfer coefficients vary depending on these. In the high speed technology research these losses have been experimentally researched /Larjola et al 1991c, Backman 1989/.

The radial gas bearing friction loss[1] can be calculated from /Gunter et al 1964/

$$P_{rb} = \frac{\omega \tau_0 R L p_0 \Lambda n c_f}{6} \tag{58}$$

The rotor free ends cause a friction loss /Polkowski 1984/

$$P_{fe} = \rho \omega^3 R^5 c_m \tag{59}$$

where

$$\mathrm{Re} = \frac{\rho \omega R^2}{\mu} \tag{60}$$

$$c_m = \frac{0.146}{\mathrm{Re}^{0.2}} \tag{61}$$

The friction losses in the air gap between motor rotor and stator for smooth surfaces are /Dibelius 1984/

$$P_{ag} = k \pi \rho \omega^3 R^4 l c_f \tag{62}$$

where

---

[1]*Here, friction loss means the equivalent power that is strained to the mechanical power of the motor*

$$\mathrm{Re} = \frac{\rho \omega R b}{\mu} \tag{63}$$

$$c_f = \frac{0.0105}{\mathrm{Re}^{0.193}} \tag{64}$$

The stator of the test facility motor has normal slots that are large in dimension compared to the air gap. Therefore, their influence to the friction coefficient is difficult to estimate. In the measurements with large molecule organic fluid the surface roughness coefficient k was in the area of 1.7—2.5 /Larjola et al 1991c/.

The axial magnetic bearing disc air gap friction coefficient is /Dibelius 1984/

$$P_{ab} = \rho \omega^3 R^5 c_m \tag{65}$$

when R is disc radius and $c_m = 0.003$ for a disc air gap of 0.2—0.5 mm.The cooling mass flow uses mechanical power in the air gap

$$P_{mf} = 0.48 q_m \omega^2 R^2 \tag{66}$$

The centrifugal compressor wheel also generates losses when exposed to high circumferential speed. These are included in the impeller isentropic efficiency and are therefore excluded here.

Table 2. The cooling calculation ofTest Facility II

Source	Loss[W]	Reynolds nr.
Rotor free end	133	126346
Rotor zylinder	67.9	7657
Impeller disc	85.0	431710
Radial gas bearings	171.6	
Gas gap	49.8	
Axial bearing	79.4	417672
Electric rotor	180.0	

Rotational Speed	Mechanical losses	Cooling mass flow
1455 1/s	382.0 W	0.005 kg/s
Electrical losses	Temperature rise	
180 W + 130 W	86.0 K	

We get the theoretical electromechanical losses by summing the rotor electric losses to Eq. (58)..(66) at the design speed and allowed temperature rise. The calculations are iterative with the cooling mass flow, and the results for internal cooling are given in Table 2. The theoretical mechanical losses are estimated to be 382 W, and the mechanical efficiency to 82%.

4.2.4 Bearings

One distinctive feature of high speed technology is the use of oil-free bearings. The reliability and long lifetime of rotational machinery depend very much on the bearings.

High speed technology research has focused on three different radial bearing types: gas, liquid and active electromagnetic bearings. This test facility is equipped with radial gas bearings and magnetic axial bearings and they are discussed next.

Radial bearings

Gas bearings mainly employ two different types, dynamic and static. The research has concentrated on dynamic bearings, because static bearings are vulnerable to the fact that there always has to be pressurized gas to ensure normal operation. The research group at LUT has a vast experience in designing dynamic gas bearings /Larjola et al 1991a/, /Larjola and Backman 1995/.

Dynamic gas bearings are tilting-pad journal bearings that use the surrounding gas — atmospheric air or process fluid vapour — to create the operative force. The bearings have several pivoted pads, which form the carrying surface of the bearing. When the shaft rotates, the friction of the surrounding gas creates a pressure distribution between the shaft and pad, which separates the solid surfaces /Larjola 1988b/.

One problem is the limited load carrying capacity, especially at the start and at low speeds. At the start, the bearing pad and the shaft contact each other, the system acts as a journal bearing and there can be some wear of the bearing system. This could be avoided with hybrid bearings, where there exist external feed of pressurized gas. However, this in turn complicates the overall system, and in tests the bearing load has been observed to rise at very small speeds /Larjola and Backman 1995/. In inverter supply this wear can be minimized by programming the start sequence to cause minimal radial forces.

The active magnetic bearings were also strongly considered, but the small size of the shaft was decisive, and gas bearings were chosen.

Axial bearing

To limit the gravitational force affecting the radial bearings, the high speed technology machines are usually built vertically. The axial bearing compensates also the forces generated by the pressure distributions around the turbomachine wheels /Backman 1988b/. The high speed technology research has worked very intensively with active magnetic bearings. This technology includes both

axial bearings /Lantto and Anttila 1995/. The chosen axial magnetic bearing was made by HST. The bearing concept consists of two stationary discs with electric coils, of rotationary disc assembled on the shaft, and of the control electronics that supplies the currents. These currents generate the magnetic field, which places the rotationary disc at the desired axial level. The displacement level can be controlled with the accuracy of 1/1000 of mm.

Fig. 34 show also the 22 mm radial gas bearings and the active magnetic axial bearing used in Test Facility II.

4.2.5 Test arrangements

Test Facility II was tested for the sub-pressure connection between September 1995 and May 1996. The main work during this time was dedicated to improving the test conditions and making necessary changes to the facility.

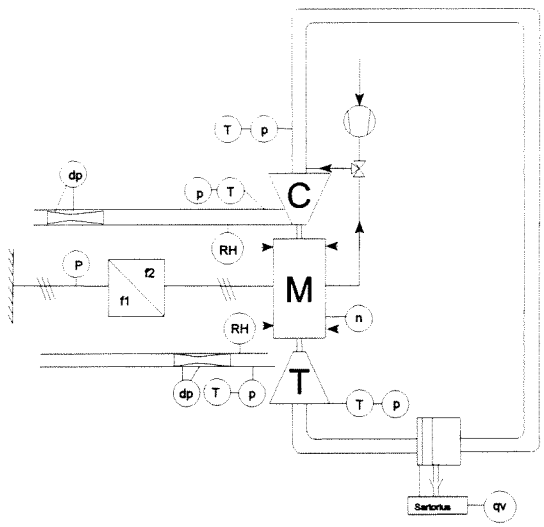

Figure 36. Test Facility II, sub-pressure connection. The cooling of the motor is either with internal cooling via the path atmospheric-motor -compressor or by external blower. The bearings are monitored with a capacitive sensor and an oscilloscope.

Goals of testing

The goals were to operate the test facility at the design point and to make measurements to ensure a satisfactory cooling of the prototype. Experimental knowledge about the process performance would also be valuable.

Test arrangements and instrumentation

The test facility was installed in the test room of the Fluid Dynamics Laboratory at LUT. The test arrangements are illustrated in Fig. 36

The measured parameters were the relative humidity before and after the test facility (*RH*), the essential pressures (*p*) and temperatures (*T*) in the compressor and the turbine, the motor power (*P*) and speed (*n*) and the water extracted from the process (*qv*). The mass flows were measured with two venturis before and after the test facility (*dp*).

The instrumentation arrangement and calibration were conducted in the following manner:

- Relative pressure transducers TRAFAG 8890.21at the inlet and outlet measuring stations with installation and calibration as in Test Facility I.

- Temperature probes were mainly K-type thermocouples with a 0.25 mm conductor diameter. The thermocouples in the compressor were situated at the flanges. The thermocouple manufacturer accuracy is ± 1 °C. The thermocouples were calibrated with a Braun Thermomix S calibrator. This calibration included the whole temperature measurement chain. The estimated accuracy in temperature instrumentation after this procedure was estimated to be ± 0.1 °C.

- The momentarily extracted water was measured with a Sartorius 1413 MP8 scale.

- The mass flows at the inlet and outlet of the cycle were measured with two classical venturis. The Reynolds number and the pipe diameter were below the recommended values /SFS-ISO 5167/, and therefore the venturis were tested against a larger orifice plate device. The discharge factor *C* was then lowered 1%, which coincided with the ISO-standard recommendation. However, the measuring accuracy was estimated to be ± 2%.

- The motor speed was obtained from the motor by a magnetic sensor. The motor supply frequency was taken from the inverter, and the slip was calculated from the supply frequency and the motor speed. The electric inlet power to the system was measured with a Norma AC-Power Analyser.

Data acquisition

The data acquisition of the process parameters was made in the same fashion as in Test Facility I. All the parameters were measured with electrical sensors, and the signals were directed to the Fluke

Hydra, and then forwarded to an IBM PC-based computer via the RS-232 serial bus. The computer runs the RBC2TEST-programme, which was upgraded from the one used in Test Facility I.

4.2.6 Test results—sub pressure cycle

There were 34 different sub-pressure connection tests which lasted totally 70 hours. The longest test lasted 4.5 hours.

In Fig. 37 there are the measured process values from a quasistationary moment of the process compared with the design programme results with the same inlet values, pressure ratio and pressure losses.

The results in Fig. 37 are with the internal cooling flow that is directed from the motor air gap to the sub-pressure piping between the turbine and the compressor. This increases the compressor mass flow and inlet temperature, and means that the cycle input power is increased. The turbine mass flow and power calculations have been corrected to the program results.
Fig. 38 shows the changes in the mass flow and the pressure ratio, and Fig. 39 the powers and the temperatures when cooling is changed on/off.

4.2.7 Errors and uncertainties

The errors in Test Facility II resemble those in Test Facility I. There are some small deviations. The temperature errors are smaller because of the more accurate calibration method. The mass flow measurement is slightly more inaccurate because of the lower mass flow.

4.2.8 Discussion on Test Facility II

The operation of the test facility proved to be reliable. The mechanical system needed only one inspection during 18 months and the inverter functioned without any faults. The tests were found to partly fill the requirements stated earlier, and the test facility was very operative.

The installation and calibration of the test facility was time consuming. In some cases the experiences of Test Facility I gave false indications in planning the measurements. Because the relative humidity measurement corresponded well with turbine operation, we decided first to use only the inlet humidity measurements. Also the mass flow measurements were decided to be taken from the

compressor manufacturer's map. All these elements were, however, added to the measurements, as can be noted from Fig. 35.

Data aquisition programme RBC2TEST

```
Time  09:44:00        10.09.96  LUT/Energy Technology       Measures   0 pcs
 Reversed Brayton       T        h        p        yi       yh        RH
 Sub pressure          [ C ]  [kJ/kg]  [ kPa ]                        %
        72.
 0 - inlet state         8.9     24.8     99.3  0.9938   0.0062     86.8
 4 - turbine outlet     -4.7      4.0     67.8  0.9962   0.0038    100.0
 1 - compressor in       5.4     15.1     67.3  0.9962   0.0038     45.8
 2 - compressor out     52.3     62.6    100.8  0.9962   0.0038      4.4

 axial bearing temperature    80.0
 Vaisala temperatur      8.2    51.8
 compressor power      Pk  =  3.2514 kW    compressor efficiency    = 0.7287
 turbine power         Pt  =  1.1262 kW    turbine efficiency       = 0.6904
 heat power            Plä =  4.6785 kW    heat Coefficient Of Pr.  = 1.7612
 calc. elect. power    Ps  =  2.6564 kW    eletromech. efficiency   = 0.7982
 mass flow turbine     qmt =  0.0543 kg/s  qmeq =  0.0548 kg/s
 mass flow compressor  qmk =  0.0684 kg/s  qmap =  0.0747 kg/s
 rotational speed       N  =   85812 rpm   Neqt =   86735 rpm
 rotational mass flow  qm  =  0.0629 kg/s  Neqk =  89472 rpm
 measured efficiency   Pco =  0.7263       blade SR  =  0.7561
 input electric power  Pel =  2.6624 kW

1EXIT     2Cont       3Temp_G     4Cond_G     5Effi_G     6FILEAJO1009A  7Step
```

Process design programme BCD

```
  Data  Input  Efficencies  PressLoss  HeatExch  Optimization  OffDesign
               Reversed Brayton Cycle in sub pressure process mode  | ©LUT&HST
  <-■->                        RBC2SUB1.rbc                        Window: 2
  Heat Exchanger connection number 5
  Cycle points                   T        h        p        wi        wh      Fii
                               [ °C ]  [kJ/kg]  [ kPa ]                        %
  0 - Cycle inlet               8.9     24.8     99.3   0.9938    0.0062    86.8
  3 - Turbine inlet             8.9     24.8     99.3   0.9938    0.0062    86.8
  4 - Turbine outlet           -4.7      5.0     67.8   0.9962    0.0038   100.0
  4*- MistElim outlet          -4.7      5.0     67.3   0.9962    0.0038   100.0
  3 - HeatEx outlet             5.4     15.2     67.3   0.9962    0.0038    45.7
  2 - Compressor outlet        52.2     62.6    100.8   0.9962    0.0038     4.5
  2*- Cycle outlet             52.2     62.6     99.3   0.9962    0.0038     4.4


  Compressor power      Pc  =   3.24 kW   compressor isentropic eff.= 0.726
  Turbine power         Pt  =   1.12 kW   turbine isentropic eff.   = 0.690
                                          mechanical eff.          = 0.877
  Motor electric power Ps   =   2.66 kW   motor electrical eff.     = 0.910
  Refrigeration power  Pre  = 694.53 W    refrigeration COP        = 0.304
  Turbine mass flow     qm  =  0.054 kg/s Compressor mass flow   qm = 0.068 kg/s
  Rotational speed       N  =  85812 rpm  Droplet separation     Ds = 100.0 %
  Condensate mass flow  qv  =  0.476 kg/h Vaporizate power      Pva = 413.4 W
  Specific energy       Psm =   5.59 Wh/g
F1 Help  F2 Save  F6 Graf  F9 Info  F10 Run  Alt+F10 Exit        | 15. 9.1995
```

Figure 37. The measured and design sub-pressure process compared to each other at a stabilized test point.

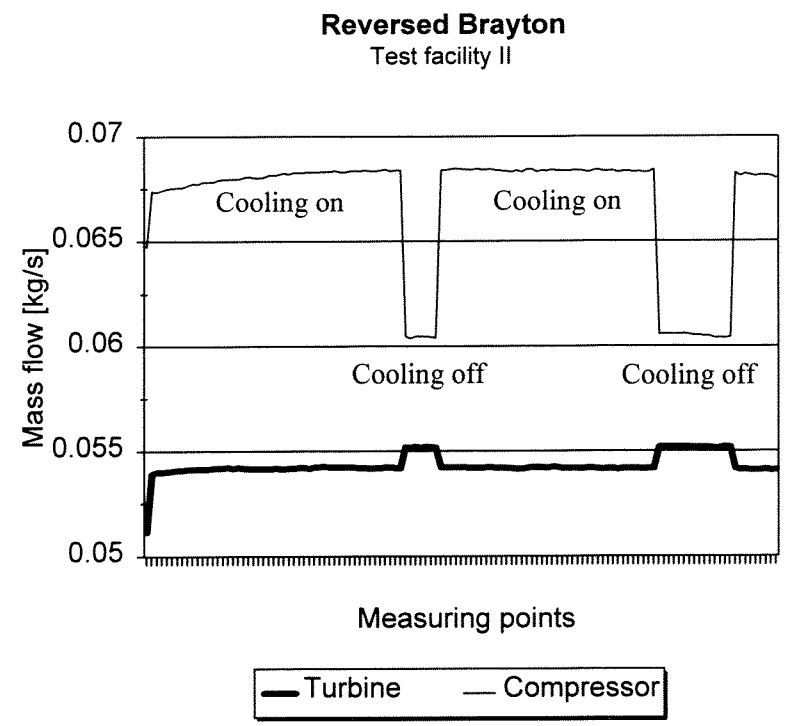

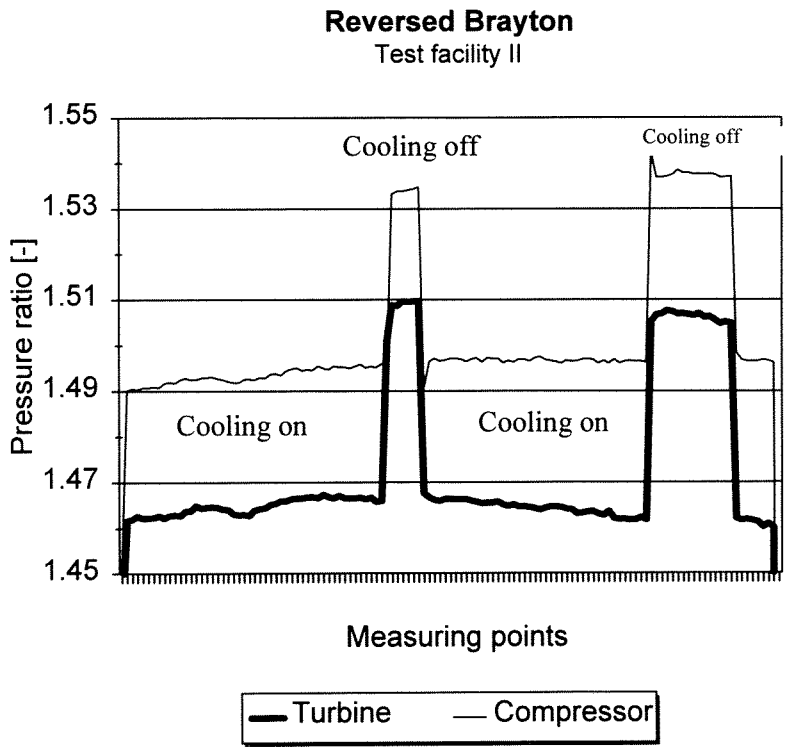

Figure 38. Mass flows and pressure ratios of the compressor and the turbine at Test Facility II

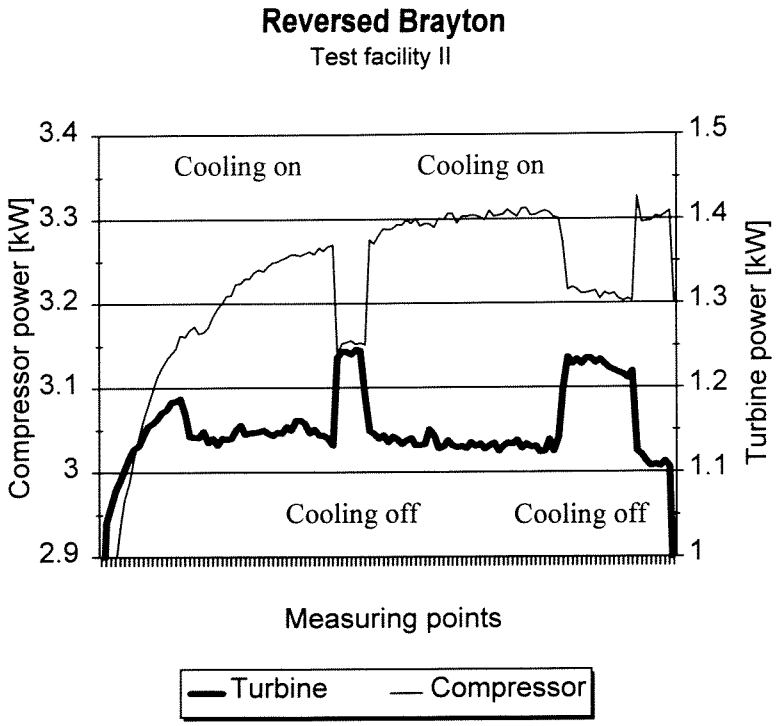

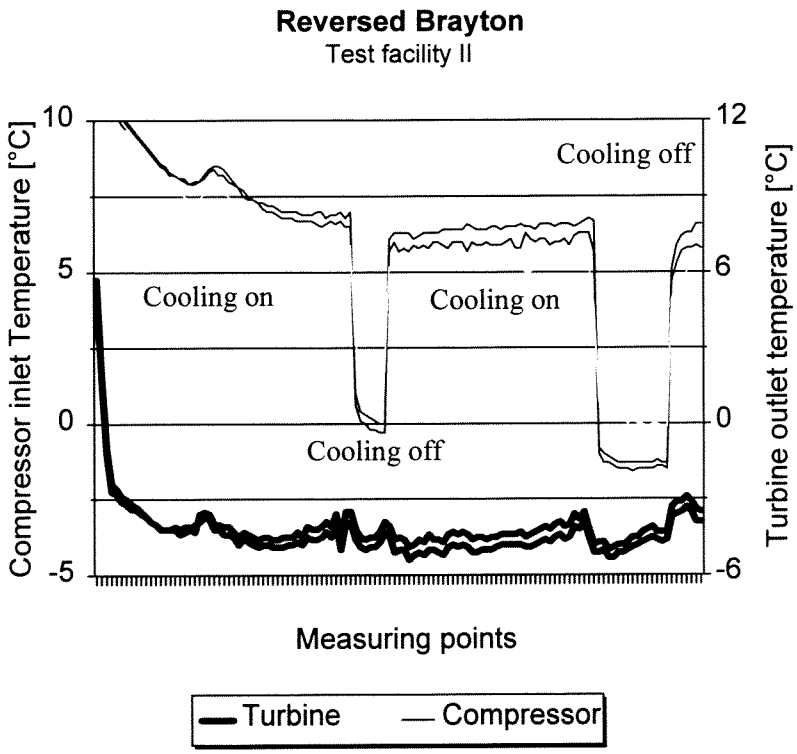

Figure 39. Powers and temperatures of the compressor and the turbine at Test Facility II

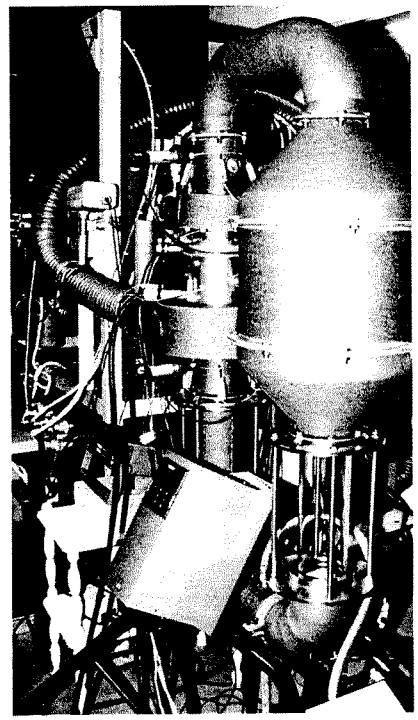

Figure 40. Test Facility II in test. In front the Vacon 2.2 CX inverter. The pipings and the droplet separator were isolated. To the right of the inverter is the glass pipe, which was used for visual mist determination. Photo Timo Mikkola.

The actual motor power measurement was troublesome. At the first measurements between May and August 1995, we measured the current and voltage from one stage before and after the inverter. The system power factor was assumed to be very close to one and therefore the motor power measurement indicated 50-70% too high values. The oscillation of the current was 20% with 1-2 Hz frequency oscillation. At the same time the mass flow of the cycle was calculated to be 20% too high. The most problematic element was the turbine operation that turned out to be moderate, the isentropic efficiency was measured to be about 70%.

The higher mass flow was due to an overestimation of the boundary layer blockage. To remedy the problem, the blades of the turbine wheels were machined 5% shorter. Also a more comprehensive, one-phase power measurement was installed before the inverter.

In the following tests from August 1995 to May 1996, the cycle measurements agreed much better with the expectations. The power factor was found to be much lower than one, which information had a considerable effect on the power calculation based on the current and the voltage. The reason for this was the relatively large capacitors in the inverter circuits. Still, the power oscillation was

about 10% with the 1-2 Hz frequency. The mass flow calculations were suspected to be erronous, because the mass flow behaved inconsistently at lower operational speeds.
The internal cooling worked with the desired effect. The maximum temperature (measured at axial magnetic bearing) was set to 110 °C and was usually achieved by opening the valve 30 %. When the valve was totally open, this temperature dropped to 90 °C. Normally the valve was kept half-open and the temperature was about 100 °C. The internal cooling raised the compressor mass flow, the inlet temperature and the motor power. The temperature mixing before compressor was not complete, and there were considerable differencies in the three inlet temperature sensors.

When the mass flow measurements were installed, it was discovered that compressor mass flow was over 10% lower than calculated. The compressor map was verified with the manufacturer representative but in the view of the above results, it does not seem to be valid.

With the reduction of the mass flow, there was again a clear difference in power. After instrument and sensor checks, a three-phase power measurement was installed to measure the inlet power. The measurement showed that the power was slightly unsymmetric, which caused the above mentioned oscillation in a single phase. The overall power was quite steady and the power was smaller than measured before. The values in Fig. 37..39 are from these last tests.

The noise at the test facility was measured to be around 85 dB, when the inlet and outlet flows were directed out of the measuring room. There was no noise filter design.

To examine the droplet size in the flow itself, a laser droplet size measurement was made in May 1996 by the Laboratory of Energy Engineering and Environmental Protection at Helsinki University of Technology. This time the measuring channel was more suited, but there were problems with the channel windows. To avoid water droplets on the surfaces, an air stream was arranged to the windows. Unfortunately, this stream proved to be difficult to control. If the stream was too weak, the water droplets gathered very rapidly on the surface. With better air stream the conditions in the channel changed and the condensation product began to vaporize. The Laboratory could confirm from the few good measurements the previous results obtained at Test Facility I.

5. APPLICATIONS

The commercial utilization of the reversed Brayton cycle is possible if target processes can be found, where high efficiency, small size and environmentally friendly fluid give competitive design properties. To demonstrate the feasibility of the system, three application concepts are presented: an air dryer, a heat pump and a refrigeration machine. There are several cases in each concept.

The performance of the Reversed Brayton cycle can be evaluated with the BCD-programme. The main parameters affecting the performance are discussed below. These application calculations are not intended to explain individual devices, but to show how a realistically designed reversed Brayton cycle machinery operates. In reality there are usually extra, case dependent connections needed to fine tune the apparatus to the actual process. All the calculations are made with the same cycle mass flow 1 kg/s, to give better understanding of the characteristic parameters in the process calculation results.

If the mass flow is kept constant, the design rotational speed varies with different pressure ratios. The rotational speed and the pressure ratio are dependent of the compressor specific speed N_s that is defined /Balje 1981/ as

$$N_s = \frac{2\pi N\sqrt{q_{v1}}}{\Delta h_s^{0.75}} \tag{67}$$

The best performance for a radial compressor can be achieved with specific speeds between 0.7 and 1.0, and it can be assumed that the turbine covers approximately half of the needed compressor power.

Eq. (67) can be used to make a chart (Fig. 41) that shows the approximated rotational speed and the power of the reversed Brayton cycle as a function of the pressure ratio. The rotational speed and power of the sub-pressure cycle is slightly lower than those of the over-pressure cycle.

It should be noted that the inverter control gives an important tool to the process control. The possibility to adjust the rotational speed of the motor permits a large range of operation. Therefore, the reversed Brayton cycle device can operate at different optimal pressure ratios, depending of the process parameters at a given time.

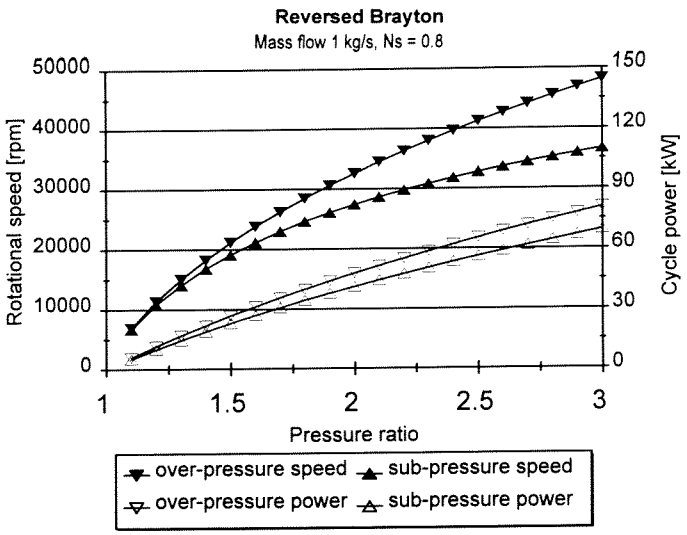

Figure 41. Reversed Brayton cycle rotational speed and power for different pressure ratios. Compressor isentropic efficiency $\eta_s = 0.8$ and motor electromechanical efficiency $\eta_{em} = 0.86$.

5.1 Air dryer

CASE 1

Let us consider a simple sub-pressure process connection (number 4 in Fig. 15) that can be used as an air dryer, such as the test facilities described in this thesis. The process calculation uses the following parameters to optimize the operation:

- the inlet air temperature is between 20 and 60 °C
- the relative humidity of the inlet air is between 60 and 100%
- the pressure ratio is between 1.1 and 3
- the mechanical efficiency is 93%, the electric efficiency 93%, the compressor isentropic efficiency 80%, and the turbine efficiency 82%. These efficiencies correlate to those achieved during the high speed technology research.
- the pressure losses are considered to be 100 Pa at the inlet of the turbine, 1 kPa at the droplet separator and 1 kPa at the outlet of the compressor

This kind of air dryers would be used to keep the ambient relative humidity at desired level in houses, offices and industrial premises, to clear the possible condensation when cooling occurs, or to dry humid or moist processes (laundry drying). The high relative humidity deteriorates products in broad fields, such as metal and electrical components corrosion. Especially in the tropics the high relative humidity affects practically all functions.

From these parameters the main cycle characteristics can be evaluated with the BCD-programme. The optimized parameters are the specific energy E_s and condensation mass flow $q_{m,wat}$, Fig 43.

One of the calculation points from the programme is shown in Fig. 42.

```
          Reversed Brayton Cycle in sub pressure process mode  | ©LUT&HST
<-■->                        CH5CAS1A.RBC                      Window: 3
Heat Exchanger connection number 4
Cycle points                    T        h        p        wi        wh       Fii
                              [ °C ]  [kJ/kg]  [ kPa ]                          %
0 - Cycle inlet                40.0    135.8    100.0    0.9624    0.0376    80.0
3 - Turbine inlet              40.0    135.8     99.9    0.9624    0.0376    79.9
4 - Turbine outlet             24.2    101.8     62.5    0.9694    0.0306   100.0
4*- MistElim outlet            24.2    101.8     61.5    0.9694    0.0306   100.0
2 - Compressor outlet          80.1    160.0    101.0    0.9694    0.0306    10.3
2*- Cycle outlet               80.1    160.0    100.0    0.9694    0.0306    10.2


Compressor power      Pc  =  57.77 kW   compressor isentropic eff.= 0.800
Turbine power         Pt  =  34.06 kW   turbine isentropic eff.   = 0.820
                                        mechanical eff.           = 0.930
Motor electric power  Ps  =  27.42 kW   motor electrical eff.     = 0.930
Heating power         Phe =   23.0 kW   heating COP               = 0.838
Turbine mass flow     qm  =  1.000 kg/s Compressor mass flow   qm  = 0.993 kg/s
Rotational speed      N   =  23000 rpm  Droplet separation     Ds  = 100.0 %
Condensate mass flow  qv  = 25.871 kg/h Vaporizate power      Pva =  17.3 kW
Specific energy       Psm =   1.06 Wh/g
```

Fig. 42. Calculation point of the sub-pressure connection nr. 4

It can be noted that the specific electricity consumption is lower, and the amount of condensed water amount is bigger at higher inlet temperatures. The optimum point of the E_s is around 1 Wh/g, when the relative humidity is high. The condensation mass flow increases when the relative humidity or the pressure ratio are increased.

CASE 2

The heat exchange connection number 9 in Fig. 15 is also rather simple. Applying the same design principles as above and having

- heat exchanger pressure loss of Δp = 200 kPa
- heat exchanger temperature difference of ΔT = 10 °C

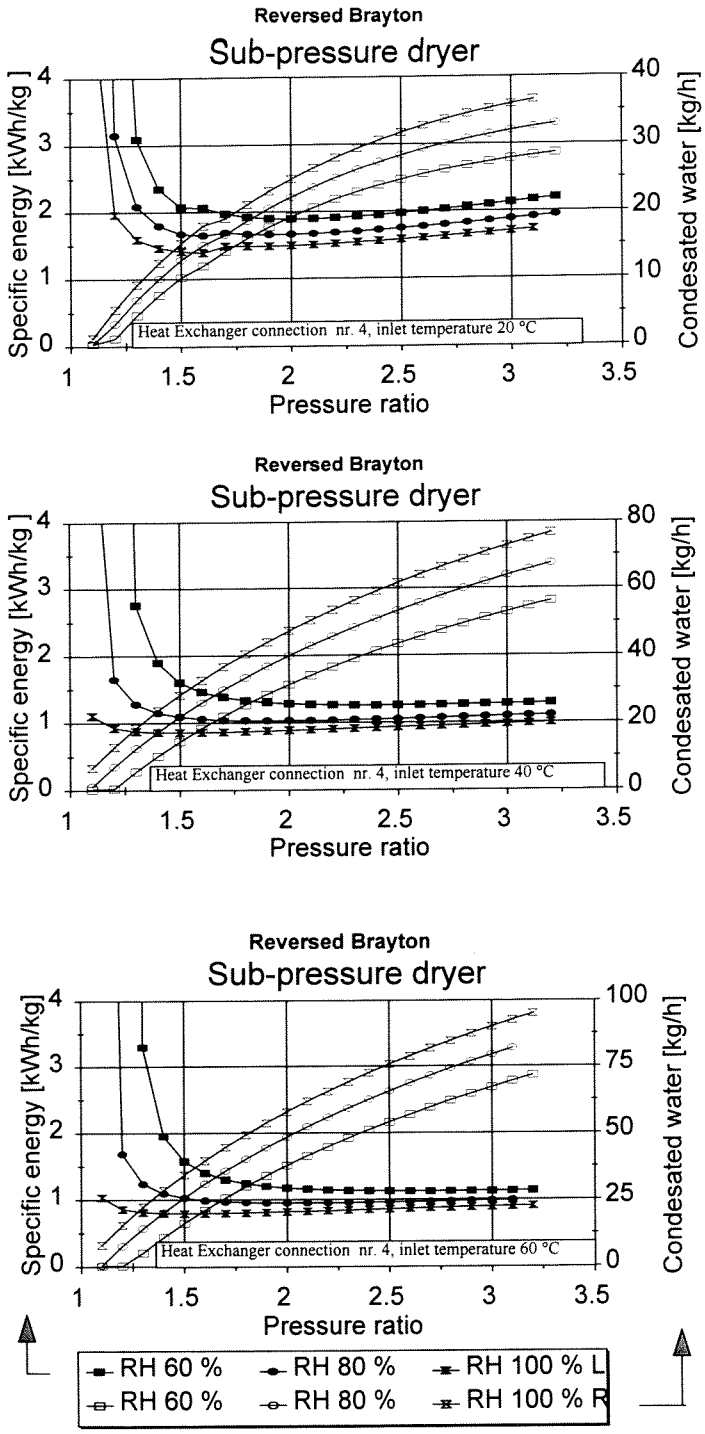

Figure 43. Sub-pressure air dryer characteristics.

Fig. 45 shows a slightly lower energy consumption with this connection. The regeneration lowers the needed pressure ratio and therefore the overall losses are smaller. The amount of condensed water is somewhat higher as is the outlet temperature. These differences are also obvious from Fig. 44, where the inlet conditions are the same as in Fig. 42.

When the pressure ratio is more than 2, the increase of condensed water at the inlet temperature of 20 °C becomes smaller. The explanation is as follows: the temperature after the turbine is so low that all water has condensed to water or ice. The values with pressure ratios above 1.7 are also unsatisfactory, because the energy consumption E_s has increased. At higher inlet temperatures this phenomenon occurs at higher pressure levels. Clearly the freezing point might limit the general use of this connection at lower relative humidity and pressure ratio values.

```
          Reversed Brayton Cycle in sub pressure process mode  | ©LUT&HST
<-■->                        CH5CAS1B.RBC                       Window: 3
Heat Exchanger connection number 9
Cycle points                    T       h       p       wi       wh      Fii
                              [ °C ]  [kJ/kg] [ kPa ]                    %
0 - Cycle inlet                40.0    135.8   100.0   0.9624   0.0376   80.0
3 - HeatEx inlet               40.0    135.8    99.9   0.9624   0.0376   79.9
3 - HeatEx outlet              35.4    128.6    99.7   0.9634   0.0366  100.0
4 - Turbine outlet             23.0     94.9    62.5   0.9716   0.0284  100.0
4*- MistElim outlet            23.0     94.9    61.5   0.9716   0.0284  100.0
5 - HeatEx outlet              30.0    102.2    61.3   0.9716   0.0284   64.8
2 - Compressor outlet          87.4    161.9   101.0   0.9716   0.0284    7.1
2*- Cycle outlet               87.4    161.9   100.0   0.9716   0.0284    7.1

Compressor power      Pc  =  59.12 kW   compressor isentropic eff.= 0.800
Turbine power         Pt  =  33.62 kW   turbine isentropic eff.   = 0.820
                                        mechanical eff.           = 0.930
Motor electric power  Ps  =  29.49 kW   motor electrical eff.     = 0.930

Turbine mass flow     qm  =  0.999 kg/s Compressor mass flow   qm = 0.991 kg/s
Rotational speed      N   =  23000 rpm  Droplet separation     Ds = 100.0 %
Condensate mass flow  qv  = 34.017 kg/h Vaporizate power      Pva =  22.8 kW
Specific energy       Psm =   0.87 Wh/g
```

Fig. 44. Calculation point of the regenerative sub-pressure connection nr. 9

When controlling the sub-pressure connections, the flow is not very sensitive to speed change. When the speed increases, the pressure ratio and volume flow increase, and the inlet pressure and density of the compressor decrease. Thus, the mass flow change is small. The decrease in the inlet temperature of the compressor, due to the increased expansion, has a smaller effect on the density.

The sub-pressure air dryer functions in two ways. It condensates water from the process and the flow from compressor outlet can be directed back to the process. This dry air at high temperature enhances the drying phenomenon.

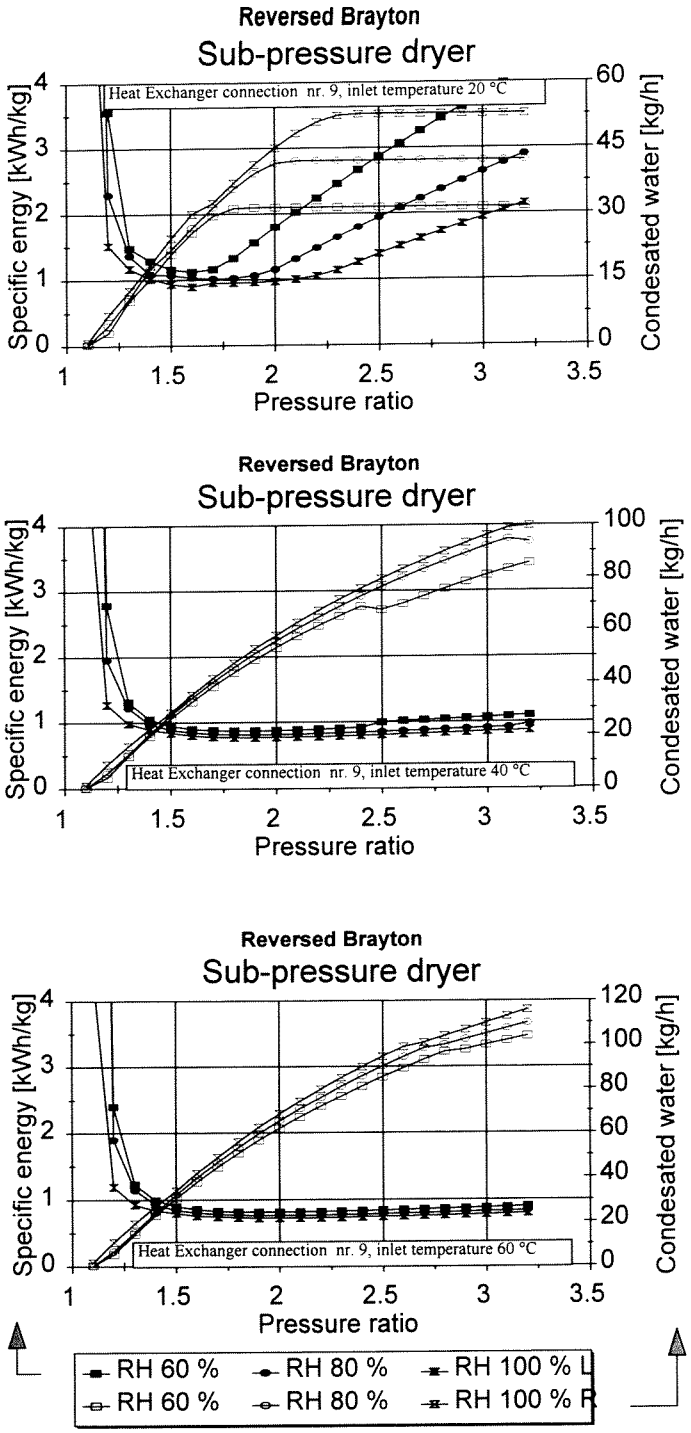

Figure 45. Regenerative sub-pressure air dryer.

CASE 3

The next dryer connection is an over-pressure connection, number 1 in Fig. 15, where the heat exchanger is between the compressor and the turbine. Water is used at the secondary side to cool the air back to the temperature of the inlet condition. The warmed water is not considered here as an asset to the calculations. One of the calculation points is shown in Fig. 46. The results in Fig. 47 show that this connection operates at lower inlet temperatures at the same level as the previous connections, but the water gives a clear increase in condensation at higher inlet temperatures.

```
          Reversed Brayton Cycle in sub pressure process mode  | ©LUT&HST
<-■->                      CH5CAS1C.RBC                        Window: 3
Heat Exchanger connection number 1
Cycle points                  T       h       p       wi       wh      Fii
                           [ °C ]  [kJ/kg] [ kPa ]                      %
0 - Cycle inlet             20.0    49.9    100.0   0.9883   0.0117   80.0
1 - Compressor inlet        20.0    49.9     99.0   0.9883   0.0117   79.2
2 - Compressor outlet       73.5   104.7    160.0   0.9883   0.0117    8.3
3 - HeatEx outlet           20.0    43.4    159.8   0.9908   0.0092  100.0
4 - Turbine outlet           1.9    12.9    101.1   0.9957   0.0043  100.0
4*- MistElim outlet          1.9    12.9    100.1   0.9957   0.0043  100.0
5 - Cycle outlet             1.9    12.9    100.0   0.9957   0.0043   98.9


Compressor power     Pc  =  54.78 kW   compressor isentropic eff.= 0.800
Turbine power        Pt  =  30.45 kW   turbine isentropic eff.   = 0.820
                                       mechanical eff.           = 0.930
Motor electric power Ps  =  28.14 kW   motor electrical eff.     = 0.930

Compressor mass flow  qm =  1.000 kg/s Turbine mass flow qm      = 0.993 kg/s
Rotational speed       N =  26000 rpm  Droplet separation     Ds = 100.0 %
Condensate mass flow  qv = 26.768 kg/h Vaporizate power      Pva =  18.3 kW
Specific energy      Psm =   1.05 Wh/g
```

Fig. 46. Calculation point of the water cooled over-pressure connection nr. 1

The results at lower pressure ratios in Fig. 47 are slightly erroneous, because the effect of water cooling is so big, and energy consumption is highly dependent on the pressure losses in the heat exchanger. Also, the pumping power of the secondary side is omitted.

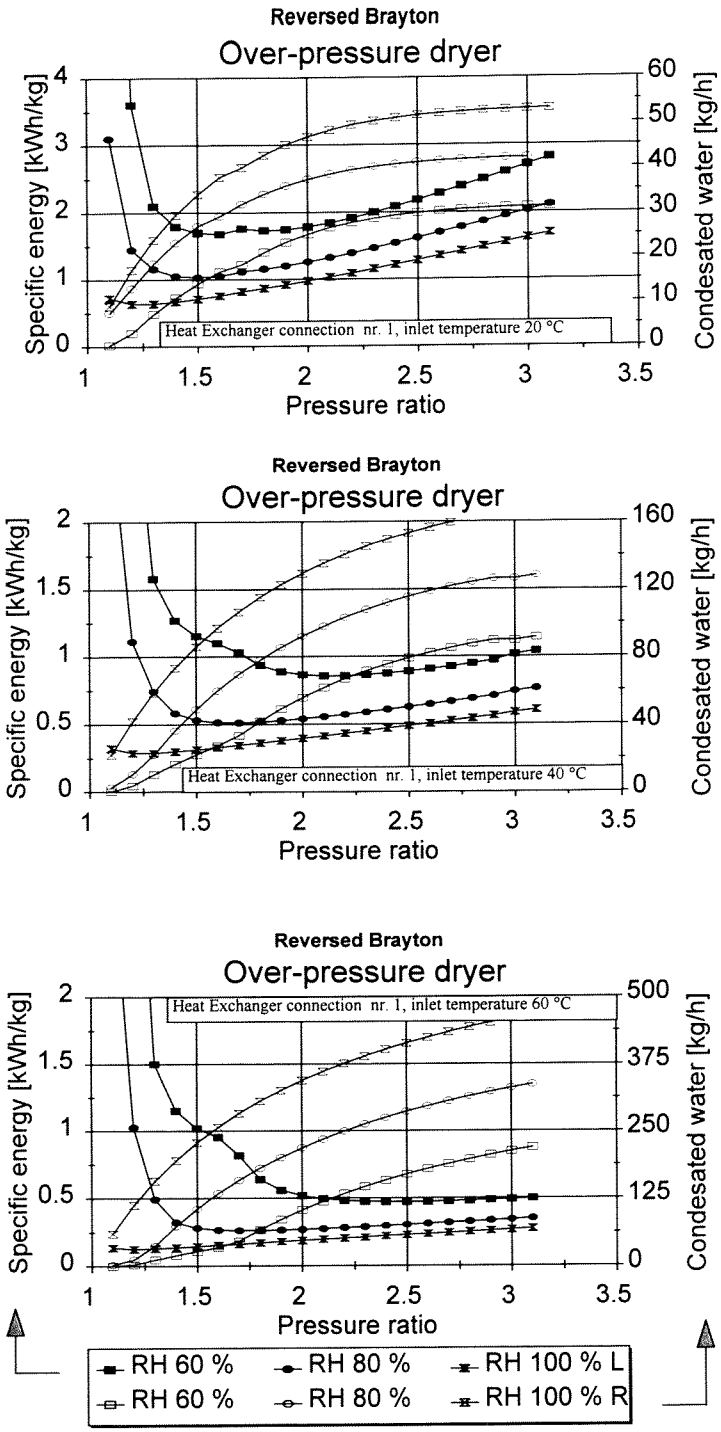

Figure 47. Water cooled over-pressure air dryer characteristics.

CASE 4

The last dryer example is a regenerative over-pressure connection, number 3 in Fig. 15. The results in Fig. 48 and Fig. 49 are quite close to those in the sub-pressure connections.

In the over-pressure cycle there are clear choices, depending of the drier application. For a drier with heating, the regenerative system would be chosen. The water cooled system would be the appropriate choice for cooled air output.

```
          Reversed Brayton Cycle in sub pressure process mode  | ©LUT&HST
<-■->                        CH5CAS1D.RBC                       Window: 3
Heat Exchanger connection number 3
Cycle points                   T       h       p       wi       wh      Fii
                             [ °C ]  [kJ/kg] [ kPa ]                     %
0 - Cycle inlet               40.0   135.8   100.0   0.9624   0.0376   80.0
1 - Compressor inlet          40.0   135.8    99.0   0.9624   0.0376   79.2
2 - Compressor outlet         96.6   195.3   160.0   0.9624   0.0376   10.5
3 - HeatEx outlet             44.3   138.3   159.8   0.9632   0.0368  100.0
4 - Turbine outlet            31.4   104.2   101.3   0.9714   0.0286  100.0
4*- MistElim outlet           31.4   104.2   100.3   0.9714   0.0286  100.0
5*- HeatEx outlet             86.6   161.7   100.1   0.9714   0.0286    7.4
5 - Cycle outlet              86.6   161.7   100.0   0.9714   0.0286    7.4

Compressor power      Pc  =  59.44 kW   compressor isentropic eff.= 0.800
Turbine power         Pt  =  33.77 kW   turbine isentropic eff.   = 0.820
                                        mechanical eff.          = 0.930
Motor electric power  Ps  =  29.68 kW   motor electrical eff.     = 0.930

Compressor mass flow  qm  =  1.000 kg/s Turbine mass flow qm      = 0.991 kg/s
Rotational speed       N  =  14000 rpm  Droplet separation     Ds = 100.0 %
Condensate mass flow  qv  = 33.064 kg/h Vaporizate power      Pva =  22.1 kW
Specific energy       Psm =   0.90 Wh/g
```

Fig. 48. Calculation point of the regenerative over-pressure connection nr. 3

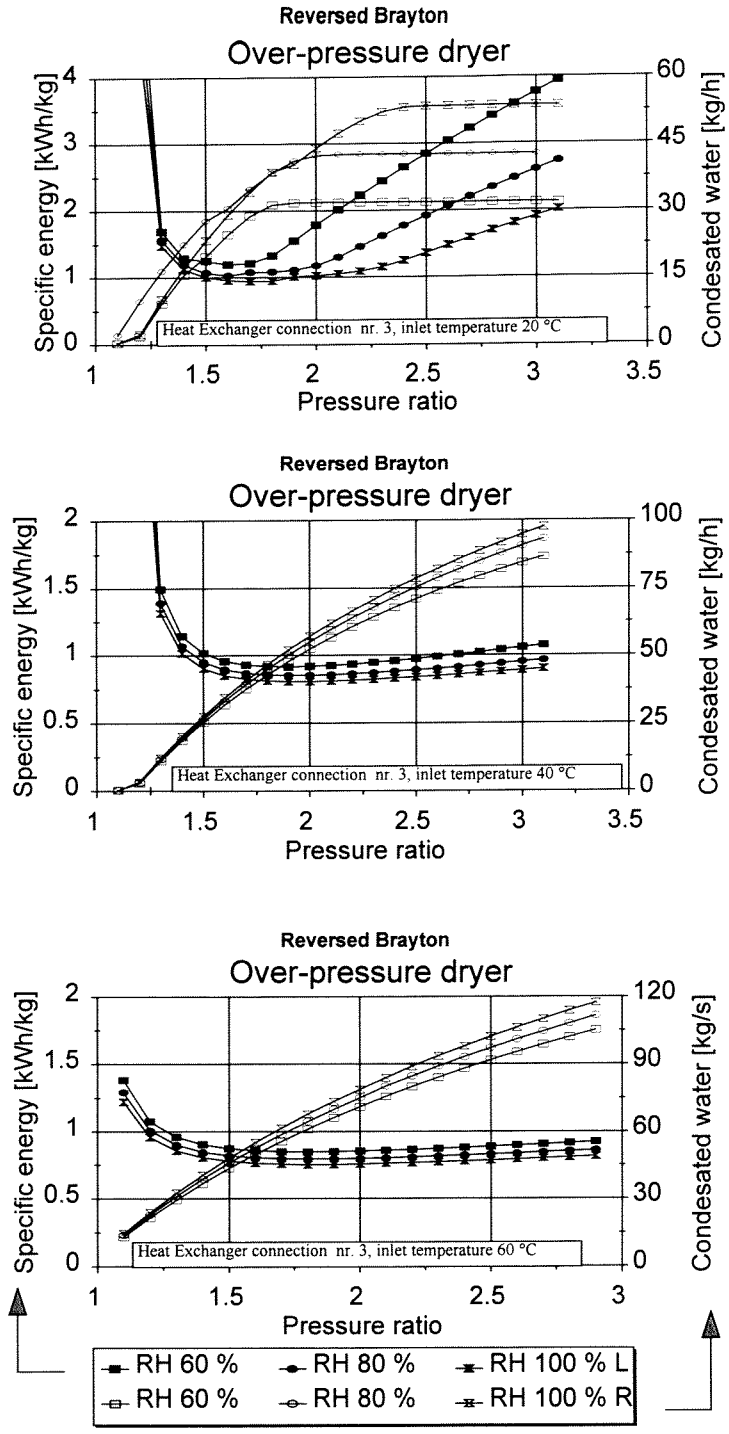

Figure 49. Regenerative over-pressure air dryer characteristics.

5.2 Heat pump

Heat pump systems are discussed separately, although the air dryers in Chapter 5.1 could also considered to be heat pumps. Heat pump connections could be used for example in milk drying as discussed in Chapter 1, in different drying applications in pulp and paper mill industry, as well as in building ventilation applications.

The heat pump concept is more complicated than the air dryer, and the connections usually involve special arrangements. Sometimes only part of the process flow is directed to the heat pump and then mixed back to the process. There can also be several heat exchangers in a series, and part of the flow can be separated from the main flow.

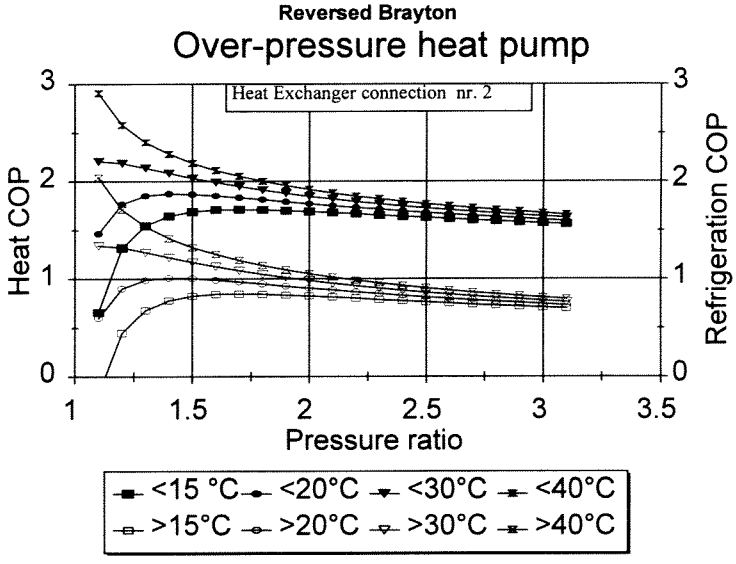

Figure 50. Over-pressure heat pump, heat exchange connection 2. Turbine inlet temperature T = 22 °C.

CASE 5

The over-pressure connection number 2 is used in the following study as a heat pump connection for heating and ventilation purposes. The same cycle parameters apply as stated in Chapter 5.1, but the temperature of the turbine inlet is set to 22 °C, which would be the temperature for example inside a building. The temperature of the compressor inlet is varied between 15 and 35 °C. The coefficients of heat ε_h and refrigeration ε_r are plotted as functions of pressure ratio in Fig. 50. The performance of the heat pump is modest but the connection is operational.

CASE 6

The second heat pump application is a which is done with heat exchange connection 1 in Fig. 15. The inlet temperature of the compressor is set to 22 °C, The flow to the building is directed through the heat exchanger secondary side, where the air is warmed with the outlet temperature of the compressor. The heat pump coefficient of performance ε_h depends of the temperature outside the building. The lower the outside temperature is, the bigger gain is achieved with the heat pump. The heat exchanger temperature difference is assumed to be 3 °C. A calculation case with outside temperature of 5 °C is shown in Fig. 51, and the heat pump characteristics with different outside temperatures are shown in Fig. 52.

```
          Reversed Brayton Cycle in sub pressure process mode  | ©LUT&HST
<-■->                        CH5CAS1A.RBC                       Window: 3
Heat Exchanger connection number 1
Cycle points                    T       h       p       wi       wh      Fii
                              [ °C ]  [kJ/kg] [ kPa ]                     %
0 - Cycle inlet                22.0    43.2   100.0   0.9917   0.0083   50.0
1 - Compressor inlet           22.0    43.2    99.0   0.9917   0.0083   49.5
2 - Compressor outlet          68.3    90.4   150.0   0.9917   0.0083    6.9
S - Outside temperature         5.0
3 - HeatEx outlet               8.0    19.5   149.8   0.9955   0.0045  100.0
4 - Turbine outlet             -9.2    -4.7   101.1   0.9983   0.0017  100.0
4*- MistElim outlet            -9.2    -4.7   100.1   0.9983   0.0017  100.0
5 - Cycle outlet               -9.2    -4.7   100.0   0.9983   0.0017   98.9


Compressor power      Pc  =  47.20 kW   compressor isentropic eff.= 0.800
Turbine power         Pt  =  25.02 kW   turbine isentropic eff.   = 0.820
                                        mechanical eff.           = 0.930
Motor electric power  Ps  =  25.64 kW   motor electrical eff.     = 0.930
Heating power         Phe =  70.90 kW   heating COP               = 2.769
Compressor mass flow  qm  =  1.000 kg/s Turbine mass flow qm      = 0.993 kg/s
Rotational speed      N   =  14000 rpm  Droplet separation     Ds = 100.0 %
Condensate mass flow  qv  = 23.581 kg/h Vaporizate power      Pva =  16.0 kW
Specific energy       Psm =   1.09 Wh/g
```

Fig. 51.Heating and ventilation heat pump at outside temperature of +5 °C

The characteristics show very high coefficients of performance at low pressure ratios. This is again slightly erroneous, because the fan power is omitted. The calculation shows very promising results with the pressure ratio levels between 1.3 and 2. If the temperature difference of the heat exchange were bigger than 3 °C, the temperatures in Fig. 52 would, respectively, be smaller.

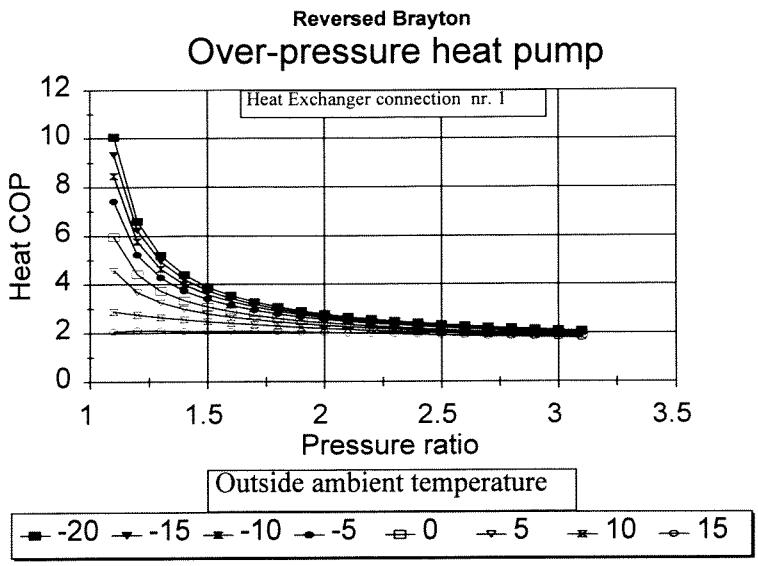

Figure 52. Over-pressure heat pump characteristic for different outside temperatures, heat exchange connection 1 for heating and ventilation. Compressor inlet temperature $T = 22$ °C.

5.3 Refrigeration machines

CASE 7

The third application group are refrigeration machines like the Kajima-concept discussed in Chapter 1. The heat pump connection in case 6 can be altered with two valves to a cooling connection. The outside, warm air on the heat exchanger secondary side is used only to cool the compressor outlet temperature, and the cool air from the turbine is directed to the building. With the temperature of 22 °C and relative humidity of 80% inside the building, the system operates with a moderate performance, Fig. 54. However, the cooling is effective as can be seen from the operation calculation with the outside temperature of 35 °C, Fig. 53.

Reversed Brayton Cycle in sub pressure process mode | ©LUT&HST
<-■-> CH5CAS2A.RBC Window: 3
Heat Exchanger connection number 1

Cycle points	T [°C]	h [kJ/kg]	p [kPa]	wi	wh	Fii %
0 - Cycle inlet	22.0	55.8	100.0	0.9867	0.0133	80.0
1 - Compressor inlet	22.0	55.8	99.0	0.9867	0.0133	79.2
2 - Compressor outlet	68.2	103.1	150.0	0.9867	0.0133	11.0
3 - HeatEx outlet	38.0	72.2	149.8	0.9867	0.0133	47.8
4 - Turbine outlet	15.9	44.4	101.1	0.9888	0.0112	100.0
4*- MistElim outlet	15.9	44.4	100.1	0.9888	0.0112	100.0
5 - Cycle outlet	15.9	44.4	100.0	0.9888	0.0112	98.9

Compressor power	Pc	=	47.34 kW	compressor isentropic eff.	=	0.800	
Turbine power	Pt	=	27.73 kW	turbine isentropic eff.	=	0.820	
				mechanical eff.	=	0.930	
Motor electric power	Ps	=	22.67 kW	motor electrical eff.	=	0.930	
Refrigeration power	Pre	=	11.43 kW	refrigeration COP	=	0.504	
Compressor mass flow	qm	=	1.000 kg/s	Turbine mass flow qm	=	0.998	kg/s
Rotational speed	N	=	14000 rpm	Droplet separation	Ds =	100.0	%
Condensate mass flow	qv	=	7.546 kg/h	Vaporizate power	Pva =	5.1	kW
Specific energy	Psm	=	3.00 Wh/g				

Fig. 53. Cooling connection at the outside temperature of +35 °C. In principle the same connection used in Fig. 49 and 50.

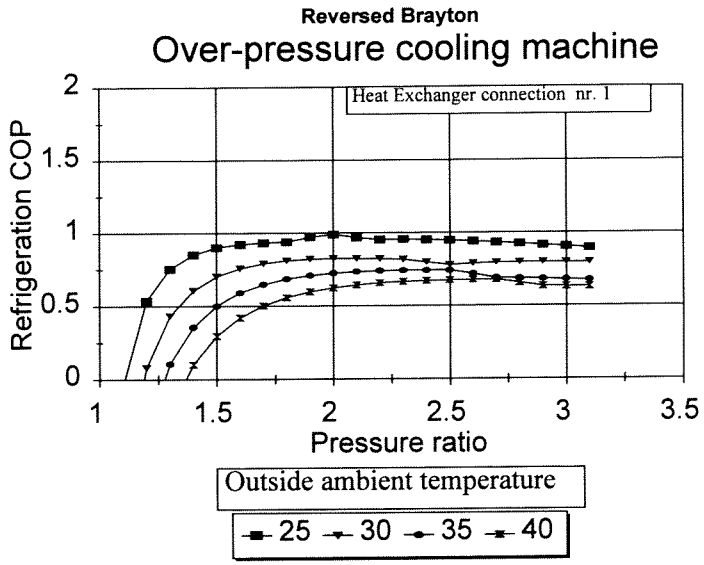

Figure 54. Over-pressure cooling device characteristics for different outside temperatures, heat exchange connection 1 for cooling. Compressor inlet temperature $T = 22$ °C.

CASE 8

A second alternative is to look at a sub-pressure connection to have the same influence.Basically with the same operating values as in Fig. 53, the sub-pressure connection number 5 in Fig.15 is calculated. The connection operates at a higher cooling performance, and the cooled air has a considerably lower temperature, Fig. 55.

```
          Reversed Brayton Cycle in sub pressure process mode  | ©LUT&HST
<-■->                        CH5CAS2B.RBC                      Window: 3
Heat Exchanger connection number 5
Cycle points                  T       h       p       wi       wh      Fii
                            [ °C ]  [kJ/kg] [ kPa ]                    %
0 - Cycle inlet              22.0    55.8    100.0   0.9867   0.0133   80.0
3 - Turbine inlet            22.0    55.8     99.9   0.9867   0.0133   79.9
4 - Turbine outlet            6.1    28.6     66.7   0.9912   0.0088  100.0
4*- MistElim outlet           6.1    28.6     65.7   0.9912   0.0088  100.0
3 - HeatEx outlet            32.0    66.0     65.5   0.9867   0.0133   29.1
2 - Compressor outlet        81.8   117.2    101.0   0.9867   0.0133    4.2
2*- Cycle outlet             81.8   117.2    100.0   0.9867   0.0133    4.1


Compressor power      Pc  =  51.16 kW   compressor isentropic eff.= 0.800
Turbine power         Pt  =  27.27 kW   turbine isentropic eff.   = 0.820
                                        mechanical eff.          = 0.930
Motor electric power  Ps  =  27.62 kW   motor electrical eff.    = 0.930
Refrigeration power   Pre =  37.47 kW   refrigeration COP        = 1.357
Turbine mass flow     qm  =  1.000 kg/s Compressor mass flow   qm = 1.000 kg/s
Rotational speed      N   =  14000 rpm  Droplet separation     Ds =   0.0 %
```

Fig. 55. Sub-pressure cooling connection at the outside temperature of +35 °C.

The optimal pressure ratio seems to be around 1.5 and the cooling operates better in warmer weather. This connection has one interesting feature; if the water is not removed from the cycle, the cooling coefficient of performance will be higher, line 30* in Fig. 56.

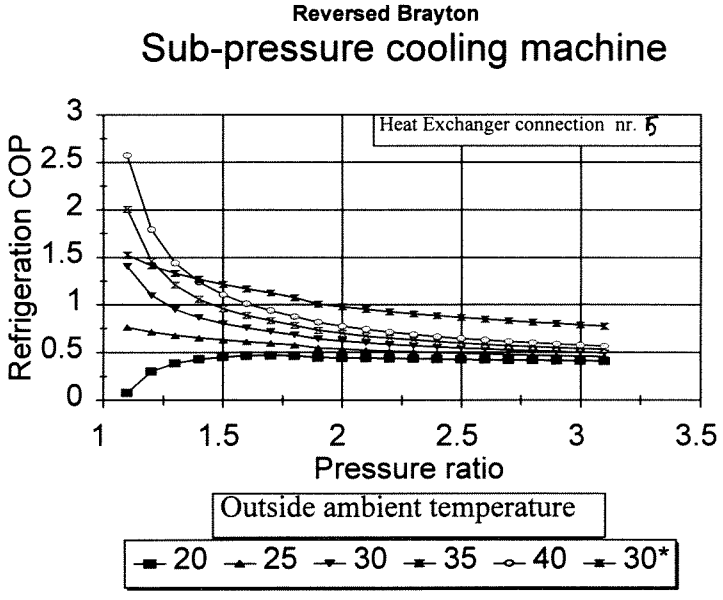

Figure 56. Sub-pressure cooling device characteristics for different outside temperatures, heat exchange connection 1 for cooling. Turbine inlet temperature $T = 22$ °C. Line 30* means operation where the water condensated in the turbine is not removed in the heat exchanger.

Both cooling device calculations assume that all the circulated air flows through the machinery, and the coefficient of performance is calculated for the whole process. By mixing the flow from inside the building with fresh ambient air, sometimes performance of the Brayton cycle can be enhanced. In the over-pressure cycle this mixing raises the compressor inlet temperature and the temperature difference. The actual power depends on the control of the cooling and is not discussed here.

CASE 9

The third refrigeration connection produces very low temperatures, number 9 in Fig. 15. The ambient air is directed through a regenerative heat exchanger, where the temperature is lowered. Then, in the actual refrigeration process, the temperature rises before entering the turbine. This connection is assumed to operate with dry air, because the heat transfer in the regenerative heat exchanger is very sensitive to inlet air humidity. The achievable process temperature curves for different pressure ratios are presented in Fig. 57.

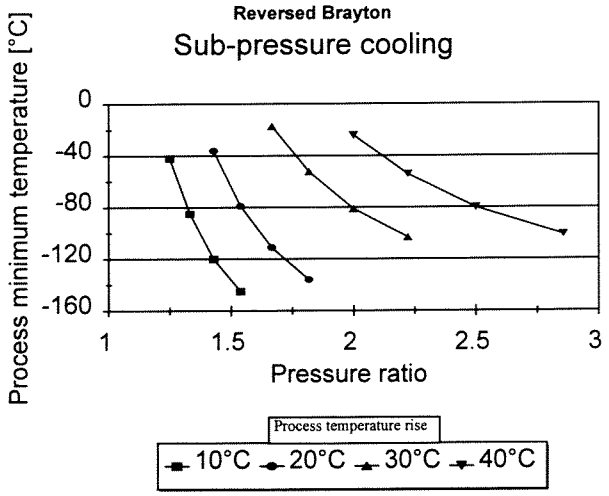

Figure 57. Sub-pressure, heat exchange connection 9 for cooling.

6. DISCUSSION AND CONCLUSIONS

This thesis introduces a high speed technology application that uses environmentally friendly working fluid, humid air. The reversed Brayton cycle is a new concept in high speed technology, and with this process it is possible to build devices with good overall efficiency. This technology can also extend the use of the reversed Brayton cycle to applications where conventional bearings and drives cannot operate.

The design programme and the test facilities described in this study give evidence of already mature technology. The inverters and gas dynamic bearings have operated well in laboratory conditions. The cooling of the high speed electric machines, due to the high power/weight ratio, can be problematic, but the internal cooling of Test Facility II has worked well. In some drying applications the fluid temperature after the compressor needs to be raised higher, and in those cases internal cooling, as realized here, would be an extra benefit for the cycle.

There are some aspects, however, that need more clarification and research in the future, and should be added into the design instruments.

The pressure losses in various parts of the cycle lower the overall performance, and for a good performance they should be minimized or at least optimized. For future Brayton cycle design, the outlet diameter of the compressor should be chosen so that it prevents the forming of a high dynamic pressure.

The selection of the droplet separator is always a question of optimization between separation efficiency and pressure loss. This is an important issue for commercial devices and needs to be researched more.

The good efficiency of the electrical motor improves the cycle efficiency in two ways as recorded at Test Facility II. It reduces the power in motor losses and the power in removing those losses from the apparatus. The research of the cooling solutions is vital.

Finally, the two test facilities showed that there are still interesting aspects in turbine design, and the work is not necessary simple. With the increased knowledge the manufacturing of compact, high efficiency machines can be realized.

REFERENCES

Ainley D.G. and Mathieson G.C.R. (1957), *A Method of Performance Estimation for Axial-Flow Turbines*. British Aeronautical Research Council, R&M 2974, London, Great Britain.

Anderson, (1990), *Modern Compressible Flow: with historical perspective*, 2nd edition, McGraw-Hill, New York, USA.

AirResearch, (1979), *Cycle Selection of a High-Temperature Heat Pump*, Report DOE/CS/ 40005-T3, Airesearch Manufacturing Company of California, Torrance, USA. 113 p.

Backman, J. (1988a), Development project on high speed compressors. *Conference on High Speed Technology*, Aug 21-28, 1988, Lappeenranta, Finland. pp 91-100

Backman, J. (1988b), Design and test results of an axial magnetic bearing. *Conference on High Speed Technology*, Aug 21-28, 1988, Lappeenranta, Finland. pp 167-174

Backman, J. (1989), *The Structural Optimization of the Low Pressure High Speed Compressor* (in Finnish), Licentiate Thesis, 1989, Lappeenranta, Finland.

Balje, O.E. (1981), *Turbomachines, A Guide to Design, Selection, and Theory.* John Wiley & Sons, Inc., New York , USA. 513 p.

Bronicki, L.H. (1982), Twenty years of ecperience with organic Rankine cycle turbines; their applicability and alternative energy systems, *17th IECEC-Conference*,

Decker, O. (1976), Advanced, high pressure gas bearing circulators, *7th International Gas Bearing Symposium*, paper C,

Dunham, J. and Came, P.M. (1970), Improvements to the Ainley/Mathieson Method of Turbine Performance Prediction. *ASME Journal of Engineering for Power*, July 1970, New York, USA. pp 252-256

Dunn, J.H. (1976), *Inspection of two Brayton Rotating Units after Extensive Endurance Testing*, Research report NASA TM X-73569, NASA Lewis Research Center, Ohio, USA.

Dibelius, G. et al. (1984), Experiments on friction, velocity and pressure distribution of rotating discs. *Heat and Mass Transfer in Rotating Machinery*, Hemisphere publication Company, Washington, USA

Dixon, S.L. (1984), Fluid Mechanics, *Thermodynamics of Turbomachinery (third edition).* Pergamon Press Ltd, Oxford, Great Britain. 263 p.

Flaux, J.P.(1984), *Study and Manufacture of a High Temperature Brayton Cycle Industrial Heat Pump*, 4. Contractors' meeting on heat pumps, Brussels, Belgium. pp. 122- 137.

Glassman, A.J. (editor 1972), *Turbine Design and Application, volume one*. Washington D.C., U.S. Goverment Printing Office. USA. 98 p.

Glassman, A.J. (editor 1975), *Turbine Design and Application, volume three*. Washington D.C., U.S. Goverment Printing Office. USA. 140 p.

Gunter, E.J. and Hinkle, J.G. and Fuller, D.D. (1964), *The Effects of Speed, Load and Film Thickness on the Performance of Gas-lubricated Tilting Pad Journal Bearings*. ASLE Transcription 7.

Habermann, H. and Brunet, M. (1984), *The Active Magnetic Bearing Enables Optimum Damping of Flexible Rotor*, ASME publication number 84-GT-117, Amsterdam, Netherlands.

Heikkinen, M.A. and Lampinen, M.J and Tamasy-Bano, M. (1992), *Thermodynamic Analysis and Optimization of Brayton Process in a Heat Recovery System of Paper Machines*. Research report 71. Helsinki University of Technology, Department of Energy Engineering, Laboratory of Thermal Engineering, Finland. 21 p.

ISO 5389 (1992), *Turbocompressors - Performance Test Code*. International standard, International Organization for Standardization, Geneve, Switzerland. 170 p.

Jokinen, T. and Luomi, J. (1988), High-speed electrical machines. *Conference on High Speed Technology*, Aug 21-28, 1988, Lappeenranta, pp 175-185

Kacker, S. and Okapuu, U. (1981). A Mean Line Prediction Method for Axial Flow Turbine Efficiency. New York, *American Society of Mechanicl Engineering Publication 81-GT-58*. New York, USA. 9 p.

Kajima Corporation (1995), *Refrigerating System using Air as Refrigerant*. Brochure.

Keenan, J. and Keyes, F. and Hill, P. and Moore, J. (1978), *Steam Tables*, John Whiley & Sons Ltd, New York, USA. 156 p.

Lantto, E. and Antila, M. (1995), Active magnetic bearings for high-speed machines, *Stockholm Power Tech*, International Symposium on Electric Power Engineering, June 18-22, 1995, Sweden.

Larjola, J. et al. (1987), *Kotimaisen kaasuturbiinin kehittäminen keski- ja matalalämpöarvoisen kaasun energiamuuntoon* (in Finnish), Research report EN B-62, Lappeenranta University of Technology, Finland.

Larjola, J. (1988a), The principle of High Speed Technology. *Conference on High Speed Technology*, Aug 21-28, 1988, Lappeenranta, Finland. pp 11-28

Larjola, J. (1988b), Basic properties of gas lubricated, titlting-pad journal bearing. *Conference on High Speed Technology*, Aug 21-28, 1988, Lappeenranta, Finland. pp 139-151

Larjola, J. (1988c), *The Design of a Radial Compressor* (in Finnish), Aalef, Lappeenranta, Finland. 60 p.

Larjola, J. et al (1991a), *Suurnopeustekniikan perustutkimuskohteet* (in Finnish), Research report EN B-71, Lappeenranta University of Technology, Finland.

Larjola, J. et al (1991b), *Electricity from Waste Heat Using the Organic Rankine Cycle*, Energy exploration & exploitation Vol 9, Nr 4.

Larjola, J. and Backman, J. (1995), Oilfree bearings in high-speed technology, *Stockholm Power Tech*, International Symposium on Electric Power Engineering, June 18-22, 1995, Sweden.

Larjola, J. et al (1995), *The Basic and Applied Research of High Speed Technology at the Department of Energy Technology of Lappeenranta University of Technology from 1/1991 to 5/1995. Final Report* (in Finnish), Research report EN D-38, Lappeenranta University of Technology, Finland.

Liepmann, H. W. and Roshko, A. (1957), *Elements of Gasdynamics*, John Wiley & Sons Inc., New York, USA.

Ling, Z. and Li, S. (1988), An Approach to Performance Prediction of Gas Wet Steam Turbo Expanders, *International Journal of Turbo & Jet-Engines 5*(1988)1-4, pp. 271- 278.

Malmqvist, A and Chudi, P. (1995), Experiences from high speed systems for hybride vehicles, *Stockholm Power Tech*, International Symposium on Electric Power Engineering, June 18-22, 1995, Sweden.

Moore, J. and Sieverding, C.H. (1976), *Two-Phase Steam Flow in Turbines and Separators*.Edited. London, Hemisphere Publishing Corp. 377 p.

Newton, I. (1686), *Philosophiae Naturalis Principia Mathematica* (in Latin), Translation in Swedish, Liber Läromedel, Kristianstad 1986, Sweden.

Pyrhönen, J. (1991), *The High-Speed Induction Motor: Caculating the Effects of Solid-Rotor Material on Machine Characteristics*, Dissertation, Acta Polytechnica Scandinavica, Electrical Engineering Series No. 68, Helsinki, Finland.

Sahlberg, P. (1993), *Thermodynamic Analysis of Reverse Brayton Cycle and Experimental Apparatus utilizing High-speed Technology* (in Finnish), Licentiate Thesis, Lappeenranta, Finland.

Sahlberg, P.-H. (1988), *Turbine Operating at the Sublimation Area of the Humid Air* (in Finnish), Graduate seminar, Helsinki University of Technology, Espoo, Finland.

Sallinen, P. (1993), *Flow Dynamic of Fluid Bearing* (in Finnish), Research report EN D-27, Lappeenranta University of Technology, Finland.

Schmidt, E. (1989), *Properties of Water and Steam in SI-units*, SpringerVerlag, Berlin, Germany. 206 p.

SFS-ISO 5167 (1987), *Measurement of Fluid Flow by Means of Orifice Plates, Nozzles and Venturi Tubes inserted in Circular Cross-section Conduits running full*

Sirén, K. (1995), *Measurements in Ventilation Technology* (in Finnish), Tietonova Oy, Espoo, Finland.

SMM,Société de Mécanique Magnétique (1984), *Application of Active Magnetic Bearings in the Machine Tool Industry*, Vernon Cedex, France.

Swift,W. and Sixsmith,H. (1982), *A Small Centrifugal Pump for Circulating Cryogenic Helium*, Advances in Cryogenic engineering, Vol. 27, Plenum Publication Company, England.

Traupel, W. (1968), *Thermische Turbomaschinen. Band 1,* Springer-Verlag, Berlin, Germany. 522 p.

Vargaftig, N.B. (1975), *Tables of the Thermophysical Properties of Liquids and Gases* (second edition). John Wiley & Sons Inc, Washington, D.C., USA. 755 p.

Watson, N. and Janota, M.S. (1982), *Turbocharging the Internal Combusting Engine*. The Macmillan Press Ltd, London, Great Britain. 595 p.

Wilson, D.G. (1991), *The Design of Gas Turbine Engines*, Thermodynamics and Aerodynamics, IGTI/ASME. Atlanta, USA. 402 p.

Young, J.B. (1989), *Wet Steam Turbines*, Whittle Laboratory, Cambridge University, England. 30 p.

Zucrow, M.J. and Hoffmann, J.D. (1976), *Gas Dynamics*, Volume I, John Wiley & Sons Inc, New York, USA.

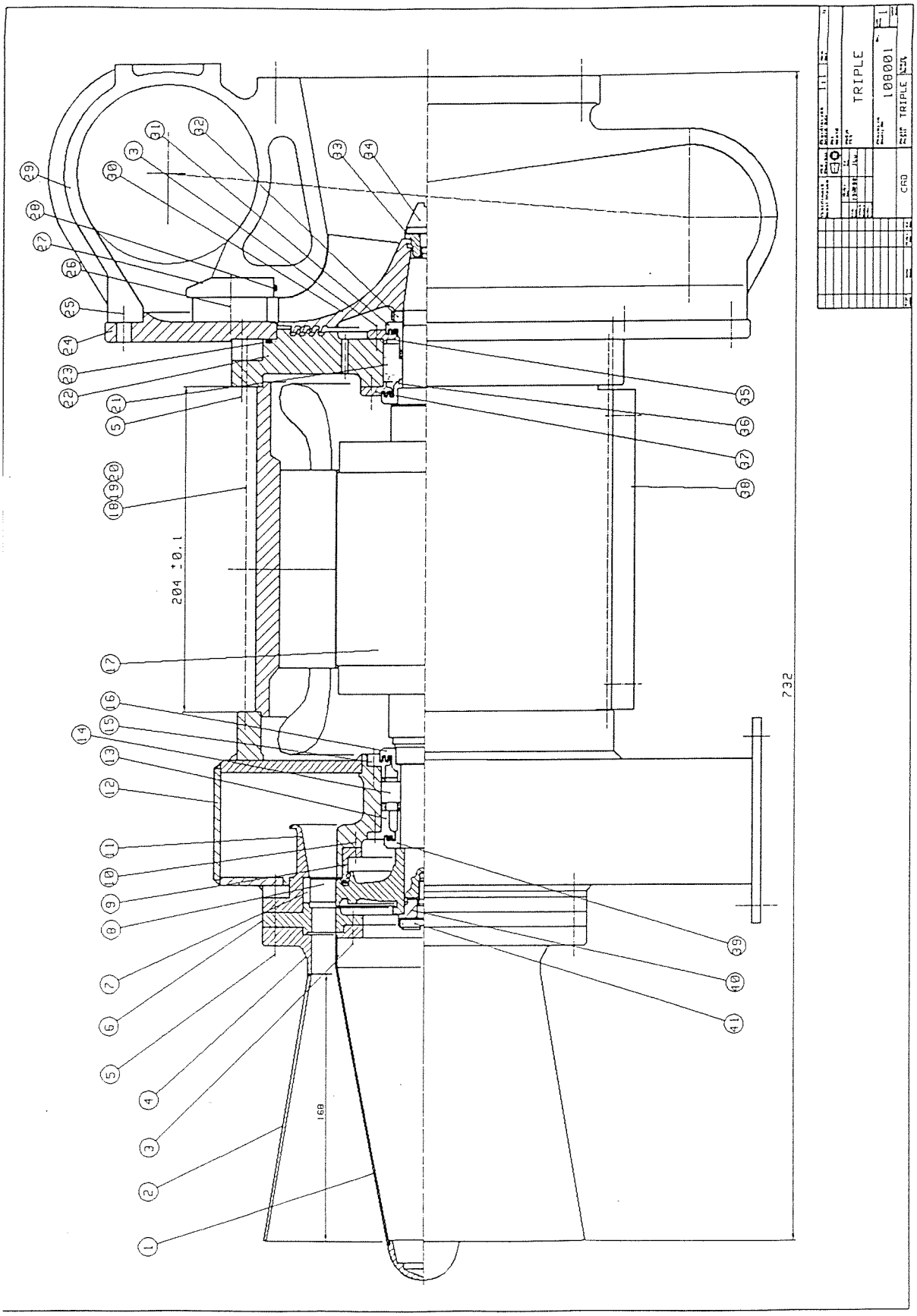
TRIPLE
100001
CAD
204 ±0.1
732
168

Uncertainty calculation **APPENDIX B.1**

1) The condensated water mass flow

$$q_{m,wat} = q_{m,t}(w_{vap0} - w_{vap1}) \tag{1}$$

where

$$w_i = \mu \frac{p'_{vapi}}{\frac{p_i}{\varphi_i} - p'_{vapi}} \tag{2}$$

The first term in the denominator uncertainty is

$$d\frac{p}{\varphi} = \pm\left[\left(\frac{1}{\varphi}\right)^2 dp^2 + \left(\frac{p}{\varphi^2}\right)^2 (d\varphi)^2\right]^{\frac{1}{2}} \tag{3}$$

The denominator (p^*) uncertainty becomes

$$dp^* = \pm\left[\left(d\frac{p}{\varphi}\right)^2 + (dp_{vap,i})^2\right]^{\frac{1}{2}} \tag{4}$$

The humidity uncertainty becomes

$$dw_i = \pm\left[\left(\frac{1}{p^*}\right)^2 (p_{vap,i})^2 + \left(\frac{p_{vap,i}}{(p^*)^2}\right)^2 (dp^*)^2\right]^{\frac{1}{2}} \tag{5}$$

Condensation uncertainty from Eq.

$$dq_{m,wat} = \left[q_{m,wat}^2 (dw_1^2 + dw_2^2) + dq_{m,wat}^2 (dw_1 - dw_2)^2\right]^{\frac{1}{2}} \tag{6}$$

For the subpressure the parameters with uncertainies are

p_1	= 101.6 kPa ± 0.2 kPa	p_1	= 76.7 kPa ± 0.2 kPa
φ_1	= 69.2 % ± 1.0 %	φ_1	= 100 %
p'_{vap}	= 1366 Pa ± 40 Pa	p'_{vap}	= 793 Pa ± 30 Pa
w_1	= 0.00848	w_2	= 0.00675
q_1	= 0.399 kg/s ± 0.004 kg/s		

With Eq. (3)...(5) we get

dp/φ	= ±2.14 kPa	dp/φ	= ±0.2 kPa
dp^*	= ±2.14 kPa	dp^*	= ±0.21 kPa
dw_1	= ±0.00030	dw_2	= ±0.0005

And the condensated mass flow is

$$dq_{m,wat} = 1.216 \pm 0.327 \text{ g/s} = 4.378 \text{ kg/h} \pm 1.177 \text{ kg/h}$$

2) The electric power P_{in}

$$P_{el} = \frac{q_{m,c}(h_{03} - h_{02}) - q_{m,t}(h_{00} - h_{04})}{\eta_{inv}\eta_{mech}\eta_{el}}$$

where we mark $\Theta_1 = T_2 - T_1$ and $\Theta_1 = T_0 - T_4$ with respective uncertainties

$$d\theta_i = \left[dT_{i2}^2 - dT_{i1}^2\right]^{\frac{1}{2}}$$

and assume constant c_p. The nominator uncertainty is

$$dP_n = \left[\left(q_{m,c}d\theta_1\right)^2 + \left(q_{m,t}d\theta_2\right)^2 + \left(dq_{m,c}\theta_1\right)^2 + \left(dq_{m,t}\theta_2\right)^2\right]^{\frac{1}{2}}$$

And the electric power uncertainty

$$dP_{el} = \left[\left(\frac{dP_n}{\eta_m\eta_e\eta_{inv}}\right)^2 + \left(-\frac{P_n}{\eta_m^2\eta_e\eta_{inv}}\right)^2 d\eta_m^2 + \left(-\frac{P_n}{\eta_m\eta_e^2\eta_{inv}}\right)^2 d\eta_e^2 + \left(-\frac{P_n}{\eta_m\eta_e\eta_{inv}^2}\right)^2 d\eta_{inv}^2\right]^{\frac{1}{2}}$$

For the subpressure the parameters with uncertainies are

$q_{m,c}$	= 0.399 kg/s ± 0,004 kg/s	T_0	= 17.3 °C ± 0,5°C
φ_1	= 0.398 kg/s ± 0,004 kg/s	T_4	= 3.5 °C ± 0,5°C
T_1	= 3.9 °C ± 0,5°C	η_m	= 0.88 ± 0.02
T_2	= 40.4 °C ± 0,5°C	η_e	= 0.88 ± 0.02
P_{el}	= 8,25 kW	η_{inv}	= 0.95 ± 0.02

First temperature difference uncertainty $d\Theta_1 = d\Theta_2 = \pm 0.71$°C
Then nominator $dP_n = \pm 0.40$ kW
The electric power becomes $P_{in} =$ 8.25 kW ± 0.57 kW

3) The specific electric energy E_s

$$E_s = \frac{P_{el}}{q_{m,wat}}$$

The uncertainty dE_s is

$$dE_s = \left[\left(\frac{1}{dq_{m,wat}}\right)^2 dP_{el}^2 + \left(\frac{P_{el}}{q_{m,wat}^2}\right)^2 dq_{m,wat}^2\right]^{\frac{1}{2}}$$

For the subpressure the parameters with uncertainies are

$q_{m,wat}$ = 3.02 kg/s ± 0.69 kg/h $\qquad$ P_{el} = 8.25 kW ± 0.57 kW

And the specific electric energy in drying is

E_s = 2.73 kWh/kg$_{wat}$ ± 067 kWh/kg$_{wat}$

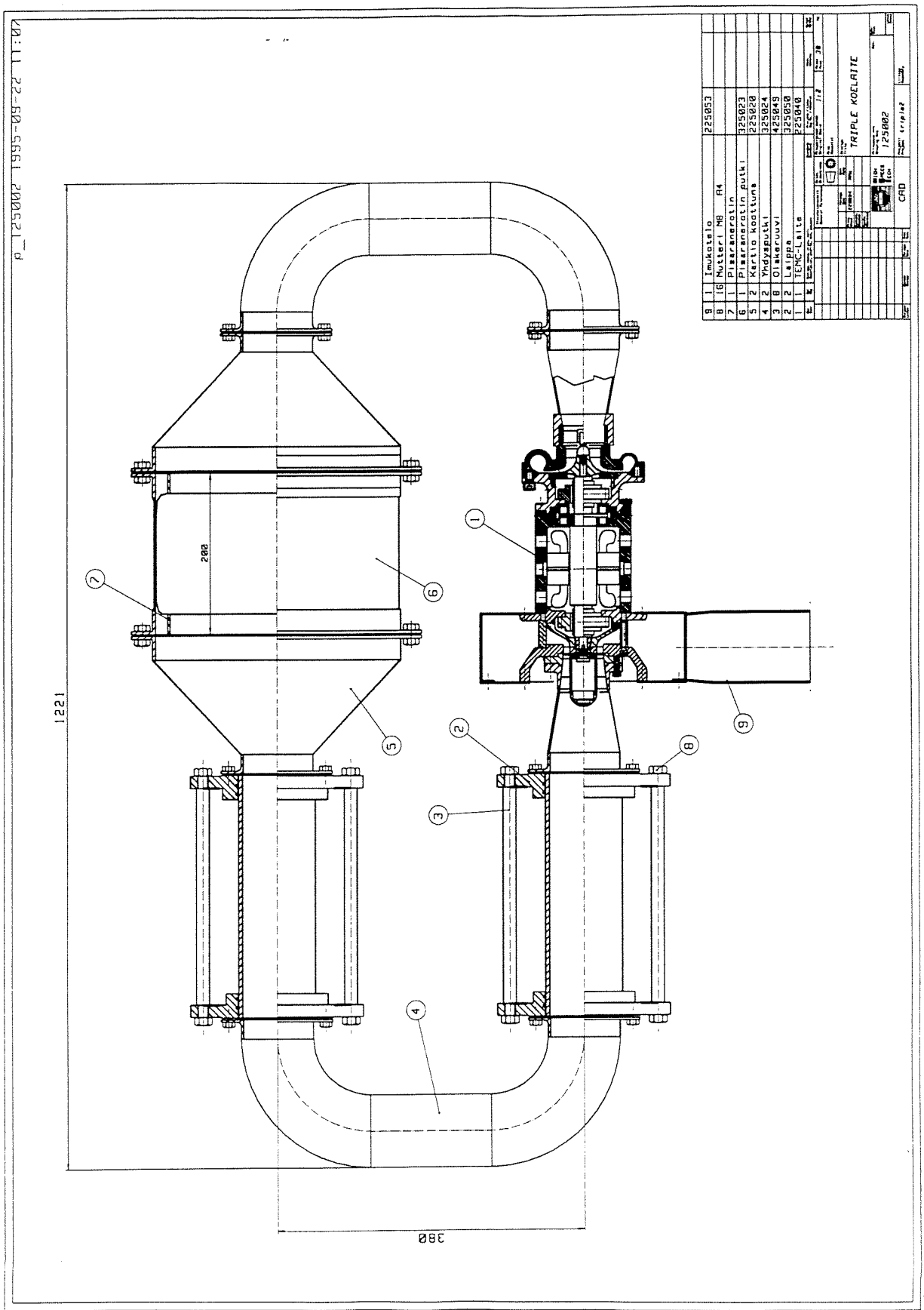
p_125002 1995-09-22 11:07
1221
200
380
TRIPLE KOELAITE
125002
CAD
9 1 Imukotelo 225053
8 16 Mutteri M8 A4
7 1 Pisaraneroitin
6 1 Pisaraneroitin putki 325023
5 2 Kartio kaotuna 225020
4 2 Yhdysputki 325024
3 8 Oikaruuvi 425045
2 2 Laippa 325030
1 1 TEMC-Laite 225040